JSCSEN 73(12)1139–1269(2008)

Journal of the Serbian Chemical Society

Electronic version

VOLUME 73

NO 12

BELGRADE 2008

Available on line at

www.shd.org.rs/JSCS

The full search of JSCS is available through

DOAJ DIRECTORY OF OPEN ACCESS JOURNALS

www.doaj.org

Journal of the Serbian Chemical Society
JSCS@tmf.bg.ac.yu • www.shd.org.rs/JSCS

J. Serb. Chem. Soc. Vol. 73, No. 12 (2008)

CONTENTS

Published by the Serbian Chemical Society
Karnegijeva 4/III, 11000 Belgrade, Serbia
Printed by the Faculty of Technology and Metallurgy
Karnegijeva 4, P.O. Box 35-03, 11120 Belgrade, Serbia

www.shd.org.rs

Journal of the Serbian Chemical Society

JSCS@tmf.bg.ac.yu • www.shd.org.rs/JSCS

J. Serb. Chem. Soc. *73* (12) 1139–1151 (2008)
JSCS–3793

UDC 547.521–326:542.913+577.15
Original scientific paper

Lipase catalyzed synthesis of flavor esters in non-aqueous media: Optimization of the yield of pentyl 2-methylpropanoate by statistical analysis

ZORICA KNEŽEVIĆ-JUGOVIĆ[1]*#, DEJAN BEZBRADICA[1#], ŽIVANA JAKOVLJEVIĆ[2], SUZANA BRANKOVIĆ-DIMITRIJEVIĆ[1#] and DUŠAN MIJIN[1#]

[1]*Faculty of Technology and Metallurgy, University of Belgrade, Karnegijeva 4, 11120 Belgrade and* [2]*Faculty of Mechanical Engineering, University of Belgrade, Kraljice Marije 16, 11120 Belgrade, Serbia*

(Received 19 March, revised 3 June 2008)

Abstract: In this study, the synthesis of pentyl 2-methylpropanoate employing a commercial lipase from *Candida rugosa* was investigated, the emphasis being placed on analyzing the effects of various process conditions on the yield of ester. The response surface methodology (RSM) and five-level-five-factor central composite rotatable design (CCRD) were used to evaluate the effects of variables, namely the initial water content, 0.0–2.0 % (w/v), the reaction temperature, 35–75 °C, the enzyme concentration, 1.0–5.0 g dm^{-3}, the acid/alcohol mole ratio, 1:2–5:2, and the reaction time, 4–48 h, on the yield (%) of ester. The production of pentyl 2-methylpropanoate was optimized and an ester yield response equation was obtained, enabling the prediction of ester yields from known values of the five main factors. It seems that the enzyme concentration, reaction time and acid/alcohol mole ratio predominantly determine the conversion process, while the amount of added water amount had no significant influence on the ester yield. Conversion of around 92 % of the substrate to ester could be realized using a concentration of lipase as low as 4.0 g dm^{-3} and in a relatively short time (26 h) at 35 °C, when a high substrate mole ratio of 2.5 was used.

Keywords: factorial design; surface response analysis; *Candida rugosa* lipase; flavor esters; esterification.

INTRODUCTION

Short chain aliphatic esters play a relevant role in the food industry as flavor and aroma constituents.[1] They are responsible for the particular fruity aroma or smell of a particular flower. Current processes for the production of esters consist

* Corresponding author. E-mail: zknez@tmf.bg.ac.yu
# Serbian Chemical Society member.
doi: 10.2298/JSC0812139K

of the esterification of a carboxylic acid with an alcohol in the presence of non-selective inorganic catalysts at high temperatures or extraction from natural sources. Esters extracted from plant materials are often either too scarce or expensive for commercial use while those produced by chemical synthesis are not considered as natural products. The replacement of inorganic catalysts by lipases in the synthesis of flavor esters avoids side product formation and is less polluting and energy consuming because of the mild conditions employed.[2] More importantly, the quality of the product of so enzyme-synthesized esters is normally better than the chemically-derived product due to the lower reaction temperature and avoidance of degradation products resulting from the strong acid-catalysis. Consequently, numerous attempts have been made to develop an efficient lipase system for the synthesis of food acceptable esters.[3–5]

Lipase from *Candida rugosa* (formerly *Candida cylindracea*) is an enzyme of considerable physiological significance and industrial potential in that it can catalyze numerous reactions, such as hydrolysis, transesterification, esterification, alcoholysis, acidolysis and aminolysis.[6–8] Several researchers have reported the synthesis of short-chain esters using free or immobilized lipase in non-aqueous, solvent-free or biphasic organic phase reaction systems.[3,9–11] In order to maximize the yield of the esters, serious attention was given to the optimization of the process parameters, the development of appropriate kinetic models of esterification and the monitoring and control of the water concentration in the reaction mixture. However, most of the studies were based on conventional one-at--a-time variation of parameters, which often do not demonstrate the interactive effects of the parameters.Moreover, the widely different substrates and reaction systems employed led to an enormous amount of quantitative data, which, however, cannot be directly compared. Thus, to make the enzymatic processes competitive, they should be studied and compared in a systematic way.

It was shown that the statistical designs could be very useful tool not only in optimizing esterification reactions, but also in explaining qualitatively and quantitatively the esterification behavior of the employed lipase.[12] In addition to reducing the number of experiments required for optimization, this technique enables the quantification of the individual effect of each factor and to investigate their possible interactions. An increasing number of results published in the field of ester synthesis in an organic solvent were based on experimental design.[13–15] Most of these studies were focused on the optimization of the conditions for the synthesis of ethanoic acid esters with immobilized lipase from *Rhizomucor miehei* as the catalyst. However, comparatively few have related to systematic studies of the synthesis of butanoic acid and 2-methyl propanoic acid esters with lipase from *C. rugosa*.[16]

The object of this study was to investigate the process conditions relevant for the synthesis of flavor esters aiming at a better control of the enzymatic process.

The results of previously reported investigations implied that the influence of reaction factors varies strongly with both substrate types. Each ester synthesis seems to be a specific problem. In this study, the synthesis of pentyl 2-methylpropanoate in isooctane was chosen as a model reaction because of its importance in the food industry. This short chain ester, which contributes to the natural aroma of fruits such as pineapple and banana, is widely used in the food industry for flavor enhancement. Lipase from *C. rugosa* was chosen for present work because of its commercial availability in large quantities at relatively low cost and the number of immobilization procedures developed with this enzyme.[17–19] Response surface methodology and 5-level-5-factor central composite rotatable design were performed to identify the factors that influence the ester synthesis and to verify whether any changes should be made in their settings to improve this reaction. In spite of the importance of pentyl 2-methylpropanoate, to the best of our knowledge, there are no reports about the use of *C. rugosa* for the synthesis of this ester in a non-aqueous system. Moreover, this is the first time that this system has been analyzed by the statistical approach at this level of detail.

EXPERIMENTAL

Materials

Commercial *Candida rugosa* lipase (EC 3.1.1.3), trizma buffer, thymolphthalein indicator solution and olive oil emulsion were purchased from Sigma Chemical Co. (St. Louis, MO, USA). The lipase was a crude preparation with 10 % protein based on the Lowry method for protein assay.[20] 2-Methylpropanoic acid and *n*-pentanol were purchased from Merck (Darmstadt, Germany). 2,2,4-Trimethylpentane of p.a. grade, purchased from Merck (Darmstadt, Germany), was dried over 0.3 nm molecular sieves for at least 24 h prior to use and, as such, was regarded as nearly anhydrous. The solvents used in the analytical procedures, standards and other reagents were reagent grade and purchased either from Aldrich Chemical Co. (St. Louis, MO, USA) or Sigma Chemical Co. (St. Louis, MO, USA).

Lipase activity assay

The lipase activity was estimated by the standard olive oil emulsion method.[21] This activity assay was performed with reaction mixtures containing 3.0 cm^3 of Sigma lipase substrate, 1.0 cm^3 of trizma buffer, and 3.5 cm^3 of distilled water. Negative and positive controls were also studied. The positive control was the reaction mixture in which investigated solution or biocatalyst was added at the beginning of the reaction time, whereas the negative control was one with samples added just before titration with NaOH. The reaction mixtures were agitated and incubated for 30 min in a water bath at 37 °C. The formed fatty acids were quantified by titration with 0.050 M sodium hydroxide. The activities are expressed as international units (IU), where 1 IU is defined as the amount of enzyme required to produce 1 μmol min^{-1} of free fatty acid under the assay conditions (37 °C, pH 7.7). The determined activity of the lipase was 1.55 IU mg^{-1} enzyme.

Pentyl 2-methylpropanoate synthesis

The esterification reactions were performed in screw-capped 100 cm^3 flasks in 2,2,4-trimethylpentane. *n*-Pentanol and 2-methylpropanoic acid were added at different molar ratios followed by different amounts of water, according to the experimental design. The reaction mixture was then diluted up to the volume of 10 cm^3 with 2,2,4-trimethylpentane and incu-

bated on a shaker at 150 rpm and at different temperatures prior to the addition of the lipase. The various quantities of enzyme were added to the reaction mixture only after the correct temperature had been attained and samples were taken for analysis after 4, 15, 26, 37 and 48 h reaction time. Control experiments were also conducted without lipase under similar conditions.

Analysis

The reactions were monitored by determination of the residual acid content by titration against standard sodium hydroxide using phenolphthalein as the indicator and methanol as a quenching agent. The molar conversion was determined from the values obtained for the blank and the test samples. The reactions were also monitored by measuring the concentrations of the products by gas chromatography (model: Varian 3400) equipped with a Carbowax 20-M column (3.0 m length, 3.175 mm internal diameter) and a flame ionization detector (FID). Nitrogen was used as the carrier gas at a flow rate of 30 cm^3 min^{-1}. The column oven, injector and detector temperatures were at 100, 200, and 250 °C, respectively.[14] The reported percentage yield of ester was defined as the amount of ester produced to the amount of initial substrate in defect ((mol ester/mol initial substrate in defect)×100). The percentage esterification determined by both GC analysis and titration were found to be in good agreement.

Experimental design and analysis

A five-level-five-factor central composite design was employed in this study, requiring 32 experiments, which consisted of 16 factorial points, 10 axial points and 6 central points.[22] The variables and their levels selected for the study of the ester synthesis were: water content (0.0–2.0 % (w/v)); temperature (35–75 °C); enzyme concentration (1.0–5.0 g dm^{-3}); acid/alcohol mole ratio (1:2–5:2) and reaction time (4–48 h). These variables were chosen based on the results obtained in a preliminary study and are the most commonly used for modeling esterification reactions. In a preliminary study, the effects of reactant concentration on the initial rate of production of pentyl 2-methylpropanoate were investigated with the reactants added in stoichiometric proportions. It seems that the initial reaction rate increases rapidly with concentration up to about 0.50 mol dm^{-3} and thereafter becomes essentially constant between 0.50 and 0.75 mol dm^{-3} before dropping at higher concentrations (data not shown). This appears to be caused by inactivation of the lipase by the alcohol. In separate experiments in which an excess of 2-methylpropanoic acid was used, it was shown that the acid did not deactivate the enzyme in concentrations up to 1.25 mol dm^{-3}. Therefore, the effect of acid/alcohol mole ratio was investigated fixing the initial alcohol concentration at a lower value (500 mmol dm^{-3}) at different concentrations of acid.

The actual and coded settings of each of the five experimental factors are given in Table I. The experiments were run at random to minimize errors due to possible systematic trends in the variables. The ester yield was taken as the response variable. The design of experiments employed is presented in Table II. The data obtained were fitted to a second-order polynomial equation:

$$Y = \beta_{k0} + \sum_{i=1}^{5} \beta_{ki} X_i + \sum_{i=1}^{5} \beta_{kii} X_i^2 + \sum_{i=1}^{4} \sum_{j=i+1}^{5} \beta_{kij} X_i X_j \quad (1)$$

where Y is the response (ester yield in mol %), β_{k0},β_{ki}, β_{kii} and β_{kij} are regression coefficients for the intercept, linear, quadratic and interaction terms, respectively and X_i and X_j are independent variables. The coefficients of the response function and their statistical significance were evaluated by the method of least squares using Matlab software (version 6.5, Release 13, The MathWorks, Juc, Matick, MA, USA). Only the significant terms ($p \leq 0.05$) were considered for the final reduced model. The lack-of-fit test was used to determine whether the

constructed model was adequate to describe the obtained data. The goodness of fit of the model was evaluated by the determination of R^2 and r coefficients, complemented by a graphic plot of the values predicted by the model *vs*. the observed experimental values. High values of both R^2 and r suggest a good fit of the model to the experimental data. Response surfaces and contour plots were obtained using the fitted model by keeping two independent variables at a constant value while changing the other two variables. The regression analysis, statistical significance and response surfaces were also realized using Matlab software.

TABLE I. Coded and actual values of the variables for the design of the experiments

Variables	Coded levels of the variables				
	–2	–1	0	1	2
Water content, X_1 / % (w/v)	0	0.5	1.0	1.5	2.0
Temperature, X_2 / °C	35	45	55	65	75
Enzyme amount, X_3 /g dm^{-3}	1	2	3	4	5
Substrate mole ratio, X_4	1:2	1:1	3:2	2:1	5:2
Reaction time, X_5 / h	4	15	26	37	48

RESULTS AND DISCUSSION

Response surface analysis

The response surface methodology (RSM) is an optimization technique, which determines the optimum process condition by testing several variables simultaneously, uses special experimental designs to reduce the number of required determinations and measures several effects by objective tests. In this study, RSM and 5-level-5-factor central composite rotatable design were employed to optimize and understand the relationship between the important reaction parameters in the lipase-catalyzed synthesis of pentyl 2-methylpropanoate in a non-aqueous system.

The data showing the predicted and experimental yields of ester for the 32 experiments of the statistical design are given in Table II. According to this study, the maximum ester yield can be obtained at a low temperature, low level of water content and high levels of lipase concentration, initial acid/alcohol mole ratio, and reaction time. Among the various syntheses, the greatest molar conversion (96.8 %) was achieved in run No. 13 (water content of 0.5 %, 45 °C, enzyme concentration of 4 g dm^{-3}, substrate mole ratio 2:1, 37 h), while the smallest conversion (only 11.85 %) was achieved in run No. 26 (water content of 1.0 %, 55 °C, enzyme concentration 3 g dm^{-3}, substrate mole ratio 3:2, 4 h).

A statistical analysis was performed on the experimental data, whereby the main effects and interaction effects of the variables were estimated. Both the *t*-test and *p*-value statistical parameters were used to confirm the significance of factors studied. The effects of the parameters on the ester synthesis and their significance are shown in the Pareto chart of effects (Fig. 1). It seems that the most relevant variables for the ester synthesis are reaction time and enzyme concentration with estimated effects of 13.00 and 11.61, respectively. The effects of substrate mole

TABLE II. Experimental setup for five-level, five-factor surface response design and the experimental data

Run No.	Water content, X_1 / %	Temperature X_2 / °C	Enzyme concentration X_3 /g dm^{-3}	Substrate mole ratio, X_4	Reaction time X_5 / h	Experimental
1	1	1	1	1	1	56.20
2	1	1	1	–1	–1	27.05
3	1	1	–1	1	–1	30.80
4	1	1	–1	–1	1	15.40
5	1	–1	1	1	–1	49.20
6	1	–1	1	–1	1	62.90
7	1	–1	–1	1	1	56.50
8	1	–1	–1	–1	–1	13.80
9	–1	1	1	1	–1	52.90
10	–1	1	1	–1	1	36.30
11	–1	1	–1	1	1	36.70
12	–1	1	–1	–1	–1	14.30
13	–1	–1	1	1	1	96.80
14	–1	–1	1	–1	–1	30.00
15	–1	–1	–1	1	–1	29.30
16	–1	–1	–1	–1	1	42.60
17	2	0	0	0	0	24.00
18	–2	0	0	0	0	36.22
19	0	2	0	0	0	13.05
20	0	–2	0	0	0	33.45
21	0	0	2	0	0	76.57
22	0	0	–2	0	0	14.25
23	0	0	0	2	0	61.75
24	0	0	0	–2	0	29.45
25	0	0	0	0	2	80.92
26	0	0	0	0	–2	11.85
27[a]	0	0	0	0	0	48.30
28[a]	0	0	0	0	0	29.10
29[a]	0	0	0	0	0	28.42
30[a]	0	0	0	0	0	41.02
31[a]	0	0	0	0	0	31.35
32[a]	0	0	0	0	0	35.92

[a]Center point

ratio, temperature, and temperature–reaction time interaction were also signifycant ($p < 0.05$). It appears that while the substrate mole ratio has a positive effect (8.87), temperature and reaction time–temperature interaction have a significant negative influence on the ester yield (–6.93 and –7.09, respectively) which is in agreement with thermal stability data for this lipase in non-aqueous medium.[10,23,24] The results also indicate the importance of working at high levels of enzyme concentration, reaction time and substrate mole ratio. Due to the bars that extend beyond the vertical line on the plot which correspond to effects that are stati-

stically significant at the 95 % confidence level, quadratic terms of incubation time, mole ratio and enzyme concentration were also significant. Interestingly, the effect of the water content on the conversion was not significant and could be neglected in the range tested. Perhaps, this is because a water content in this range was sufficient to preserve the catalytic conformation of the enzyme and the lipase itself contained sufficient water to maintain its activity. In general, it was observed that only a very small amount of water was required to successfully employ enzymes in organic solvents.[10] However the optimal level of water should be determined for each particular reaction system. In the present experimental setup, the water content did not significantly influence the ester yield. Therefore, the added water was constant at 0 level (1 %) in the following discussion.

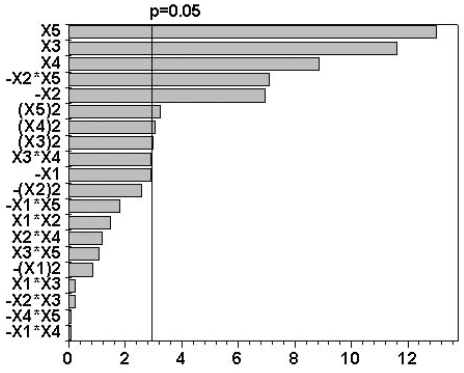

Fig. 1. Pareto diagram of the effect of the reaction parameters on the ester synthesis and their significance calculated from the experimental design. For abbreviations, see Table I.

The multiple regression coefficients, obtained by employing a least squares technique to predict a second-order polynomial model (Eq. (1)) for ester yield (Y, %), after backward elimination, their significance (student's t-test and p-values) and the results of the statistical analysis are summarized in Table III. According to the results of the student's t-test, four linear coefficients and one cross-product term had a highly significant effect at the 99 % confidence level. Three quadratic terms were also significant ($p < 0.05$). The quadratic term of temperature and nine cross-product terms corresponding to X_1 with X_2, X_3, X_4 and X_5, X_2 with X_3 and X_4, X_3 with X_4 and X_5 and X_4 with X_5 were found to be insignificant ($p > 0.05$). The final response equation obtained after eliminating the insignificant terms is as follows:

$$Y = 31.959 - 6.935X_2 + 11.767X_3 + 9.019X_4 + 12.849X_5 - 7.093X_2X_5 + \\ + 3.207\,X_3^2 + 3.254\,X_4^2 + 3.451\,X_5^2 \quad (2)$$

The fit of the model was checked by the R^2 values, which was calculated to be 0.912, indicating that 91.2 % of the variability in the response could be explained by the model. The model also showed statistically insignificant lack of fit, as is evident from the lower calculated F value (1.06) than the theoretical $F_{0.05}$ value (4.58) at the 5 % level. The plot of experimental values of ester yield

(%), *versus* those calculated from the above equation, indicated a good fit (Fig. 2), with a correlation coefficient, r of 0.944. Overall, these results revealed good agreement between the predicted and experimental values, implying that the empirical model derived from RSM can be used to adequately describe the relationship between the factors and the response in the lipase-catalyzed synthesis of pentyl 2-methylpropanoate.

TABLE III. Regression coefficients (β) and significance (student's t-test and p-values) of the predicted second-order polynomial model for the response (Y) after backward elimination and the results of the statistical analysis

Factors	Coefficient (β)	Standard error	t-Values	p-Values
Average	31.9595	±3.11	11.31	0.0000
Temperature, X_2	–6.9348	±1.68	–4.23	0.0027[a]
Lipase concentration, X_3	11.7673	±1.68	6.93	0.0002[a]
Substrate mole ratio, X_4	9.0193	±1.68	5.29	0.0009[a]
Reaction time, X_5	12.8494	±1.68	7.76	0.0001[a]
X_2X_5	–7.0930	±2.32	–3.50	0.0064[a]
X_3^2	3.2070	±1.45	2.06	0.0422[b]
X_4^2	3.2539	±1.44	2.10	0.0404[b]
X_5^2	3.4507	±1.45	2.23	0.0335[b]

Results of the statistical analysis

Source of variation	Sum of square	Degrees of freedom	Mean square	F-test
Regression	1455.8	23	63.3	–
Lack of fit	1153.2	18	64.1	1.06
Pure error	302.6	5	60.5	–

[a]$p < 0.01$; [b]$p < 0.05$

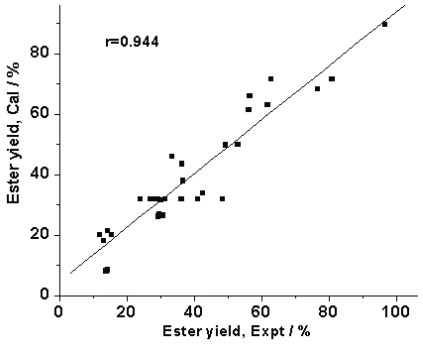

Fig. 2. Correlation of the calculated *versus* the experimental values for the synthesis of pentyl 2-methylpropanoate catalyzed by lipase from *C. rugosa*.

Influence of process conditions on the molar conversion

The influence of the variables, reaction temperature, enzyme concentration, substrate mole ratio and reaction time on the yield of ester is discussed using the statistical model shown by Eq. (2).

Temperature showed an interactive effect with the reaction time of esterification. The shape of the three-dimensional surface, representing yield of ester *versus* temperature and reaction time, is shown in Fig. 3a. It appears that the

surface is smooth showing an increase/decrease in one axis and a decrease/ /increase in the other axis, which reflects that the temperature may affect the reaction rate in opposite ways. Specifically, as the temperature increases, the expected increase in reaction rate resulting from more productive molecule collisions per unit time is offset by the increasing rate of enzyme denaturation. The effect of temperature on the ester synthesis during the initial period was observed to follow Arrhenius law (between 298 and 338 K) with an activation energy of 18.34 kJ mol^{-1}, which is typical for enzymatic reactions occurring in a reaction--limited regime.[25] At intermediate and high levels of reaction time, however, a different behavior was observed as the surface decreased with increasing reaction temperature. This could be the result of a negative temperature–reaction time interaction, probably caused by thermal deactivation of the enzyme. The maximum yield of ester could be obtained when working at low temperatures and a high level of reaction time. The result suggests that the *C. rugosa* lipase, like some other lipases such as Novozym SP 435 from *Candida antarctica*[26,27] or porcine pancreatic lipase,[12] was inactivated when it was subjected to a high temperature for a long period under non-aqueous conditions.

Another important parameter affecting the economic feasibility of the process is the acid to alcohol mole ratio. Figure 3b shows the predicted percentage of esterification as a function of the substrate molar ratio at different temperatures for an enzyme concentration of 3 g dm^{-3} (4.5 IU cm^{-3}) and an incubation period of 26 h. It seems that while the temperature exerted a negative influence, excess of acid had a significant positive effect on the ester yield, indicating the importance of using an excess of acid over the stoichiometric amount for the maximum conversion to ester. Minimum esterification was observed at a substrate mole ratio of 0.8 at 55 °C (11 %) and a maximum esterification was observed at a substrate ratio of 2.5 at 35 °C (≈ 77 %). The beneficial effect of excess acyl donor was also observed for the synthesis of short-chain esters using microbial lipases by several authors. For example, studying the synthesis of ethyl butanoate with the same lipase as the catalyst, Chen[9] verified that the mole ratio between ethanol and butanoic acid was a critical factor for attaining a high yield of ethyl butanoate, requiring an amount of butanoic acid of the order of 3.3 times that of ethanol. Yadav and Lathi[27] also found that there was an increase in the reaction rate with increasing amount of 2-methylpropanoic acid using Novozym SP 435 lipase during the synthesis of butyl 2-methylpropanoate. The possible explanation is related to reaction mechanism. Lipase is known to catalyze esterification through an acyl-intermediate formed between the fatty acid substrate and the enzyme. Free enzyme can either bind the fatty acid to produce this intermediate or the ester product. In an excess of fatty acid, most of the enzyme is found in the acylated form, preventing it from binding the product. In addition, a higher concentration of free 2-methylpropanoic acid in the reaction system was

beneficial for the incorporation of acid from the view of reaction equilibrium, but excessive free fatty acid could also result in substrate inhibition.[10,25,28] In the present experimental setup, the substrate mole ratio had a positive influence on the ester yield and it was found that the acid did not deactivate the catalyst at concentrations up to 1.25 mol dm^{-3}.

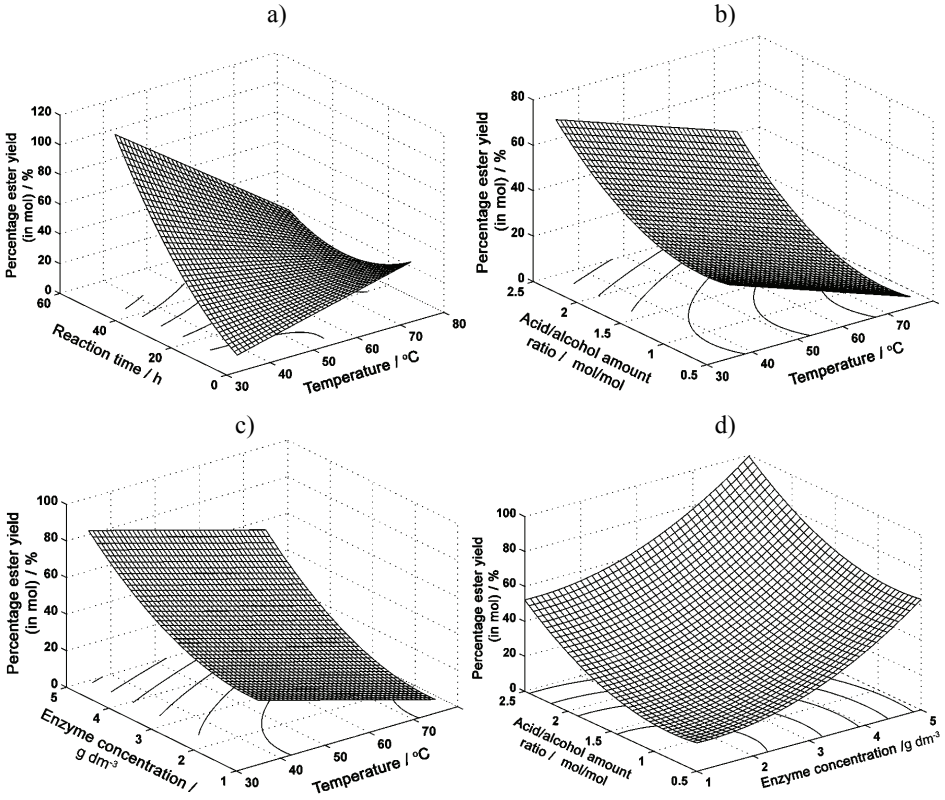

Fig. 3. Correlation of the calculated *versus* the experimental values for the synthesis of pentyl 2-methylpropanoate catalyzed by lipase from *C. rugosa*.

The response surface plot for the predicted values for the yield of ester *versus* temperature and catalyst concentration after 26 h at a fixed substrate mole ratio of 1.5 are shown in Fig. 3c. It appears that predicted yield of ester increased with increasing enzyme concentration at all temperatures. For an illustration, at 55 °C, the response varied from 21.2 to 68.3 % on increasing the enzyme concentration from 1–5 g dm^{-3} (1.5–7.5 IU cm^{-3}). A similar behavior was observed during the *Rhizopus* lipase-catalyzed synthesis of 3-methylbutyl butanoate, since an increase in yield by 32.2 % was recorded when the amount lipase was changed from 1 to 10 %.[29] Therefore, to maximize the ester yield, the enzyme concentration must be kept at the highest tested levels.

Similar trends were observed for the interaction of both enzyme concentration and substrate mole ratio *versus* reaction time. However, the most interesting result of the part of study focused on the statistically analyzed influence of enzyme concentration and mole ratio in a 3-dimensional graph (Fig. 3d). In addition, the contour plot could also indicate the desirable combination of variables, which can be selected by the manufacturer, because there were several optimal combinations available to obtain the highest ester yield (Fig. 4). The ester production is represented by a concave surface described by a second order polynomial with a minimum at an enzyme concentration of about 1.2 g dm^{-3} (3.6 IU cm^{-3}) for a mole acid/alcohol ratio equal to 0.8. Figure 4 shows the contour plot for the predicted values for the yield of ester *versus* catalyst concentration and substrate mole ratio after 26 h at 35 °C. The results indicate that high yields are possible with small amounts of enzyme when high substrate mole ratio levels are used,

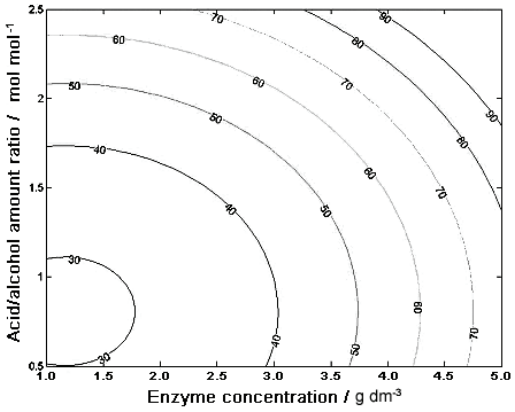

Fig. 4. Contour plot for the yield of ester as a function of enzyme concentration and substrate mole ratio after 26 h at 35 °C.

which is beneficial from the economic viewpoint since the cost of enzyme is usually higher than that of substrates. In general, for enzymatic esterification reactions, the lipase concentrations required to achieve higher yields of esters are often too high and the reaction times relatively too long for industrial application. Welsh *et al.*[4] reported 75.8 % conversion in 48 h with 2 % native lipase from *C. cylindracea* at 0.050 M substrate (the E/S ratio was 400 g mol^{-1}). Chowdary *et al.*[30] reported an 85 % conversion of 3-methylbutanoic acid to 3-methylbutyl 3-methylbutanoate with 0.50 M acid concentration and 1.0 % enzyme concentration during an incubation time of 144 h in *n*-hexane (the E/S ratio was 20), by using Lipozyme IM-20 lipase from *R. miehei*. In this study, it was shown that a high conversion of 91.9 % could be achieved at 0.50 M alcohol concentration (substrate in deficit), using amounts of enzyme as low as 4.0 g dm^{-3} and in a relatively short time (26 h) at 35 °C at a fixed acid/alcohol mole ratio of 2.5, as can be inferred from the contour plot in Fig. 4. Namely, under this condition (E/S ratio of $\approx$ 8 g mol^{-1}), a rather high ester concentration of around 70 g dm^{-3} was

achieved, which was in the proximity of results previously reported in related studies[28,30] or much higher.[4,5,31] The feasibility of the ester synthesis by *C. rugosa* lipase under solvent-free condition was also explored, and a reasonably high yield of esters (62 %) was achieved under optimal conditions (data not shown).

CONCLUSIONS

The aim of this work was to evaluate the performance of lipase from *C. rugosa* in the synthesis of pentyl 2-methylpropanoate using a reaction system of interest from an industrial point of view. A surface response methodology based on CCRD design was employed to study the effects of the five most important factors influencing the yield of ester. An ester yield response equation was obtained, making it possible to predict the operating conditions required to obtained well--defined amounts of the ester. It seems that the lipase concentration, reaction time and substrate mole ratio have positive influences on the ester synthesis while the temperature and reaction time–temperature interaction have negative influences on the process. It appears that high yields of esters are possible with small amounts of enzyme when high substrate mole ratios are used, which is beneficial from the economic viewpoint. These findings should stimulate the application of such lipase-catalyzed reactions for the preparation of food acceptable short chain esters. Further studies should be concentrated on improvement of the lipase stability by its immobilization and extension of its application to other non-aqueous and solvent-free reaction systems.

Acknowledgements. The authors thank Ministry of Science and Technological Development of the Republic of Serbia for the financial support (Project: TR-20064).

ИЗВОД

СИНТЕЗА МИРИСНИХ ЕСТАРА КАТАЛИЗОВАНА ЛИПАЗАМА У НЕВОДЕНОЈ СРЕДИНИ: ОПТИМИЗАЦИЈА ПРИНОСА ПЕНТИЛ-2-МЕТИЛПРОПАНОАТА СТАТИСТИЧКОМ АНАЛИЗОМ

ЗОРИЦА КНЕЖЕВИЋ-ЈУГОВИЋ[1], ДЕЈАН БЕЗБРАДИЦА[1], ЖИВАНА ЈАКОВЉЕВИЋ[2], СУЗАНА БРАНКОВИЋ-ДИМИТРИЈЕВИЋ[1] и ДУШАН МИЈИН[1]

[1]*Технолошко–металуршки факултет, Универзитет у Београду, Карнегијева 4, 11120 Београд и* [2]*Машински факултет, Универзитет у Београду, Краљице Марије 16, 11120 Београд*

У раду су испитани утицаји различитих процесних параметара на синтезу пентил-2-метилпропаноата катализовану липазом из *Candida rugosa.* У циљу оптимизације ензимске синтезе естара примењена је методологија одзивних површина у складу са одабраним централним композиционим ротабилним планом (пет фактора на пет нивоа). Испитани су утицаји процесних параметара на принос естра у следећим интервалима: почетног садржаја воде (0,0–2,0 %), температуре (35–75 °C), концентрације ензима (1,0–5,0 g dm^{-3}), почетног молског удела супстрата (1:2–5:2) и реакционог времена (4–48 h). Добијен је адекватан математички модел на основу кога се може предвидети понашање система у функцији ових пет фактора. Показано је да концентрација ензима, почетни молски однос супстрата и реакционо време имају нај-

већи утицај на процес, док садржај воде не утиче значајно на принос естра. Под оптималним условима ензимске синтезе остварен је принос естра око 92 %.

(Примљено 19. марта, ревидирано 3. јуна 2008)

REFERENCES

1. M. Liaquat, R. K. Owusu, *Food Chem. Toxicol.* **65** (2000) 295
2. U. Krings, R. G. Berger, *Appl. Microbiol. Biotechnol.* **49** (1998) 1
3. F. W. Welsh, R. E. Williams, *Enzym. Microb. Technol.* **12** (1990) 743
4. F. W. Welsh, R. E. Williams, K. H. Dawson, *J. Food Sci.* **55** (1990) 1679
5. H. Razafindralambo, C. Blecker, G. Lognoy, M. Marlier, J. P. Wathlet, M. Severin, *Biotechnol. Lett.* **16** (1994) 247
6. S. Benjamin, A. Pandey, *Yeast* **14** (1998) 1069
7. D. Bezbradica, I. Karalazić, N. Ognjanović, D. Mijin, S. S. Marinković, Z. Knežević, *J. Serb. Chem. Soc*. **71** (2006) 31
8. Z. Knežević, S. S. Marinković, L. Mojović, *Appl. Microbiol. Biotechnol.* **49** (1998) 267
9. J. P. Chen, *J. Ferment. Bioeng.* **82** (1996) 404
10. G. Carta, J. L. Gainer, A. H. Benton, *Biotechnol. Bioeng*. **37** (1991) 1004
11. D. Bezbradica, D. Mijin, S. S. Marinković, Z. Knežević, *J. Mol. Catal. B: Enzym*. **38** (2006) 11
12. B. Manohar, S. Divakar, *Process Biochem.* **39** (2004) 847
13. C. J. Shieh, S. W. Chang, *J. Agric. Food Chem.* **49** (2001) 1203
14. S. H. Krishna, B. Manohar, S. Divakar, S. G. Prapulla, N. G. Karanth, *Enzym. Microb. Technol.* **26** (2000) 131
15. B. Manohar, S. Divakar, *World J. Microbiol. Biotechnol.* **18** (2002) 745
16. I. L. Shih, S. H. Hung, F. Y. Chen, H. Y. Ju, C. J. Shieh, *Food Chem.* **100** (2007) 1223
17. S. H. Chiou, W. T. Wu, *Biomaterials* **25** (2004) 197
18. Z. Knežević, L. Mojović, B. Adnađević, *J. Serb. Chem. Soc*. **63** (1998) 257
19. J. M. Moreno, J. V. Sinisterra, *J. Mol. Catal.* **93** (1994) 357
20. O. H. Lowry, N. J. Resebrough, A. L. Farr, R. J. Randall, *J. Biol. Chem.* **193** (1951) 265
21. N. Tietz, E. Fiereck, *Clin. Chim. Acta* **13** (1966) 352
22. G. E. P. Box, W. G. Hunter, J. S. Hunter, *Statistics for experimenters: an introduction to design, data analysis and model building*, Wiley, New York, 1978, p. 653
23. F. M. Gomes, E. B. Pereira, H. F. Castro, *Biomacromolecules* **5** (2004) 17
24. Z. Knežević, N. Milosavić, D. Bezbradica, Ž. Jakovljević, R. Prodanović, *Biochem. Eng. J.* **30** (2006) 269
25. A. Zaidi, J. L. Gainer, G. Carta, A. Mrani, T. Kadiri, Y. Belarbi, A. Mir, *J. Biotechnol.* **93** (2002) 209
26. J. M. Rodriguez-Nogales, E. Roura, E. Contreras, *Process Biochem.* **40** (2005) 63
27. G. D. Yadav, P. S. Lathi, *Biochem. Eng. J.* **16** (2003) 245
28. S. H. Krishna, S. G. Prapulla, N. G. Karanth, *J. Ind. Microbiol. Biotechnol.* **25** (2000) 147
29. G. A. Macedo, G. M. Pastore, M. I. Rodrigues, *Process Biochem.* **39** (2004) 687
30. G. V. Chowdary, M. N. Ramesh, S. G. Prapulla, *Process Biochem.* **36** (2000) 331
31. G. Langrand, N. Rondot, C. Triantaphylides, J. Baratti, *Biotechnol. Lett.* **18** (1990) 581.

www.shd.org.rs

Journal of the Serbian Chemical Society

JSCS@tmf.bg.ac.yu • www.shd.org.rs/JSCS

J. Serb. Chem. Soc. 73 (12) 1153–1160 (2008)
JSCS–3794

UDC 546.732+547.582.4:615.281–188
Original scientific paper

Antibacterial activity of cobalt(II) complexes with some benzimidazole derivatives

S. O. PODUNAVAC-KUZMANOVIĆ[1]*#, V. M. LEOVAC[2#] and D. D. CVETKOVIĆ[1]

[1]*Faculty of Technology, Bul. Cara Lazara 1, 21000 Novi Sad and* [2]*Department of Chemistry, Faculty of Sciences, Trg D. Obradovića 3, 21000 Novi Sad, Serbia*

(Received 21 March, revised 26 May 2008)

Abstract: The antibacterial activities of cobalt(II) complexes with two series of benzimidazoles were evaluated *in vitro* against three Gram-positive bacterial strains (*Bacillus cereus*, *Staphylococcus aureus*, and *Sarcina lutea*) and one Gram-negative isolate (*Pseudomonas aeruginosa*). The minimum inhibitory concentration was determined for all the complexes. The majority of the investtigated complexes displayed *in vitro* inhibitory activity against very persistent bacteria. They were found to be more active against Gram-positive than Gram-negative bacteria. It may be concluded that the antibacterial activity of the compounds is related to the cell wall structure of the tested bacteria. Comparing the inhibitory activities of the tested complexes, it was found that the 1-substituted--2-aminobenzimidazole derivatives were more active than complexes of 1-substituted-2-amino-5,6-dimethylbenzimidazoles. The effect of chemical structure on the antibacterial activity is discussed.

Keywords: benzimidazole derivatives; complexes; cobalt(II); antibacterial; *in vitro* studies.

INTRODUCTION

The benzimidazole nucleus, which is a useful structure for further research and for the development of new pharmaceutical molecules, has received a great deal of attention in the last decade. Due to their antimicrobial activities, new benzimidazoles have been synthesized and investigated for medical applications. The position and type of the substituents on the benzimidazole ring are responsible for the variety of their biological activities. Many derivatives of benzimidazole are well known as antibacterial agents.[1–7] This class of compounds has been found to show antimicrobial activities against Gram-positive and Gram-negative bacteria, primarily because of the potential bio-activity of benzimidazole--based ligands.[8–10] Hence, the incorporation of imidazole and benzimidazole nuclei is an important synthetic strategy in drug discovery.

* Corresponding author. E-mail: sanya@uns.ns.ac.yu
# Serbian Chemical Society member.
doi: 10.2298/JSC0812153P

Extensive biochemical and pharmacological activities have confirmed that these molecules are effective against RNA viruses and inhibit the formation of virus-induced RNA polymerase, thereby preventing or retarding RNA synthesis of various strains of microorganisms.[11–14] Antimicrobial activity of this class of compounds against *Helicobacter pylori*[15] and oral *Streptococci*[16] has also been reported. The synthesis of benzimidazoles fused to another heterocyclic ring has attracted widespread attention due to their diverse application as antioxidant,[17,18] antifungal,[19] antitubercular,[20] anticancer,[21,22] and antiallergic drugs.[23] Various benzimidazoles are also effective inhibitors of the growth of the HIV-virus.[24,25]

In the last period, possible therapeutical properties of metal complexes with derived benzimidazoles have also excited wide interest. It was found that the complexes of transition metal salts with benzimidazole derivatives showed greater antimicrobial activity than the ligands applied alone.[26]

The development of resistance to current antibacterial therapy continues to drive the search for more effective agents. In order to obtain more potent compounds, our previous studies[4–9] prompted us to investigate the antibacterial activity of cobalt(II) complexes containing 1-benzylbenzimidazoles against three Gram-positive bacterial strains and one Gram-negative isolate. The effect of the ligand and complex structure on the inhibitory activity of tested compounds was also examined.

EXPERIMENTAL

In the present study, the antibacterial activity of cobalt(II) complexes with the following starting ligands: 2-amino-1-(3-chlorobenzyl)benzimidazole (L^1), 2-amino-1-(3-fluorobenzyl)–benzimidazole (L^2), 2-amino-1-(3-chlorobenzyl)-5,6-dimethylbenzimidazole (L^3), 2-amino-1--(3-fluorobenzyl)-5,6-dimethylbenzimidazole (L^4) and 2-amino-5,6-dimethyl-1-(3-methylbenzyl)benzimidazole (L^5), was evaluated (Table I).

TABLE I. Structural formulae of the ligands

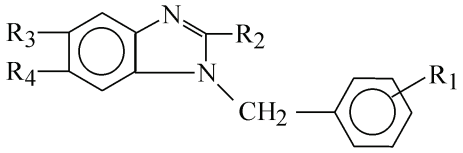

	R_1	R_2	R_3	R_4
		Series I		
L^1	–*m*-Cl	NH_2	H	H
L^2	–*m*-F	NH_2	H	H
		Series II		
L^3	–*m*-Cl	NH_2	CH_3	CH_3
L^4	–*m*-F	NH_2	CH_3	CH_3
L^5	–*m*-CH_3	NH_2	CH_3	CH_3

All the ligands were synthesized by Vlaović *et al.* according to a procedure described earlier.[27] The cobalt(II) complexes were prepared following the same procedure described in a previous paper.[7]

Antibacterial investigations

All the cobalt(II) complexes were tested for their *in vitro* growth inhibitory activity against *Bacillus cereus* ATCC 10876, *Staphylococcus aureus* ATCC 25923, *Sarcina lutea* ATCC 9341 and *Pseudomonas aeruginosa* ATCC 27853.

The antibacterial activities of the complexes were tested by the disc-diffusion method under standard conditions using Mueller-Hinton agar medium, as described by NCCLS.[28] Each of the investigated isolates of bacteria was seeded in tubes with nutrient broth (NB). 1 cm^3 of seeded NB was homogenized in tubes with 9 cm^3 of melted (45 °C) nutrient agar (NA). The homogenous suspension was poured out in Petri dishes. The discs of filter paper (diameter 5 mm) were ranged on the cool medium. After cooling on the formed solid medium, 0.02 cm^3 of the investigated compounds (c = 1000 μg/ml) were placed by micropipette. After incubation of 24 h at 25–27 °C, the inhibition (sterile) zone diameters (including disc) were measured (in mm). An inhibition zone diameter over 8 mm indicates the tested compound is active against the microorganism. Every test was done in triplicate. Antimicrobial activities of the free ligands against the same bacteria were tested in a previous study.[8]

Minimum inhibitory concentration (*MIC*) was determined by the agar dilution method according to guidelines established by the NCCLS standard M7-A5.[29] The *MIC* is described as the lowest concentration of a compound that visibly inhibited the growth of a colony. Stock solutions of the compounds were prepared in dimethylformamide (DMF). Further dilutions were performed with distilled water. The concentration range of the compounds tested was between 60–750 μg/ml in two-fold dilution steps. The inoculated plates were than incubated at 35 °C for 16–20 h. A control using DMF without any test complex was included for each organism. It was found that the solvent had no activity against any of the test micro-organisms.

RESULTS AND DISCUSSION

The results of the antibacterial studies of the cobalt(II) complexes with the two series of 1-benzylbenzimidazole derivatives tested by the agar disc-diffusion method are summarized in Table II.

TABLE II. *In vitro* antibacterial activity of the complexes at a concentration of 1000 μg/ml

Complex	Inhibition zone diameter, mm			
	Pseudomonas aeruginosa	*Bacillus cereus*	*Staphylococcus aureus*	*Sarcina lutea*
$Co(L^1)_2Cl_2$	22	26	26	29
$Co(L^2)_2Cl_2$	17	24	24	25
$Co(L^3)_2Cl_2$	9	17	17	18
$Co(L^4)_2Cl_2$	8	16	17	17
$Co(L^5)_2Cl_2$	5	16	17	16

It is evident that the majority of the investigated compounds displayed *in vitro* antimicrobial activity against very persistent micro-organisms. The investigated complexes were found to be more active against Gram-positive than Gram-negative bacteria (*P. aeruginosa*). In the case of Gram-negative isolate, only com-

plexes of ligands from Series I exhibited significant antibacterial activity. The cobalt(II) complexes of L^3, L^4 and L^5 were slightly active against *P. aeruginosa*. In the case of *B. cereus* and *S. aureus*, the cobalt(II) complexes of ligands L^1 and L^2 also expressed higher activity than the complexes of ligands from Series II. The Gram-positive bacterium *S. lutea* was persistent in all investigated cases. The cobalt(II) complexes containing L^1 and L^2 were very highly or highly active, respectively. On the other hand, complexes of L^3, L^4 and L^5 were moderately active against the same bacteria.

In the second phase, the *MIC* of the tested compounds was determined by the agar dilution method. The results are presented in Tables III–VI. The compounds which are not shown in the tables had no antibacterial activity at the tested concentration.

TABLE III. Antibacterial activities of the complexes against *P. aeruginosa* at different concentrations (inhibition zone diameter in mm)

Complex	*MIC* / μg ml^{-1}				
	750	500	250	125	62.5
$Co(L^1)_2Cl_2$	18	8	5	0	0
$Co(L^2)_2Cl_2$	15	6	0	0	0
$Co(L^3)_2Cl_2$	5	0	0	0	0
$Co(L^4)_2Cl_2$	5	0	0	0	0
$Co(L^5)_2Cl_2$	0	0	0	0	0

From the results presented in Table III, it is seen that cobalt(II) complex containing L^1 was active against *P. aeruginosa* with a *MIC* value of 250 μg/ml, whilst $Co(L^2)_2Cl_2$ was less toxic with a *MIC* value of 500 μg/ml. However, $Co(L^3)_2Cl_2$ and $Co(L^4)_2Cl_2$ had the same activity with a *MIC* value of 750 μg/ml, but the complex of L^5 had a low activity against the same bacteria.

TABLE IV. Antibacterial activities of the complexes against *B. cereus* at different concentrations (inhibition zone diameter in mm)

Complex	*c* / μg ml^{-1}				
	750	500	250	125	62.5
$Co(L^1)_2Cl_2$	20	16	10	5	0
$Co(L^2)_2Cl_2$	19	14	8	3	0
$Co(L^3)_2Cl_2$	14	9	4	0	0
$Co(L^4)_2Cl_2$	12	7	4	0	0
$Co(L^5)_2Cl_2$	11	5	0	0	0

In the case of *B. cereus* and *S. aureus* (Tables IV and V, respectively), the complexes containing ligands of Series I were more active (*MIC* = 125 μg/ml) than the complexes of second series. $Co(L^3)_2Cl_2$ had the same activity as $Co(L^4)_2Cl_2$ with a high *MIC* value of 250 μg/ml against the same bacteria, whilst the complex containing L^5 expressed a *MIC* value of 500 μg/ml.

TABLE V. Antibacterial activities of the complexes against *S. aureus* at different concentrations (inhibition zone diameter in mm)

Complex	c / μg ml^{-1}				
	750	500	250	125	62.5
$Co(L^1)_2Cl_2$	20	15	9	4	0
$Co(L^2)_2Cl_2$	19	13	8	3	0
$Co(L^3)_2Cl_2$	14	9	5	0	0
$Co(L^4)_2Cl_2$	13	9	4	0	0
$Co(L^5)_2Cl_2$	12	6	0	0	0

On the other hand, the complexes of both series were more active against *S. lutea* (Table VI). The complex of L^3 with a *MIC* value of 125 μg/ml had the same activity as $Co(L^4)_2Cl_2$ but the complexes of Series I were more active and a *MIC* value of 62.5 μg/ml was obtained. $Co(L^5)_2Cl_2$ had the lowest activity against this Gram-positive bacterium (*MIC* = 250 μg/ml).

TABLE VI. Antibacterial activities of the complexes against *S. lutea* at different concentrations (inhibition zone diameter in mm)

Complex	c / μg ml^{-1}				
	750	500	250	125	62.5
$Co(L^1)_2Cl_2$	25	20	16	8	5
$Co(L^2)_2Cl_2$	21	17	14	7	3
$Co(L^3)_2Cl_2$	14	10	7	3	0
$Co(L^4)_2Cl_2$	13	9	5	3	0
$Co(L^5)_2Cl_2$	11	7	3	0	0

Comparing the activities of the tested complexes, it was found that the 1-substituted-2-aminobenzimidazole derivatives (L^1, L^2) formed cobalt(II) complexes which were more active than the complexes of the 1-substituted-2-amino-5,6-dimethylbenzimidazoles (L^3, L^4, L^5). It can be concluded that the basic antibacterial activity of the benzimidazoles was produced by the presence of an amino group at position 2 of the benzimidazole ring. Simultaneously, methyl groups at the 5 or 6 positions decreased the general antibacterial activity of the relevant benzimidazoles. Also, the antibacterial results show that if the benzimidazole nucleus was substituted with a 3-chlorobenzyl group at the N1 atom, the antibacterial activity was increased.

By comparing the antimicrobial activity of the ligands[8] and their complexes, it was found that the complexes were more effective against all bacteria. This is the result of the coordinated cobalt which plays a significant role for the antibacterial activity. The chelation theory explains that a decrease in the polarizability of the metal can change the lipophilicity or hydrophobicity of complexes. These properties are now seen as important parameters related to membrane permeation in biological systems. Many of the processes of drug disposition depend on the ability or inability to cross membranes and hence there is a high correlation with

measures of lipophilicity. Moreover, many of the proteins involved in drug disposition have hydrophobic binding sites, further adding to the importance of lipophilicity.

By consideration of the structures of compounds that exhibit antimicrobial activity, it can be concluded that substituted ligands and the metal moiety may play a role in determining the antibacterial activity. From the results which indicated that the tested compounds were more active against Gram-positive than Gram-negative bacteria, it may be concluded that the inhibitory activity of the studied compounds is related to the cell wall structure of the bacteria. This is possible because the cell wall is essential to the survival of bacteria and some antibiotics are able to kill bacteria by inhibiting a step in the synthesis of peptidoglycan. Gram-positive bacteria possess a thick cell wall containing many layers of peptidoglycan and teichoic acids, but in contrast, Gram-negative bacteria have a relatively thin cell wall consisting of a few layers of peptidoglycan surrounded by a second lipid membrane containing lipopolysaccharides and lipoproteins. These differences in cell wall structure can produce differences in antibacterial susceptibility and some antibiotics can kill only Gram-positive bacteria and is ineffective against Gram-negative pathogens.[30]

CONCLUSIONS

The antibacterial activity of cobalt(II) complexes with two series of 1-benzylbenzimidazole derivatives was tested against very persistent microorganisms: *Pseudomonas aeruginosa*, *Bacillus cereus*, *Staphylococcus aureus* and *Sarcina lutea*. All the complexes displayed *in vitro* inhibitory activity, but the 1-substituted-2-aminobenzimidazole derivatives formed cobalt(II) complexes which were more active than the complexes of the 1-substituted-2-amino-5,6-dimethylbenzimidazoles. The basic antibacterial activity of the benzimidazoles was produced by the presence of an amino group at position 2 of the benzimidazole ring. Methyl groups at the 5 or 6 position decreased the general antibacterial activity of the relevant benzimidazole. Also, the results indicated that the tested complexes were more active against Gram-positive than Gram-negative bacteria. It may be concluded that the antibacterial activity of the compounds is related to the cell wall structure of the bacteria. This is possible because the cell wall is essential to the survival of many bacteria and some antibiotics are able to kill bacteria by inhibiting a step in the synthesis of peptidoglycan.

Acknowledgement. These results are the part of the project No. 142028, supported by the Ministry of Science of the Republic of Serbia.

И З В О Д

АНТИБАКТЕРИЈСКА АКТИВНОСТ КОБАЛТ(II)-КОМПЛЕКСА СА НЕКИМ ДЕРИВАТИМА БЕНЗИМИДАЗОЛА

С. О. ПОДУНАВАЦ-КУЗМАНОВИЋ[1], В. М. ЛЕОВАЦ[2] и Д. Д. ЦВЕТКОВИЋ[1]

[1]Технолошки факултет, Булевар Цара Лазара 1, 21000 Нови Сад и [2]Департман за хемију, ПМФ, Трг Доситеја Обрадовића 3, 21000 Нови Сад

Испитана је *in vitro* антибактеријска активност кобалт(II) комплекса са две серије бензимидазола према три грам-позитивне бактерије (*Bacillus cereus*, *Staphylococcus aureus* и *Sarcina lutea*) и једној грам-негативној бактерији (*Pseudomonas aeruginosa)*. За све комплексе одређена је минимална инхибиторна концентрација. Већина испитиваних комплекса показала је *in vitro* инхибиторну активност према веома отпорним бактеријама. Утврђено је да испитивани комплекси показују већу активност према грам-позитивним него према грам-негативној бактерији, што указује на то да антибактеријска активност једињења зависи од грађе ћелијског зида. Поређењем инхибиторне активности тестираних комплекса дошло се до закључка да су комплекси деривата 1-супституисаних-2-аминобензимидазола активнији од деривата 1-супституисаних-2-амино-5,6-диметилбензимидазола. Продискутован је утицај хемијске структуре на антибактеријску активност.

(Примљено 21. марта, ревидирано 26. маја 2008)

REFERENCES

1. Z. Kazimiercyuk, J. A. Upcroft, P. Upcroft, A. Gorska, B. Starosciak, A. Laudy, *Acta Biochim. Polon*. **49** (2002) 185
2. H. Goker, C. Kus, D. W. Boykin, S. Yildiz, N. Altanlar, *Bioorg. Med. Chem*. **17** (2007) 2233
3. O. G. Ozden, T. Erdogan, H. Goker, S. Yildiz, *Bioorg. Med. Chem*. **13** (2005) 1587
4. S. O. Podunavac-Kuzmanović, D. M. Cvetković, *Centr. Eur. J. Occupat. Environ. Med.* **12** (2006) 55
5. S. O. Podunavac-Kuzmanović, S. L. Markov, *Centr. Eur. J. Occupat. Environ. Med.* **12** (2006) 61
6. N. U. Perišić-Janjić, S. O. Podunavac-Kuzmanović, J. S. Balaž, Đ. Vlaović, *J. Planar Chromatogr*. **13** (2000) 123
7. S. O. Podunavac-Kuzmanović, V. M. Leovac, N. U. Perišić-Janjić, J. Rogan, J. Balaž, *J. Serb. Chem. Soc.* **64** (1999) 381
8. S. O. Podunavac-Kuzmanović, D. Cvetković, *J. Serb. Chem. Soc.* **75** (2007) 459
9. S. O. Podunavac-Kuzmanović, S. L. Markov, D. J. Barna, *J. Theor. Comput. Chem.* **6** (2007) 687
10. H. Kucukbay, R. Durmaz, E. Orhan, S. Gunal, *Farmaco* **58** (2003) 431
11. V. K. Pandey, M. Upadhay, V. Dev Gupta, M. Tandon, *Acta Pharm.* **55** (2005) 47
12. L. Garuti, M. Roberti, C. Cermelli, *Bioorg. Med. Chem. Lett.* **9** (1999) 2525
13. V. K. Pandey, M. N. Joshi, M. Tandon, S. K. Bajpai, *Acta Pharm.* **50** (2000) 293
14. V. K. Pandey, Z. Tusi, S. Tusi, M. N. Joshi, S. K. Bajpai, *Indian J. Heterocycl. Chem.* **111** (2002) 309
15. L. Gata, F. Perna, N. Figura, C. Ricci, J. Holton, L. D′Anna, M. Miglioli, D. Vaira, *J. Antimicrob. Chemother.* **51** (2003) 439

16. P. T. M. Nguyen, J. D. Baldeck, J. R. Olsson, R. E. Marquis, *Oral Microbiol. Immunol.* **20** (2005) 93
17. C. Kus, G. Ayhan-Kilcigil, B. Can-Eke, M. Iscan, *Arch. Pharm. Res.* **27** (2004) 156
18. G. Ayhan-Kilcigil, C. Kus, T. Coban, B. Can-Eke, M. Iscan, *J. Enzyme Inhib. Med. Chem.* **19** (2004) 129
19. G. Ayhan-Kilcigil, N. Altanlar, *Turk. J. Chem.* **30** (2006) 223
20. B. G. Mohamed, M. A. Hussein, A. M. Abdel-Alim, M. Hashem, *Arch. Pharm. Res.* **29** (2006) 26
21. S. A. El-Hawash, E. A. Badawey, T. Kappe, *Pharmazie* **54** (1999) 341
22. K. J. Soderlind, B. Gorodetsky, A. Singh, N. Bachur, G. Miller, J. Lown, *Anti-Cancer Drug Des*. **14** (1999) 19
23. H. Nakano, T. Inoue, N. Kawasaki, H. Miyataka, H. Matsumoto, T. Taguchi, N. Inagaki, H. Nagai, T. Satoh, *Chem. Pharm. Bull.* **47** (1999) 1573
24. S. Demirayak, U. Abu-Mohsen, A. Cagri Karaburun, *Eur. J. Med. Chem.* **37** (2002) 255
25. S. M. Rida, S. A. El-Hawash, H. T. Fahmy, A. A. Hazzaa, M. M. El-Meligy, *Arch. Pharm. Res*. **29** (2006) 826
26. F. Gumus, O. Algul, G. Eren, H. Eroglu, N. Diril, S. Gur, A. Ozkul, *Eur. J. Med. Chem*. **38** (2003) 303
27. Đ. Vlaović, J. Čanadanović-Brunet, J. Balaž, I. Juranić, D. Đoković, K. Mackenzie, *Biosci., Biotechnol., Biochem.* **56** (1992) 199
28. National Committee for Clinical Laboratory Standards, NCCLS Approval Standard Document M2-A7, Vilanova, PA, 2000
29. National Committee for Clinical Laboratory Standards, NCCLS Approval Standard Document M7-A5, Vilanova, PA, 2000
30. A. L. Koch, *Clin. Microbiol. Rev.* **16** (2003) 673.

www.shd.org.rs

Journal of the Serbian Chemical Society

JSCS@tmf.bg.ac.yu • www.shd.org.rs/JSCS

J. Serb. Chem. Soc. 73 (12) 1161–1167 (2008)
JSCS–3795

UDC 54+582.33:547.261:547.56
Original scientific paper

HPLC–DAD of phenolics in bryophytes *Lunularia cruciata*, *Brachytheciastrum velutinum* and *Kindbergia praelonga*

NEBOJŠA JOCKOVIĆ[1], PAULA B. ANDRADE[2], PATRÍCIA VALENTÃO[2] and MARKO SABOVLJEVIĆ[3]*

[1]*Institute of Pharmaceutical Biology, Martin-Luther-University Halle-Wittenberg, Hoher Weg 8, 06120 Halle/Saale, Germany,* [2]*Requimte, Institute of Pharmacognosy, Faculty of Pharmacy, University of Oporto, Rua Aníbal Cunha, 4050-047, Porto, Portugal and* [3]*Institute of Botany and Garden, Faculty of Biology, University of Belgrade, Takovska 43, 11000 Belgrade, Serbia*

(Received 27 March, revised 30 May 2008)

Abstract: The chemistry of bryophytes is not well known. The available data indicate interesting chemical constitutions of some bryophyte species, *i.e.*, active and new compounds are to be found within bryophytes, especially liverworts. In this study, one liverwort and two moss species were studied: *Lunularia cruciata* (L.) Dumort, *Brachytheciastrum velutinum* (Hedw) Ignatov & Huttunen and *Kindbergia praelonga* (Hedw) Ochyra. The phenolic compositions of these bryophyte species have not hitherto been reported. Their methanolic extracts were analyzed by reversed-phase HPLC, coupled to a diode-array detector (DAD). Luteolin-7-*O*-glucoside and quercetin were found in the *L. cruciata* extract. The extract obtained from *B. velutinum* contained four phenolic acids (4-*O*-caffeoylquinic, 5-*O*-caffeoylquinic, caffeic and ellagic acids) and three flavonoids (apigenin-7-*O*-glucoside, luteolin and apigenin). The *K. praelonga* extract was characterized by the presence of several phenolic acids and their derivatives (4-*O*-caffeoylquinic, 5-*O*-caffeoylquinic, caffeic, *p*-coumaric, ferulic and ellagic acids, and caffeic and *p*-coumaric acid derivatives) and three flavonoids (apigenin-7-*O*-glucoside, luteolin, apigenin and an unidentified flavanone).

Keywords: bryophytes; phenolics; *Lunularia cruciata*; *Brachytheciastrum velutinum*; *Kindbergia praelonga*.

INTRODUCTION

Bryophytes (mosses, liverworts and hornworts) with approximately 15,000–25,000 species[1] are, after flowering plants, worldwide the most diverse plant group. They are to be found in all ecosystems, from desert to alpine, except marine, and the bryophyte biomass productivities can vary in each ecosystem, from

* Corresponding author. E-mail: marko@bfbot.bg.ac.rs
doi: 10.2298/JSC0812161J

negligible to the most significant producers. However, the ecological role of bryophytes in any ecosystems is significant.

The chemistry of bryophytes is poorly known and the results on are very scattered.[2–4] The reason for this is the difficulty in identification and small amount of the same species available for analyses, usually by sophisticated methods. Liverworts are very interesting for chemical analysis due to their oil bodies containing many scientifically new compounds.

However, worldwide bryophytes are known to be used in ethno-botany and are applied to cure diseases, threat to plants and animals, or in the household.[5–7] Therefore, bryophytes are indicated as a source of chemically new and unknown compounds.[3,4,8–10] Studies of the chemical constituents of bryophytes were recently performed but are still inadequate and neglected.[2,11–18] These data help in the systematics of barely morphologically classified bryophytes.[19] Also, some scattered data on the biological activities of bryophyte extracts and/or chemical constituents are available for not very many bryophyte taxa.[20–23]

Generally, based on the species studied to date, bryophytes are known to possess extremely high amounts of terpenoids, phenolics (flavonoids and bibenzyl derivatives), glycosides, fatty acids and also some rare aromatic compounds. Bryophytes are considered as a "remarkable reservoir" of new, natural products or secondary compounds, many of which have shown interesting biological activity. These activities of bryophytes include antimicrobial, antifungal, cytotoxic, antitumor, vasopressin (VP) antagonist, cardiotonic, allergy causing, irritancy and tumour effecting, insect anti-feedant, insecticidal, molluscicidal, pesticidal, plant growth regulatory, superoxide anion radical release inhibition and 5-lipoxygenase, calmodulin, hyaluronidase and cyclooxygenase inhibition features. Some latest results also predict a beneficial influence of bryophytes in AIDS therapy (some bibenzyls of liverworts).[24–36]

The liverwort *Lunularia cruciata*, a Mediterranean Atlantic species, expresses antimicrobial and, to a less extent, antifungal activities.[37–39] The plant--growth-regulator lunularic acid was isolated for the first time from this species.[40] The chemical constituents of *L. cruciata* are unknown.[4,41]

The palearctic mosses *Brachytheciastrum velutinum* and *Kindbergia praelonga* have hitherto not been chemically screened; nor are their bioactive effects known.[4]

EXPERIMENTAL

Samples

Fresh material was collected in July 2003 in the Oporto City Park (Portugal). A voucher of each Bryophyte sample is deposited in the Bryophyte Collection of Belgrade University (BEOU).

The material was cleaned and dried to constant weight at room temperature.

Extraction of phenolics

5 g dry mass of each bryophyte sample was used for the extraction of the phenolics. The material was previously ground in an electric mill to a rough powder. The extraction consisted of two consecutive steps employing 175 and 125 mL methanol, respectively, on a magnetic stirrer for 10 min. These two extracts were combined and the solvent removed under reduced pressure at 30 °C To this residue, 20 mL of 2.0 M HCl were added and the obtained solution was passed through a C18 Bond Elut cartridge, preconditioned with methanol and 2.0 M HCl. The retained phenolics were eluted with methanol. This solution was taken to dryness under reduced pressure (30 °C), dissolved in methanol and 20 μL were analyzed by HPLC–DAD.

HPLC–DAD analysis of the phenolics

The extracts were analyzed on an analytical HPLC instrument (Gilson), using a Spherisorb ODS2 column (25.0 cm×0.46 cm; 5 μm particle size Waters, Milford, MA, USA) with a C18 ODS guard column. The mobile phase consisted of solvent A (water–formic acid (19:1)) and solvent B (methanol) (Table I).

The flow rate was 0.9 mL/min and the injection volume 20 μL. Detection was performed using a Gilson diode array detector. The phenolic compounds in each sample were identified by comparing their retention times and UV–Vis spectra in the 200–600 nm range with individual standards. The chromatograms were registered at 280, 320 and 350 nm.

TABLE I. Gradient flow

Time, min	Solvent A content, %	Solvent B content, %
0.00	95	5
3.00	85	15
13.00	75	25
25.00	70	30
35.00	65	35
39.00	60	40
42.00	55	45
44.00	50	50
47.00	45	55
50.00	30	70
56.00	25	75
60.00	0	100
62.00	5	95

RESULTS AND DISCUSSION

The chromatogram of the methanol extract of *Lunularia cruciata* is presented in Fig. 1. Based on a comparison of the retention time (R_t) and UV–Vis spectra with standard substances, the presence of the flavonoid heteroside luteolin-7-*O*-glucoside and the flavonoid aglycone quercetin was confirmed. The presence of these two compounds is for the first time reported in *L. cruciata.*

The chromatogram of the methanol extract of *Brachytheciastrum velutinum* is presented in Fig. 2. The following substances were evidenced as constituents of this species: phenolic acids, *i.e.*, 4-*O*-caffeoylquinic, 5-*O*-caffeoylquinic, caffeic and ellagic acid, flavonoids, *i.e.*, heteroside apigenin-7-*O*-glucoside, and flavonoid aglycones, *i.e.*, luteolin and apigenin.

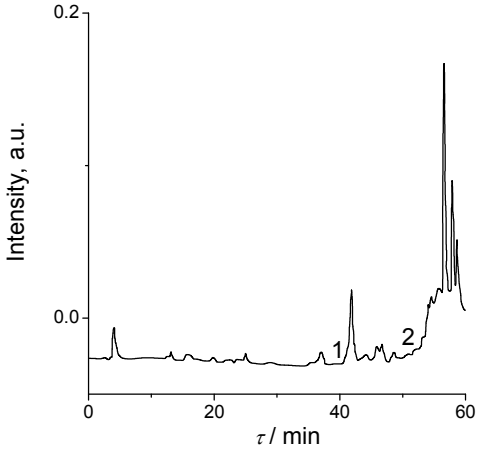

Fig. 1. Chromatograms of the methanol extract of liverwort *L. cruciata*: luteolin-7-*O*--glucoside (1) and quercetin (2).

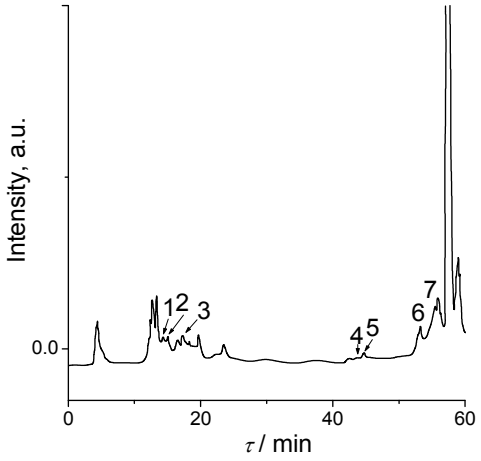

Fig. 2. Chromatogram of the moss methanol extract of *B. velutinum*: 4-*O*-caffeoylquinic acid (1), 5-*O*-caffeoylquinic acid (2), caffeic acid (3) and ellagic acid (5), apigenin-7-*O*-glucoside (4), luteolin (6) and apigenine (7).

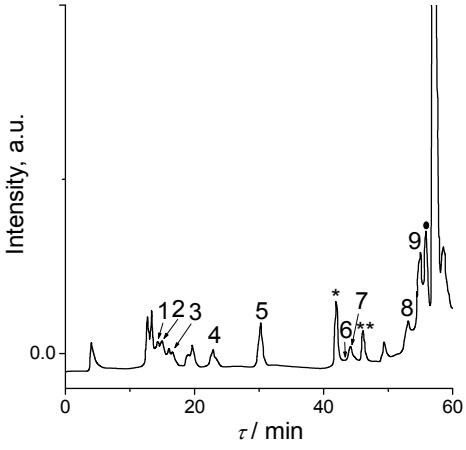

Fig. 3. Chromatogram of the methanol extract of the moss *K. praelonga*: 4-*O*-caffeoylquinic acid (1), 5-*O*-caffeoylquinic acid (2), caffeic acid (3), *p*-coumaric acid (4), ferulic acid (5), ellagic acid (7), caffeic acid derivative (*), *p*-coumaric acid derivative (**), apigenin-7-*O*--glucoside (6), luteolin (8), apigenin (9) and unidentified flavanone (●).

In the methanol extract of the moss *Kindbergia praelonga*, 4-*O*-caffeoylquinic, 5-*O*-caffeoylquinic, caffeic, *p*-coumaric, ferulic and ellagic acid, caffeic acid derivative, *p*-coumaric acid derivative, flavonoid heteroside apigenin-7-*O*-glucoside, aglycones luteolin and apigenin, as well as one unidentified flavanone were evidenced, as shown in Fig. 3.

The chemical contents of *B. velutinum* and *K. praelonga* have not been screened previously.

Luteolin is present in many vascular plants, especially from the family Resedaceae, *Genista tinctoria* (Fabaceae) and *Petroselinum crispum* (Apiaceae).[42] However, the heteroside form of luteolin-7-*O*-glucoside is not common and this compound was not previously known from *L. cruciata*. This form is known from some *Mentha* plants.[43] The yellowish pigment quercetin is widespread in many plants but was not detected previously in *L. cruciata*. Quercetin was found to be the most biologically active of the flavonoids and many medicinal plants owe much of their activity to their high quercetin content.[44]

Artichoke (*Cynara scolymus*) is known to have rich content of 4-*O*-caffeoylquinic and 5-*O*-caffeoylquinic acids.[45] Previously they were not evidenced from mosses among the other phenolic acids.[4]

Caffeic acid is already known from some mosses.[46] Apigenine is a pale yellow pigment present in many plants from the families Apiaceae and Asteraceae with an antitumor effect. Apigenin and its derivates are known to be present in mosses and to have biological effects.[47] In mosses, *p*-coumaric and ferulic acids are known to be present in moss spores. They are precursors of lignin, which is not common in moss gametophytes, but both *p*-coumaric and ferulic are present in moss gametophytes where lignin was not detected.[48]

Although phenolic compounds are known to be present in bryophytes, this knowledge is mainly based on liverworts not mosses and their presence; diversity and distribution within different species remain for further studies.[49–51]

Thus, the paper presents one first approach to the identification of phenolics in the bryophytes *L. cruciata*, *B. velutinum* and *K. praelonga*, until now unknown.

Acknowledgements. M. Sabovljević thanks the Serbian Ministry of Science for support (Grant No. 143015).

ИЗВОД

HPLC–DAD ФЕНОЛА КОД БРИОФИТА *Lunularia cruciata*, *Brachytheciastrum velutinum* И *Kindbergia praelonga*

НЕБОЈША ЈОЦКОВИЋ[1], PAULA B. ANDRADE[2], PATRÍCIA VALENTÃO[2] и МАРКО САБОВЉЕВИЋ[3]

[1]Institute of Pharmaceutical Biology, Martin-Luther-University Halle-Wittenberg, Hoher Weg 8, 06120 Halle/Saale, Germany, [2]Requimte, Institute of Pharmacognosy, Faculty of Pharmacy, University of Oporto, Rua Aníbal Cunha, 4050-047, Porto, Portugal и [3]Институт за ботанику и ботаничка башта,Биолошки факултет, Универзитет у Београду, Таковска 43, 11000 Београд

Хемијски састав бриофита је слабо познат. Досадашњи подаци указују на интересантне хемијске састојке бриофита, биолошки активна и нова једињења, нарочито код јетрењача. У овом раду изучаване су једна јетрењача *Lunularia cruciata* (L.) Dumort и две маховине *Brachytheciastrum velutinum* (Hedw) Ignatov & Huttunen и *Kindbergia praelonga* (Hedw) Ochyra. Фенолни састав ових врста бриофита од раније није познат. Њихови метанолни екстракти су анализирани путем HPLC типа реверсне фазе, повезаног са DAD детектором. U екстракту *L. cruciata* пронађени су лутеолин-7-*O*-глукозид и кверцетин. Екстракт добијен од *B. velutinum* показао је присуство четири фенолне киселине (4-*O*-кафеоилхина, 5-*O*-кафеоилхина, кофеинска и елагинска киселина) и три флавоноида (флавоноидни агликони лутеолин и апиге-

нин, и његов хетерозид апигенин-7-*O*-глукозид). Екстракт од *K. praelonga* је окарактерисан присуством неколико фенолних киселина и њихових деривата (4-*O*-кафеоилхина, 5-*O*-кафеоилхина, кофеинска, *н*-кумаринска, ферула и елагинска киселина, деривати кофеинске и *н*-кумаринске киселине) и следећих флавоноида: апигенина, апигенин-7-*O*-глукозида, лутеолина и једног неидентификованог флаванона.

(Примљено 27. марта, ревидирано 30. маја 2008)

REFERENCES

1. J. M. Glime, *Bryophyte ecology*, Michigan Technological University and the International Association of Bryologists, Houghton, MI, 2007, p. 714
2. Y. Asakawa, in *Chemical Constituents of the Bryophytes*, W. Herz, G. W. Kirby, R. W. Moore, W. Steglich, Ch. Tamm, Eds., Springer Verlag, Wien, 1995, p. 266
3. H. D. Zinsmeister, H. Becker, T. Eicher, *Angew. Chem.* **30** (2003) 130
4. A. Sabovljević, M. Sabovljević, in *Phytopharmacology and Therapeutic Values IV*, J. N. Govil, V. K Singh, Eds., Studium Press LLC, Houston, TX, 2008, p. 9
5. H. Ando, *Proc. Bryol. Soc. Japan* **3** (1983) 124
6. H. Ando, H. Matsuo, *Appl. Bryol. Adv. Bryol.* **2** (1984) 133
7. K. Kumar, K. Singh, A. K. Asthana, V. Nath, *Pharm. Biol.* **38** (2001) 353
8. Y. Asakawa, *Pure Appl. Chem*. **66** (1994) 2193
9. Y. Asakawa, *Phytochemistry* **56** (2001) 297
10. M. Sabovljević, A. Bijelović, D. Grubišić, *Lek. Sirov.* **21** (2001) 17 (in Serbian)
11. M. Toyota, K. Masuda, Y. Asakawa, *Phytochem.* **48** (1998) 297
12. H. Edelmann, C. Neinhuis, M. C. Jarvis, B. Evans, E. Fischer, W. Barthlott, *Planta* **206** (1998) 315
13. A. Speicher, K. Hollemeyer, E. Heinzle, *Rapid Commun. Mass Spectrom*. **15** (2000) 124
14. A. Speicher, K. Hollemeyer, E. Heinzle, *Phytochemistry* **57** (2001) 303
15. J. W. van Klink, J. Zapp, H. Becker, *Z. Naturforsch*. **57** (2002) 413
16. Z. A. Popper, S. C. Fry, *Ann. Bot.* **91** (2003) 1
17. U. M. Hertewich, J. Zapp, H. Becker, *Phytochemistry* **63** (2003) 227
18. N. Jocković, M. Pavlović, M. Sabovljević, N. Kovačević, *Natura Montenegrina* **6** (2007) 123
19. Y. Asakawa, *Phytochemistry* **65** (2004) 623
20. A. Basile, S. Sorbo, S. Giordano, A. Lavitola, R. Castaldo-Cobianchi, *Int. J. Antimicrob. Agents* **10** (1998) 169
21. A. Basile, S. Giordano, S. Sorbo, M. L. Vuotto, M. T. L. Ielpo, R. Castaldo Cobianchi, *Pharm. Biol.* **36** (1998) 25
22. A. Dulger, Ö. Tonguç-Yayintas, A. Gonuz, *Fitoterapia* **76** (2005) 730
23. A. Sabovljević, M. Soković, M. Sabovljević, D. Grubišić, *Fitoterapia* **77** (2006) 144
24. Y. Asakawa, *Prog. Chem. Org. Nat. Prod*. **42** (1982) 1
25. Y. Asakawa, M. Toyota, T. Takemoto, *Phytochemistry* **19** (1980) 1799
26. Y. Asakawa, R. Matsuda, M. Toyota, T. Takemoto, J. D. Connolly, W. P. Phillips, *Phytochemistry* **22** (1983) 961
27. Y. Asakawa, L. J. Harrison, M. Toyota, *Phytochemistry* **24** (1985) 261
28. R. D. Banerjee, S. P. Sen, *Bryologist* **82** (1979) 141
29. J. L. Hartwell, *Lloydia* **34** (1971) 386
30. T. Hashimoto, H. Suzuki, M. Tori, Y. Asakawa, *Phytochemistry* **30** (1991) 1523
31. T. Kanaski, K. Ohta, *Agric. Biol. Chem.* **40** (1976) 1239

32. J. A. McCleary, P. S. Sypherd, D. L. Walkington, *Science* **131** (1960) 108
33. Y. Ohta, N. H. Andersen, C. B. Liu, *Tetrahedron* **33** (1977) 617
34. L. Van Hoof, D. A. Vanden Berghe, E. Petit, A. J. Vlietinck, *Fitoterapia* **52** (1981) 223
35. J.-P. Frahm, K. Kirchhoff, *Cryptog. Bryol.* **23** (2002) 271
36. T. Mekuria, U. Steiner, H. Hindorf, J.-P. Frahm, H.-W. Dehne *J. Appl. Bot. Food Qual.* **79** (2005) 89
37. A. Basile, S. Giordano, S. Sorbo, R. Castaldo Cobianchi, M. L. Vuotto, M. T. L. Ielpo, *Pharm. Biol.* **36** (1998) 25
38. A. Basile, S. Giordano, S. Sorbo, M. L. Vuotto, M. T. L. Ielpo, R. C. Cobianchi, *Int. J. Pharm.* **36** (1998) 1
39. M. T. Ielpo, P. De Sole, A. Basile, V. Moscatiello, E. Laghi., R. C. Cobianchi, M. L. Vuotto, *Immunopharmacol. Immunotoxicol.* **20** (1998) 555
40. R. J. Pryce, *Planta* **97** (1971) 354
41. A. Basile, V. Spagnuolo, S. Giordano, R. C. Cobianchi, *Giorn. Bot. Ital.* **112** (1993) 549
42. J. Mann, *Secondary Metabolism*, 2nd Ed., Oxford University Press, Oxford, 1992, p. 280
43. T. Cserháti, *Monograph. J. Chrom. Lib.* **71** (2006) 587
44. H. Su-Lan, H. Yu-Chi, W. Yao-Horng, T. Chih-Wan, S. Sheng-Fang, L. C. Pei-Dawn, *Life Sci.* **72** (2002) 227
45. K. Schütz, D. Kammerer, R. Carle, A. Schieber, *J. Agric. Food Chem.* **52** (2004) 4090
46. V. Chobot, L. Kubicová, S. Nabbout, L. Jahodář, J. Vytlačilová, *Fitoterapia* **77** (2006) 598
47. A. Basile, S. Giordano, J. A. López-Sáez, R. Castaldo-Cobianchi, *Phytochemistry* **52** (1999) 1479
48. S. M. Siegel, *Am. J. Bot.* **56** (1969) 175
49. Y. Asakawa, *Current Pharm. Des.* **14** (2008) 3067
50. J.-P. Frahm, *Biologie der Moose*, Gustav Fischer, Verlag, 2001, p. 357
51. H. D. Zinsmeister, R. Mues, *Bryophytes, their chemistry and chemical taxonomy*, Clarendon Press, Oxford, 1990, p. 470.

www.shd.org.rs

Journal of the Serbian Chemical Society

JSCS@tmf.bg.ac.yu • www.shd.org.rs/JSCS

J. Serb. Chem. Soc. 73 (12) 1169–1180 (2008)
JSCS–3796

UDC 547.466.64+546.3+54–145.2:66.011
Original scientific paper

Computer augumented modelling studies of Pb(II), Cd(II), Hg(II), Co(II), Ni(II), Cu(II) and Zn(II) complexes of L-glutamic acid in 1,2-propanediol–water mixtures

MAHESWARA RAO VEGI, PADMA LATHA MUDDAPU, SIVA RAO TIRUKKUVALLURI and NAGESWARA RAO GOLLAPALLI*

School of Chemistry, Andhra University, Visakhapatnam-530003, India

(Received 25 April 2007, revised 16 June 2008)

Abstract: Chemical speciation of Pb(II), Cd(II), Hg(II), Co(II), Ni(II), Cu(II) and Zn(II) complexes of L-glutamic acid was studied at 303 K in 0–60 vol. % 1,2-propanediol–water mixtures, whereby the ionic strength was maintained at 0.16 mol dm^{-3}. The active forms of the ligand are LH_3^+, LH_2 and LH^-. The predominant detected species were ML, ML_2, MLH, ML_2H and ML_2H_2. The trend of the variation in the stability constants with changing dielectric constant of the medium is explained based on the cation stabilizing nature of the co-solvents, specific solvent–water interactions, charge dispersion and specific interactions of the co-solvent with the solute. The effect of systematic errors in the concentrations of the substances on the stability constants is in the order alkali > > acid > ligand > metal. The bioavailability and transportation of metals are explained based on distribution diagrams and stability constants.

Keywords: chemical speciation; L-glutamic acid; 1,2-propanediol; bioavailability; metals.

INTRODUCTION

Investigations of acido–basic equilibria of amino acids, their interaction with metal ions in media varying ionic strength, temperature and dielectric constant throw light on the mechanism of enzyme-catalyzed reactions. Although it is known that the polarity of the active site cavities in proteins is lower than that of the bulk, a direct measurement of the dielectric constant is not possible. Comparing the formation constants of acido–basic equilibria and/or metal complex equilibria with those at biological centres offers a way to estimate the effective dielectric constant or equivalent solution dielectric constant for the active site cavity.[1] This brought a renaissance in the study of complex equilibria in aqua–organic mixtures apart from its established utility in understanding solute–solvent interactions, increasing sensitivity of reactions of analytical and industrial importance and solubilising ligands or their metal complexes.

* Corresponding author. E-mail: gollapallinr@yahoo.com
doi: 10.2298/JSC0812169V

Chemical speciation of metals is important for an understanding of their distribution, mobility, bioavailability, toxicity and for setting environmental quality standards.[2] Bioavailability of a particular metal depends on its complex chemical reactions of dissolution, binding and complexation with the constituents of the environmental aquatic phase.[3] The activities of bacteria increase the concentration of dissolved organic carbon and decreases the pH value of water. This causes an increase in the complexation and mobility of a metal.[4] Complexation signifycantly decreases bioavailability.[5]

Due to the multiple biological roles of glutamic acid,[6–9] speciation studies of L-glutamic acid (Glu) with Co(II), Cu(II) and Zn(II) in DMF–water mixtures and Pb(II), Cd(II), Hg(II), Co(II), Ni(II), Cu(II) and Zn(II) in urea–water mixtures were reported earlier.[10,11] Ionic strength dependence of the formation constants of Glu with uranium(VI) and beryllium(II) and pH-metric and spectrophotometric studies of oxovanadium(IV) with Glu, aspartic acid and imidazoles were also reported.[12–14] Herein, the results of chemical speciation of Glu complexes of Pb(II), Cd(II), Hg(II), Co(II), Ni(II), Cu(II) and Zn(II) in 1,2-propanediol–water mixtures are reported.

EXPERIMENTAL

Chemicals

1,2-Propanediol (propylene glycol, PG), obtained from Merck, Mumbai, was used as received. Aqueous solutions of L-glutamic acid, Pb(II), Cd(II) and Hg(II) nitrates, Co(II), Ni(II), Cu(II) and Zn(II) chlorides, nitric acid, sodium hydroxide and sodium nitrate were prepared by dissolving GR Grade (Merck, Germany) samples in triple distilled water. To increase the solubility of Glu and to suppress the hydrolysis of metal salts, the nitric acid concentration was maintained at 0.050 mol dm^{-3}. All the solutions were standardized by usual standard methods. To assess the errors that might have entered into the determinations of the concentrations, the data were subjected to analysis of variance of one way classification (Anova).[15] The strength of the alkali was determined using the Gran plot method.[16]

Apparatus

The titrimetric data were obtained with a calibrated Elico (Model L1-120) pH meter (readability 0.01), which can monitor changes in the H^+ concentration. The pH meter was calibrated with a 0.050 mol dm^{-3} potassium hydrogen phthalate solution in the acidic region and a 0.010 mol dm^{-3} borax solution in the basic region. The glass electrode was equilibrated in a well-stirred PG–water mixture containing an inert electrolyte. The effects of variations in the asymmetry potential, liquid junction potential, activity coefficient, sodium ion error and dissolved carbon dioxide on the response of the glass electrode were accounted for in the form of correction factors.[17,18]

Procedure

The titrations were performed at 303±0.1 K in media containing 0–60 vol. % PG, whereby the ionic strength was maintained constant at 0.16 mol dm^{-3} with sodium nitrate. The electrode was kept, usually for 2–3 days, in the required solvent system for equilibration. To verify whether the electrode was equilibrated, a strong acid was titrated with an alkali every day until no appreciable differences were observed between the pH values of two titrations at

the corresponding volumes of titrant. Under the above conditions, the electrode was assumed to be equilibrated. A calomel electrode was refilled with PG–water mixture of the equivalent composition to that of the titrand. Free acid titrations were performed before the metal–ligand titrations to calculate the correction factor. In each of the titrations, the titrand consisted of a mineral acid of approximately 1 mmol in a total volume of 50 cm^3. Titrations with different ratios (1:2.5, 1:3.5 and 1:5) of metal–ligand were performed with 0.40 mol dm^{-3} sodium hydroxide. Other experimental details are given elsewhere.[19]

Modelling strategy

The approximate complex stability constants of metal–Glu complexes were calculated with the computer program SCPHD.[20] The best fit chemical model for each investigated system was arrived at using Miniquad75.[21]

RESULTS AND DISCUSSION

The results of the best fit models that contain the type of species and overall formation constants along with some of the important statistical parameters are given in Tables I and II. A very low standard deviation in the log β values indi

TABLE I. Parameters of the best fit chemical models of Pb(II), Cd(II) and Hg(II)–glutamic complexes in PG–water mixtures. Temperature 303 K, ionic strength 0.16 mol dm^{-3}

y(PG) vol. %	log $\beta_{mlh}(SD)$				*NP**	U^{**}_{corr} 10^{-8}	Skewness	χ^2	*R* factor	Kurtosis	pH Range
	ML	MLH	ML_2	ML_2H_2							
					Pb(II)						
00.00	6.58(14)	–	–	–	15	3.817	–0.57	10.64	0.0137	2.79	3.7–4.7
10.00	6.81(11)	–	–	–	13	1.778	–0.81	9.21	0.0090	3.50	3.7–4.6
20.00	6.54(9)	–	–	–	29	0.448	–0.80	34.47	0.0091	3.73	3.8–4.7
30.00	6.78(8)	–	–	–	36	3.332	–0.68	47.26	0.0135	2.85	3.7–4.9
40.00	6.85(8)	–	–	–	34	3.096	–0.71	31.96	0.0129	3.39	3.8–4.9
50.00	6.70(7)	–	–	–	28	1.267	–0.70	22.86	0.0080	3.52	4.0–4.9
60.00	6.74(8)	–	–	–	29	1.358	–0.84	39.99	0.0082	4.23	4.0–5.0
					Cd(II)						
00.00	3.99(12)	–	7.22(10)	22.38(50)	23	0.892	0.26	4.16	0.0090	3.08	5.0–9.3
10.00	4.14(7)	–	7.46(6)	23.21(10)	55	1.015	0.19	27.44	0.0076	5.46	3.0–9.5
20.00	4.10(8)	–	7.05(8)	22.36(71)	21	0.363	–0.11	3.92	0.0061	4.24	6.0–9.5
30.00	4.33(13)	–	7.69(12)	22.96(54)	22	0.732	0.16	16.42	0.0084	7.41	5.6–9.5
40.00	4.46(13)	–	7.83(12)	23.20(43)	22	0.622	0.16	16.91	0.0078	6.15	5.6–9.5
50.00	4.49(9)	–	7.96(9)	22.72(71)	27	0.526	0.35	6.60	0.0074	4.72	5.5–9.8
60.00	4.48(10)	–	7.95(11)	23.39(33)	34	1.756	0.23	20.20	0.0127	5.14	5.0–10
					Hg(II)						
00.00	10.96(4)	13.41(5)	–	–	82	7.997	1.00	85.84	0.0028	6.66	1.7–2.6
10.00	11.60(4)	14.32(4)	–	–	48	0.365	–0.08	9.78	0.0025	4.75	2.1–2.6
20.00	11.52(8)	14.48(5)	–	–	31	0.206	–0.14	16.68	0.0018	5.36	2.1–2.5
30.00	12.13(2)	14.81(4)	–	–	29	0.059	–0.52	11.30	0.0011	6.14	2.1–2.5
40.00	12.68(3)	15.02(11)	–	–	25	0.416	0.11	2.55	0.0024	3.45	2.1–2.5
50.00	12.71(3)	15.48(4)	–	–	19	0.070	–0.78	7.14	0.0009	7.02	2.1–2.5
60.00	12.24(7)	15.63(3)	–	–	10	0.014	0.18	0.93	0.0004	3.01	2.3–2.5

*NP = number of experimental points; **$U_{corr} = U/(NP - m)$, where m = number of species

Table II. Parameters of the best fit chemical models of Co(II), Ni(II), Cu(II) and Zn(II)–glutamic acid complexes in PG–water mixtures. Temperature 303 K, ionic strength 0.16/mol dm^{-3}

y(PG) vol. %	Log β_{mlh}(*SD*)					*NP*	U_{corr} / 10^{-8}	Skewness	χ^2	*R*-Factor	Kurtosis	pH-Range
	ML	MLH	ML_2	ML_2H	ML_2H_2							
					Co(II)							
00.00	4.58(4)	–	7.75(4)	–	22.94(34)	23	0.939	0.14	6.94	0.0096	6.79	
10.00	4.69(3)	–	8.12(3)	–	23.16(8)	12	0.124	–0.03	3.11	0.0014	5.14	
20.00	4.65(4)	–	7.96(4)	–	22.92(14)	12	0.055	–0.17	10.67	0.0021	2.77	
30.00	4.87(6)	–	8.43(6)	–	22.92(27)	12	0.137	–0.27	10.22	0.0034	2.03	
40.00	4.73(7)	–	8.30(9)	–	22.24(64)	37	1.069	0.06	30.33	0.0080	3.76	
50.00	5.08(4)	–	8.79(6)	–	23.14(10)	38	0.488	–0.28	38.98	0.0054	3.72	
60.00	4.88(22)	–	8.22(7)	–	23.62(81)	16	2.653	0.14	13.00	0.0148	4.16	
					Ni(II)							
00.00	5.14(7)	–	9.56(50)	16.47(2)	-	22	6.939	2.23	27.30	0.0288	6.90	
10.00	5.78(3)	–	10.07(5)	–	23.36(5)	29	0.257	–0.02	14.79	0.0042	3.43	
20.00	5.66(3)	–	9.91(6)	–	22.98(6)	31	0.227	–0.05	4.12	0.0039	3.11	
30.00	5.85(3)	–	10.14(5)	–	23.32(4)	33	0.225	–0.12	21.81	0.0038	4.57	
40.00	6.36(2)	–	10.91(3)	–	23.83(3)	34	0.135	0.00	4.98	0.0030	2.89	
50.00	6.31(2)	–	10.85(4)	–	23.79(3)	36	0.205	0.01	8.59	0.0035	2.48	
60.00	6.23(2)	–	10.42(5)	–	24.20(3)	39	0.207	0.15	13.94	0.0034	3.58	
					Cu(II)							
00.00	7.99(11)	12.52(2)	14.49(5)	19.50(19)	24.11(7)	38	0.438	–0.08	10.77	0.0055	4.15	
10.00	8.32(11)	12.91(4)	15.29(3)	20.81(5)	24.49(13)	43	0.123	–0.31	12.21	0.0025	4.37	
20.00	8.11(8)	12.62(3)	14.75(3)	20.26(5)	24.32(9)	45	0.110	–1.50	19.73	0.0023	9.34	
30.00	8.42(8)	13.02(2)	15.12(2)	20.69(5)	24.75(9)	45	0.083	–0.37	10.36	0.0020	4.09	
40.00	8.61(9)	13.48(21)	16.44(18)	21.74(18)	26.06(17)	43	4.636	–0.08	75.34	0.0151	1.55	
50.00	8.90(31)	13.84(5)	16.32(5)	21.86(8)	26.14(10)	43	0.312	–0.05	7.62	0.0037	2.24	
60.00	9.12(20)	14.16(3)	15.93(5)	22.21(5)	26.59(9)	47	0.153	–0.69	76.09	0.0026	10.09	
					Zn(II)							
00.00	4.90(5)	–	8.88(5)	–	22.94(5)	45	0.418	0.29	17.24	0.0047	5.61	
10.00	4.90(7)	–	8.89(7)	–	23.13(9)	37	0.692	0.08	11.16	0.0063	3.82	
20.00	4.90(2)	–	8.82(20)	–	22.86(82)	15	1.899	0.20	9.93	0.0125	3.55	
30.00	4.89(18)	–	8.87(17)	–	22.80(96)	21	1.515	0.06	4.94	0.0121	3.59	
40.00	5.20(13)	–	9.35(13)	–	23.20(46)	16	0.707	0.22	6.33	0.0079	3.43	
50.00	5.41(5)	–	9.61(6)	–	23.14(18)	19	0.355	0.10	4.89	0.0053	5.47	
60.00	5.05(18)	–	8.77(19)	–	23.51(74)	11	1.158	–0.06	31.73	0.0098	1.83	

cates the precision of these parameters. The small values of U_{corr} (sum of the squares of the deviations in the concentrations of ligand and hydrogen ions at all experimental points corrected for degrees of freedom) indicate that the experimental data can be represented by the model. Small values of the mean, standard deviation and mean deviation for the systems corroborate that the residuals are around a zero mean with little dispersion. For an ideal normal distribution, the values of the kurtosis and skewness should be three and zero, respectively. The kurtosis values in the present study indicate that the residuals form a leptokurtic pattern and a few form a platykurtic pattern. The values of the skewness given in the Tables are between –1.50 and 2.23. These data evince that the residuals form a part of a normal distribution, hence, the least squares method can be applied to the present data. The sufficiency of the model is further evident from the low crystallographic *R*-value recorded. Thus, these statistical parameters show that the best fit models portray the metal–ligand species in PG–water mixtures. The stability constants of the metal–ligand species are compared with literature reported values in Table III.

TABLE III. Comparison of the results of the present study with the binary stability constants of Glu complexes reported in the literature in aqueous medium

Metal ion	Species	Presented values	Literature reported value	Ref.
Co(II)	ML, ML_2	4.58, 7.75	4.56, 7.86	22
Ni(II)	ML, ML_2	5.14, 9.56	5.62, 9.82	22
	ML, ML_2	5.14, 9.56	5.60, 9.76	23
Cu(II)	ML	7.99	7.87	23
	ML, MLH	7.99, 12.52	8.07, 12.39	24
	ML, MLH	7.99, 12.52	8.39, 12.49	25
	ML, MLH, ML_2, ML_2H, ML_2H_2	7.99, 12.52, 14.49, 19.50, 24.11	8.55, 12.73, 15.22, 20.57, 25.18	26
Zn(II)	ML, ML_2	4.90, 8.88	4.69, 8.55	27

Effect of systematic errors on best fit model

Miniquad75 does not provide for a study of the effect of systematic errors in influential parameters, such as the concentrations of the reactants, on the magnitude of the equilibrium constant. In order to rely upon the best chemical model for critical evaluation and application under varied experimental conditions with different accuracies of data acquisition, an investigation was made by introducing pessimistic errors in the concentrations of alkali, mineral acid, ligand and metal (Table IV). The order of the compounds that influence the magnitudes of the stability constants due to incorporation of errors is alkali > acid > ligand > metal. Some species, such as ML_2 and ML_2H_2, were even rejected when errors were introduced in the concentrations of the components. This shows that any deviation from the experimental concentrations of the components increases the standard deviation in the log β values and results ultimately in the rejection of the species.

This study infers that the experimental concentrations are appropriate and the proposed models are adequate for the experimental data.

TABLE IV. Effect of errors in the influential parameters on the metal–glutamic acid equilibria in a 30 vol. % v/v PG–water mixture

Component	Error, %	Log $\beta(SD)$		
		ML	ML_2	ML_2H_2
		Cd(II)		
Alkali	0	4.33(13)	7.69(12)	22.96(53)
	–5	2.13(60)	Rejected	Rejected
	–2	3.76(30)	6.15(33)	22.48(256)
	+2	4.73(17)	8.78(14)	Rejected
	+5	6.10(69)	10.97(66)	Rejected
Acid	–5	5.74(36)	10.19(37)	Rejected
	–2	4.97(32)	8.82(31)	23.63(64)
	+2	3.84(29)	6.61(26)	22.16(467)
	+5	3.12(24)	Rejected	Rejected
Ligand	–5	4.44(10)	8.28(9)	Rejected
	–2	4.36(12)	7.92(11)	22.64(84)
	+2	4.29(20)	7.43(19)	23.16(61)
	+5	4.22(33)	6.98(33)	23.34(82)
Metal	–5	4.32(15)	7.81(13)	22.95(59)
	–2	4.33(14)	7.74(13)	22.96(56)
	+2	4.33(13)	7.64(12)	22.97(52)
	+5	4.33(12)	7.56(11)	22.97(50)
		Zn(II)		
Alkali	0	4.89(18)	8.88(16)	22.80(96)
	–5	3.13(42)	Rejected	Rejected
	–2	4.41(39)	7.26(43)	22.53(340)
	+2	5.35(12)	9.96(11)	Rejected
	+5	6.31(52)	11.72(43)	Rejected
Acid	–5	6.06(28)	11.09(26)	Rejected
	–2	5.24(9)	9.69(8)	Rejected
	+2	4.46(16)	7.74(21)	Rejected
	+5	3.83(29)	Rejected	Rejected
Ligand	–5	5.07(8)	9.46(7)	Rejected
	–2	4.94(14)	9.10(12)	22.38(154)
	+2	4.85(25)	8.63(24)	23.03(94)
	+5	4.80(38)	8.20(38)	23.27(105)
Metal	–5	4.85(18)	9.00(16)	22.66(115)
	–2	4.88(18)	8.93(16)	22.75(101)
	+2	4.90(18)	8.82(17)	22.85(91)
	+5	4.92(19)	8.74(18)	22.92(86)

Effect of solvent

The presence of PG in aqueous solutions considerably decreases the dielectric constant of the medium and these solutions are expected to mimic physio-

logical conditions where the concept of equivalent solution dielectric constant for protein cavities is applicable. Hence, PG was selected for the biomimetic study. The dielectric constants of PG at different percentages (0–60 vol. %) of water were taken from literature.[28] PG is an amphiprotic and coordinating solvent. It is a structure former and hence it enhances the structure of water in PG–water mixtures. It also removes water from coordination sphere of metal ions, making them more reactive towards ligands. As a result, the stability of the complexes is expected to increase with increasing concentration of PG. On the other hand, PG is a coordinating solvent and competes with ligands for coordination with the metals. This decreases the stability of the complexes. Hence, variation in the stability of complex with solvent is a result of both the opposing behaviours.

The variation of the values of the overall stability constant or change in free energy with content of co-solvent depends upon two factors, *viz*. electrostatic and non-electrostatic. The Born classical treatment accounts well for the electrostatic contribution to the free energy change.[29] According to this treatment, the energy of electrostatic interaction is related to the dielectric constant. Hence, the log β values should vary linearly with the reciprocal of the dielectric constant of the medium. The plots given in Fig. 1 show that the values of log β increase linearly with decreasing value of the dielectric constant. This trend indicates the dominance of the structure forming nature of PG over its complexing ability. The cation stabilizing nature of co-solvents, specific solvent–water interactions, charge dispersion and specific interactions of the co-solvent with the solute (indicated by the changes in the solubility of different species in aqua–organic mixtures) account for the small deviation from a linear relationship. Since the complex formation can be viewed as the competition between pure and solvated forms of the ligand and metal ion, solute–solvent interactions, relative thermodynamic stabilities, kinetic labilities play an important role.[30,31]

Distribution diagrams

Glu has two dissociable carboxyl protons and an amino group that can associate with a proton. The different forms of Glu that exist in the pH regions 2.0–4.0, 2.0–5.0, 4.0–9.0 and 8.0–10.0 are LH_3^+, LH_2, LH^- and L^{2-}, respectively. Hence, the probable species existing in different systems can be predicted from these data. The species formed in the present study for different metals, as given in Tables I and II, are ML for Pb(II); ML and MLH for Hg(II); ML, ML_2 and ML_2H_2 for Cd(II), Co(II), Ni(II) and Zn(II); ML, MLH, ML_2, ML_2H and ML_2H_2 for Cu(II).

Distribution diagrams were drawn for various complex species using the formation constants of the best fit models as shown in Figs. 2 and 3. These diagrams indicate that the percentage of the ML species of Pb(II) increases with increasing PG content. With increasing percentage of solvent, the percentage of protonated species decreases and the unprotonated species increases for Cd(II). For Hg(II), the

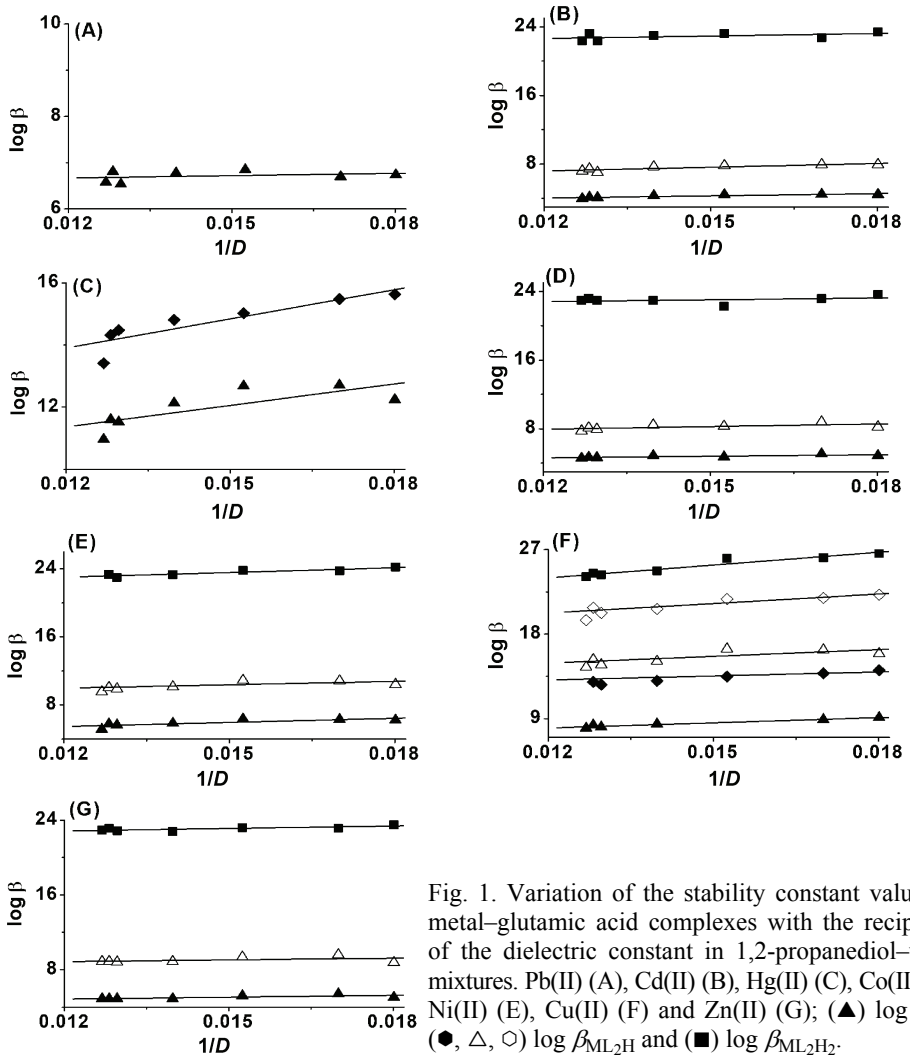

Fig. 1. Variation of the stability constant values of metal–glutamic acid complexes with the reciprocal of the dielectric constant in 1,2-propanediol–water mixtures. Pb(II) (A), Cd(II) (B), Hg(II) (C), Co(II) (D), Ni(II) (E), Cu(II) (F) and Zn(II) (G); (▲) log β_{ML}, (●, △, ○) log β_{ML_2H} and (■) log $\beta_{ML_2H_2}$.

species exist at very low and narrow pH region. For Co(II), the percentages of ML, ML_2 are not affected by the solvent. For Ni(II), the distribution of all the species is almost the same in all proportions of the solvent. The percentages of MLH, ML_2H and ML_2 are greater at high solvent concentrations and that of ML_2H_2 is very low in all compositions of the solvent. The percentage of ML_2H_2 is lower when compared to ML and ML_2. The formation of various binary complex species is shown in the following equilibria:

$$M(II) + LH_3^+ \rightleftharpoons MLH_2^{2+} + H^+ \quad \text{(minor process)} \tag{1}$$

$$MLH_2^{2+} \rightleftharpoons MLH^+ + H^+ \tag{2}$$

$$M(II) + LH_2 \rightleftharpoons MLH^+ + H^+ \quad (3)$$

$$MLH^+ \rightleftharpoons ML + H^+ \quad (4)$$

$$MLH^+ + LH_2 \rightleftharpoons ML_2H_2 + H^+ \quad (5)$$

$$M(II) + 2LH_2 \rightleftharpoons ML_2H_2 + 2H^+ \quad (6)$$

$$ML_2H_2 \rightleftharpoons ML_2H^- + H^+ \quad (7)$$

$$M(II) + LH^- \rightleftharpoons ML + H^+ \quad (8)$$

$$ML_2H^- \rightleftharpoons ML_2^{2-} + H^+ \quad (9)$$

$$M(II) + 2LH^- \rightleftharpoons ML_2^{2-} + 2H^+ \quad (10)$$

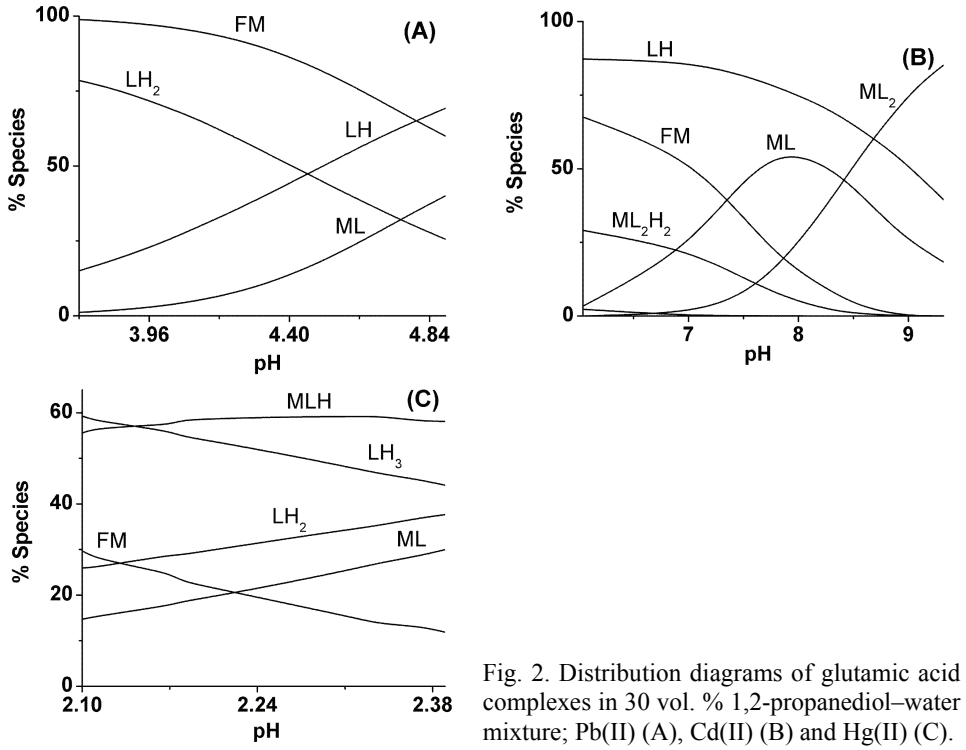

Fig. 2. Distribution diagrams of glutamic acid complexes in 30 vol. % 1,2-propanediol–water mixture; Pb(II) (A), Cd(II) (B) and Hg(II) (C).

The species shown in Equilibrium (1) was not detected, may be because the process is minor or the species is unstable. Soluble metal species are more bioavailable than insoluble ones.[32] Complexation of the metals by natural complexing agents, such as amino acids and humic acids, alter their bioavailability.[5,33] Bioavailability is also affected by pH value, composition of interfering anions and cations, dissolved organic matter, sequestration and binding in plants, species-dependent regulation mechanisms for the uptake, amount of metal and the oxidation state of mineral components.[34,35] Thus, the distribution of the species over the entire pH range is useful to understand the pH where a particular species

is likely to form. By using these data, the bioavailability of a metal can be predicted. For example, in Figs. 2 and 3 the concentration of free metal ion (FM) is very high in acidic pH values, more so with the toxic metals. Hence, in these pH ranges the metals are more bioavailable than in higher pH ranges. Hence, the concentrations of the complex chemical species have more significance than the total concentrations for the bioavailability and toxicity of trace metals in soils and water.

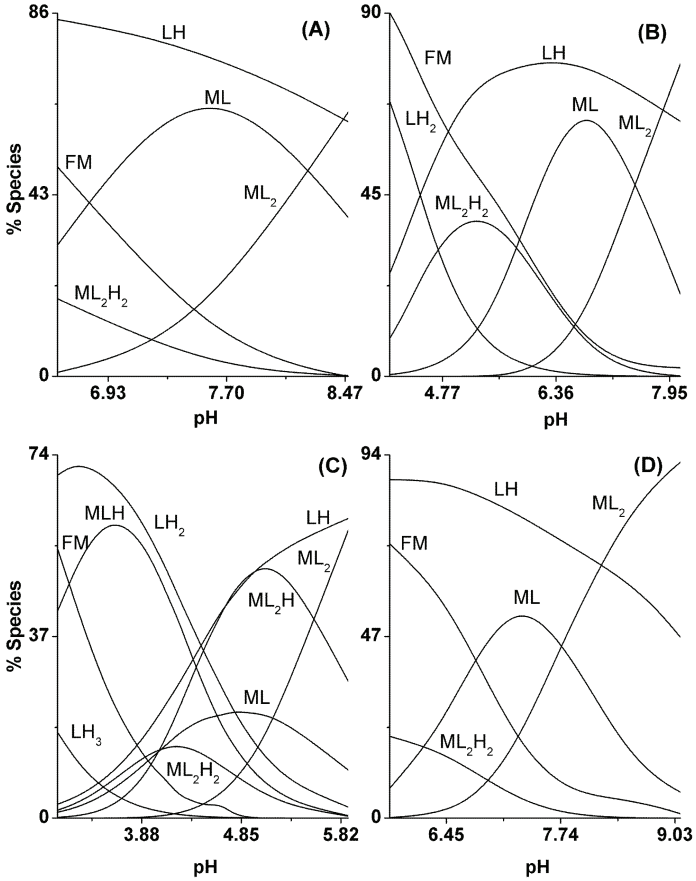

Fig. 3. Distribution diagrams of glutamic acid complexes in 30 vol. % 1,2-propanediol–water mixture; Co(II) (A), Ni(II) (B), Co(II) (C) and Zn(II) (D).

CONCLUSIONS

1. The present biomimetic studies of metal ion complexes with L-glutamic acid in PG–water mixtures indicate that all the complexes were protonated in acidic pH values.

2. The predominant species detected were ML, ML_2, MLH, ML_2H and ML_2H_2.

3. The log β values linearly increased with 1/D values of the medium, indicating the dominance of electrostatic forces over non-electrostatic forces.

4. The order of the compounds influencing the magnitudes of the stability constants due to the incorporation of errors was alkali > acid > ligand > metal.

5. The higher concentration of free metal in low pH values make the metal more bioavailable, more so in the case of toxic metals. At higher pH values, the higher concentrations of complex chemical species indicate that the metals are more amenable for transportation at higher pH values.

И З В О Д

Pb(II), Cd(II), Hg(II), Co(II), Ni(II), Cu(II) И Zn(II) КОМПЛЕКСИ СА L-ГЛУТАМИНСКОМ КИСЕЛИНОМ У СМЕШИ 1,2-ПРОПАНДИОЛ–ВОДА ПРОУЧАВАНИ МОДЕЛОВАЊЕМ ПОТПОМОГНУТИМ КОМПЈУТЕРОМ

MAHESWARA RAO VEGI, PADMA LATHA MUDDAPU, SIVA RAO TIRUKKUVALLURI и NAGESWARA RAO GOLLAPALLI

School of Chemistry, Andhra University, Visakhapatnam-530003, India

Проучавана је хемијска специјација Pb(II), Cd(II), Hg(II), Co(II), Ni(II), Cu(II) и Zn(II) комплекса са L-глутаминском киселином у 0–60 vol. % 1,2-пропанол–вода смешама при јонској јачини од 0,16 mol dm^{-3} на 303 K. Активни облици лиганда су LH_3^+, LH_2, LH^-. Предоминантне детектоване специје су ML, ML_2, MLH, ML_2H and ML_2H_2. Тренд варијације константи стабилности са променом диелектричне константе средине објашњен је на основу природе ко-растварача који стабилизује катјон, специфичних интеракција растварача и воде, дисперзије наелектрисања, специфичних интеракција ко-растварача са растворком. Утицај систематских грешака у концентрацијама састојака на константе стабилности следи редослед алкални метал > киселина > лиганд > метал. Транпорт метала и биолошка доступност објашњени су дистрибуционим дијаграмима и константама стабилности.

(Примљено 25. априла 2007, ревидирано 16. јуна 2008)

REFERENCES

1. H. Sigel, R. B. Martin, R. Tribolet, U. K. Haring, R. M. Balakrishnan, *Eur. J. Biochem.* **152** (1985) 187
2. S. Teigen, R. Andersen, *Programme on marine pollution (PMF). Trace metals in the marine environment: State of The Art and Research Needs*, Croatian Society of Chemical Engineers, Zagreb, 1992, p. 124
3. D. M. Di Toro, H. E. Allen, H. L. Bergman, J. S. Meyer. P. R. Paquin, R. C. Santore, *Environ. Toxicol. Chem.* **20** (2001) 2383
4. S. C. Wu, Y. M. Luo, K. C. Cheung, M. H. Wong, *Environ. Pollut.* **144** (2006) 765
5. H. R. Felix, A. Kayser, R. Schulin, in *Proceedings of 5th International Conference on Biogeochemistry of Trace Elements*, Vienna, Austria, (1997), p. 138
6. A. Satako, T. Abe, T. Yoshioka, S. Kyoritsu, *Busshitsu to Shite* (2003) 107
7. V. Sauvinet, S. Parrot, N. Benturquia, E. Bravo-Moraton, B. Renaud, L. Denoroy, *Electrophoresis* **24** (2003) 3187
8. M. Kalloniatis, G. Tomisich, *Prog. Retin Eye Res.* **18** (1999) 811
9. K. Ajito, C. Han, K. Torimitsu, *Anal. Chem.* **76** (2004) 2506

10. M. S. Babu, J. S. Sukumar, G. N. Rao, M. S. P. Rao, *Indian J. Chem.* **34** (1995) 567
11. V. M. Rao, M. P. Latha, T. S. Rao, G. N. Rao, *J. Indian Chem. Soc.* **83** (2006) 925
12. F. Gharib, K. Zare, R. Cheraghali, *Zh. Neorg. Khim.* **49** (2004) 1039
13. V. Lubes, F. Brito, M, L, Araufo, A, Sabatini, A. Vacca, S. Midollini, A. Mederos, *Comision Editora de la Revista Ciencia*, **12** (2004) 78
14. R. N. Patel, V. K. Soni, S. Sharma, K. K. Shukla, K. B. Pandeya, *Oxidation Commun*. **26** (2003) 358
15. R. S. Rao, G. N. Rao, *Computer Applications in Chemistry*, Himalaya Publishing House, Mumbai, 2005, p. 302
16. (a) G. Gran, *Analyst*. **77** (1952) 661; (b) G. Gran, *Anal. Chim. Acta* **206** (1988) 111
17. G. Gonzalez, D. Rosales, J. L. Gomez Ariza, A. Guiraum Perez, *Talanta* **33** (1986) 105
18. L. G. Van Uitert, C. G. Haas, *J. Am. Chem. Soc.* **75** (1953) 451
19. N. Padmaja, M. S. Babu, G. N. Rao, R. S. Rao, K. V. Ramana, *Polyhedron* **9** (1990) 2497
20. G. N. Rao, *PhD Thesis*, Andhra University, Visakhapatnam, 1989
21. P. Gans, A. Sabatini, A. Vacca, *Inorg. Chim. Acta* **18** (1976) 237
22. J. H. Ristma, G. A. Wiegers, F. Jellink, *Rec. Trav. Chim.* **84** (1965) 1577
23. D. S. Barnes, L. D. Pettit, *J. Inorg. Nucl. Chem.* **33** (1971) 2177
24. I. Nagypal, A. Gergely, E. Farakas, *J. Inorg. Nucl. Chem.* **36** (1974) 699
25. J. H. Ristma, *Rec. Trav. Chim.* **94** (1975) 210
26. G. Brooks, L. D. Pettit, *J. Chem. Soc. Dalton Trans*. (1977) 1918
27. A. Gergely, E. Farakas, *Magy Kem. Foly.* **81** (1975) 471
28. R. J. Sengwa, R. Chaudhary, S. C. Mehrotra, *Mol. Phys.* **99** (2001) 1805
29. M. Born, *Z. Phys*. **1** (1920) 4
30. M. P. Latha, V. M. Rao, T. S. Rao, G. N. Rao, Proc. *Nat. Acad. Sci. India* **77A** (2007) 109
31. G. N. Rao, R. S. Rao, *J. T. R. Chem.* **2** (1995) 15
32. W. Lund, *Fresenius J. Anal. Chem.* **337** (1990) 557
33. C. Vetriani, Y. S. Chew, S. M. Miller, J. Yagi, J. Coombs, R. A. Lutz, T. Barkay, *Appl. Environ. Microbiol.* **71** (2005) 220
34. K. Hund-Rinke, W. Kordel, *Ecotoxicol. Environ. Safety* **56** (2003) 52
35. J. E. Darnell, *PhD Thesis*, Mississippi State University, Starkville, MS, 2004.

Journal of the Serbian Chemical Society
JSCS@tmf.bg.ac.yu • www.shd.org.rs/JSCS
J. Serb. Chem. Soc. 73 (12) 1181–1186 (2008) UDC 544.354–128.4+547.545/.548:66.061:532.74
JSCS–3797 *Short communication*

SHORT COMMUNICATION

Solvent extraction of Ca^{2+}, Ba^{2+}, Cu^{2+}, Zn^{2+}, Cd^{2+}, Pb^{2+}, UO_2^{2+}, Mn^{2+}, Co^{2+} and Ni^{2+} into nitrobenzene using strontium dicarbollylcobaltate and tetra-*tert*-butyl *p-tert*-butylcalix[4]arene tetraacetate

E. MAKRLÍK[1]*, J. BUDKA[2], P. VAŇURA[2] and P. SELUCKÝ[3]

[1]*Faculty of Applied Sciences, University of West Bohemia, Husova 11, 306 14 Pilsen,*
[2]*Institute of Chemical Technology, Technická 5, 166 28 Prague and*
[3]*Nuclear Research Institute, 250 68 Řež, Czech Republic*

(Received 4 February, revised 26 May 2008)

Abstract: The exchange extraction constants corresponding to the general equilibrium $M^{2+}(aq) + SrL^{2+}(nb) \rightleftarrows ML^{2+}(nb) + Sr^{2+}(aq)$ occurring in the two-phase water–nitrobenzene system ($M^{2+} = Ca^{2+}$, Ba^{2+}, Cu^{2+}, Zn^{2+}, Cd^{2+}, Pb^{2+}, UO_2^{2+}, Mn^{2+}, Co^{2+} or Ni^{2+}; L = tetra-*tert*-butyl *p-tert*-butylcalix[4]arene tetraacetate; aq = aqueous phase; nb = nitrobenzene phase) were evaluated from extraction experiments and γ-activity measurements. Furthermore, the stability constants of the ML^{2+} complexes in water saturated nitrobenzene were calculated; they were found to increase in the cation order $Ba^{2+} < Mn^{2+} < Pb^{2+}$, $Co^{2+} < Cu^{2+}$, $Zn^{2+} < Cd^{2+}$, $Ni^{2+} < UO_2^{2+} < Ca^{2+}$.

Keywords: divalent cations; calix[4]arene compound; extraction and stability constants; water–nitrobenzene system.

INTRODUCTION

The dicarbollylcobaltate anion and some of its halogen derivatives are very useful reagents for the extraction of alkali metal cations (especially Cs^+), and also, in the presence of polyoxyethylene compounds, for the extraction of Sr^{2+} and Ba^{2+} from an aqueous solution into a polar organic phase, both under laboratory conditions for purely theoretical or analytical purposes,[1] and on the technological scale for the separation of some high-activity isotopes in the reprocessing of spent nuclear fuel and acidic radioactive waste.[2–4]

Calix[*n*]arenes are a well-known family of macrocyclic molecules with many potential applications in various branches of chemistry. Due to their simple one-pot preparation, easy derivatization and unique complexation abilities, calix[*n*]arenes

* Corresponding author. E-mail: makrlik@centrum.cz
doi: 10.2298/JSC0812181M

are widely used as building blocks for the constructions of more sophisticated molecular systems. Their unique three-dimensional pre-organization make them very attractive as the receptors for the complexation of cations, anions, and even neutral molecules. Calix[*n*]arenes find applications as selective binders and carriers, as analytical sensors, as catalysts and model structures for biomimetic studies.[5,6] In the field of host–guest chemistry, many studies have focused on the binding ability of calixarene derivatives with carbonyl groups at their lower rims toward metal ions, predominantly alkali and alkaline-earth, but also transition and heavy metal cations.[7–15]

In the present communication, the solvent extraction of Ca^{2+}, Ba^{2+}, Cu^{2+}, Zn^{2+}, Cd^{2+}, Pb^{2+}, UO_2^{2+}, Mn^{2+}, Co^{2+} and Ni^{2+} into nitrobenzene by using a synergistic mixture of strontium dicarbollylcobaltate and tetra-*tert*-butyl *p*-*tert*-butylcalix[4]arene tetraacetate (see Scheme 1), similar to a previous study[16], was investigated. Furthermore, the stability constants of the proved divalent cation complexes with the mentioned calix[4]arene ligand in the organic phase of the water–nitrobenzene extraction system were determined.

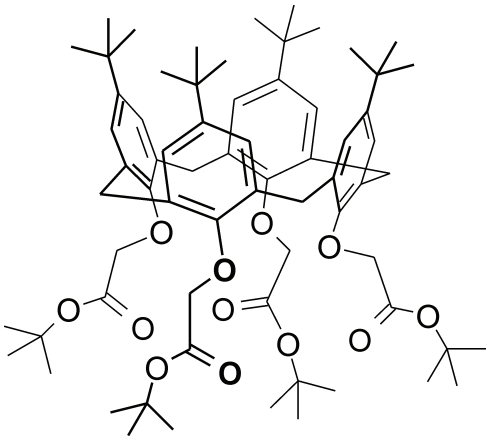

Scheme 1. Structural formula of tetra-*tert*-butyl *p*-*tert*-butylcalix[4]arene tetraacetate (abbrev. L).

EXPERIMENTAL

Tetra-*tert*-butyl *p*-*tert*-butylcalix[4]arene tetraacetate was synthesized using the procedure published by Arnaud-Neu *et al.*[9] Cesium 3,3'-*commo*-bis (undecahydro-1,2-dicarba-3-cobalta-*closo*-dodecabor)ate, $Cs^+\{[\pi\text{-}(3)\text{-}1,2\text{-}B_9C_2H_{11}]Co(III)\}^-$ (also called cesium dicarbollylcobaltate, Cs(DCC), was supplied by Katchem, Řež, Czech Republic. A nitrobenzene solution of hydrogen dicarbollylcobaltate (HDCC)[1] was prepared from CsDCC by the method described elsewhere.[17] The other employed chemicals were of reagent grade purity (Lachema, Brno, Czech Republic). The equilibration of the nitrobenzene solution of HDCC with stoichiometric $Sr(OH)_2$ yielded the corresponding $Sr(DCC)_2$ solution in nitrobenzene. The radionuclide $^{85}Sr^{2+}$ (DuPont, Belgium) was of standard radiochemical purity.

The extraction experiments were performed in 10 ml glass test-tubes covered with polyethylene stoppers: 2.0 ml of an aqueous solution of $M(NO_3)_2$ (M^{2+} = Ca^{2+}, Ba^{2+}, Cu^{2+}, Zn^{2+}, Cd^{2+}, Pb^{2+}, UO_2^{2+}, Mn^{2+}, Co^{2+} or Ni^{2+}) of concentration in the range from 1.0×10^{-3} to 1.0×10^{-2}

mol/l and micro amounts of $^{85}Sr^{2+}$ were added to 2.0 ml of a nitrobenzene solution of tetra--*tert*-butyl *p*-*tert*-butylcalix[4]arene tetraacetate and $Sr(DCC)_2$, the initial concentrations of which also varied from 1.0×10^{-3} to 1.0×10^{-2} mol/l (in all experiments, the initial concentration of tetra-*tert*-butyl *p*-*tert*-butylcalix[4]arene tetraacetate in nitrobenzene, $c_L^{in,nb}$, was always equal to the initial concentration of $Sr(DCC)_2$ in this medium, $c_{Sr(DCC)_2}^{in,nb}$). The test-tubes filled with the solutions were shaken for 12 h at 25±1 °C, using a laboratory shaker. Then the phases were separated by centrifugation. Afterwards, 1.0 ml samples were taken from each phase and their γ-activities were measured using a well-type NaI(T1) scintillation detector connected to a γ-analyzer NK/350 (Gamma, Budapest, Hungary).

The equilibrium distribution ratio of strontium, D_{Sr}, was determined as the ratio of the measured radioactivities of $^{85}Sr^{2+}$ in the nitrobenzene and aqueous samples.

RESULTS AND DISCUSSION

According to the results of previous papers,[1,18–21] the two-phase water––$M(NO_3)_2$ (M^{2+} = Ca^{2+}, Ba^{2+}, Cu^{2+}, Zn^{2+}, Cd^{2+}, Pb^{2+}, UO_2^{2+} Mn^{2+}, Co^{2+}, Ni^{2+})–nitrobenzene–$Sr(DCC)_2$ extraction system can be described by the following general equilibrium:

$$M^{2+}(aq) + Sr^{2+}(nb) \rightleftharpoons M^{2+}(nb) + Sr^{2+}(aq) \quad (1)$$

with the corresponding exchange extraction constant $K_{ex}(M^{2+},Sr^{2+})$; aq and nb denote the presence of the species in the aqueous and nitrobenzene phases, respectively. For the constant $K_{ex}(M^{2+},Sr^{2+})$, one can write:

$$\log K_{ex}(M^{2+},Sr^{2+}) = \log K^{i}_{M^{2+}} - \log K^{i}_{Sr^{2+}} \quad (2)$$

where $K^{i}_{M^{2+}}$ and $K^{i}_{Sr^{2+}}$ are the individual extraction constants for M^{2+} and Sr^{2+}, respectively, in the water–nitrobenzene system.[18] Knowing $\log K^{i}_{Ca^{2+}} = -11.2$,[18,19] $\log K^{i}_{Ba^{2+}} = -10.5$,[21] $\log K^{i}_{Cu^{2+}} = \log K^{i}_{Cd^{2+}} = -11.5$,[22] $\log K^{i}_{Zn^{2+}} = \log K^{i}_{Ni^{2+}} =$ $= -11.6$,[22] $\log K^{i}_{Pb^{2+}} = -10.6$,[22] $\log K^{i}_{UO_2^{2+}} = -11.8$,[22] $\log K^{i}_{Mn^{2+}} = -11.1$,[22] $\log K^{i}_{Co^{2+}} = -11.4$[22] and $\log K^{i}_{Sr^{2+}} = -10.7$,[18,20] the single exchange extraction constants $K_{ex}(M^{2+}, Sr^{2+})$ were simply calculated from Eq. (2). The corresponding data are given in Table I.

TABLE I. Equilibrium data for the M^{2+} and ML^{2+} cations in the two-phase water–nitrobenzene extraction system at 25 °C (M^{2+} = Ca^{2+}, Sr^{2+}, Ba^{2+}, Cu^{2+}, Zn^{2+}, Cd^{2+}, Pb^{2+}, UO_2^{2+}, Mn^{2+}, Co^{2+}, Ni^{2+}; L = tetra-*tert*-butyl *p*-*tert*-butylcalix[4]arene tetraacetate; for the meaning of the constants, see text)

Quantity	Ca^{2+}	Sr^{2+}	Ba^{2+}	Cu^{2+}	Zn^{2+}	Cd^{2+}	Pb^{2+}	UO_2^{2+}	Mn^{2+}	Co^{2+}	Ni^{2+}
$\log K^{i}_{M^{2+}}$	–11.2[a]	–10.7[b]	–10.5[c]	–11.5[d]	–11.6[d]	–11.5[d]	–10.6[d]	–11.8[d]	–11.1[d]	–11.4[d]	–11.6[d]
$\log K_{ex}(M^{2+},Sr^{2+})$[e]	–0.50	–	0.20	–0.80	–0.90	–0.80	0.10	–1.1	–0.40	–0.70	–0.90
$\log K_{ex}(M^{2+},SrL^{2+})$[f]	1.0	–	–0.70	–1.1	–1.2	–1.0	–0.30	–1.0	–1.0	–1.1	–1.1
$\log \beta_{nb}(ML^{2+})$[g]	8.6	7.1[h]	6.2	6.8	6.8	6.9	6.7	7.2	6.5	6.7	6.9

[a]Inferred from Refs. 18 and 19; [b]inferred from Refs. 18 and 20; [c]Ref. 21; [d]Ref. 22; [e]calculated from Eq. (2) using data from Refs. 18–22; [f]calculated from Eq. (5); [g]calculated from Eq. (6) using data from Refs. 18–22; [h]determined by the method described in detail in Ref. 23

Previous results[24–26] showed that the two-phase water–$M(NO_3)_2$ (M^{2+} = Ca^{2+}, Ba^{2+}, Cu^{2+}, Zn^{2+}, Cd^{2+}, Pb^{2+}, UO_2^{2+}, Mn^{2+}, Co^{2+} or Ni^{2+})–nitrobenzene–L (L = = tetra-*tert*-butyl *p*-*tert*-butylcalix[4]arene tetraacetate)–$Sr(DCC)_2$ extraction system (see Experimental), chosen for the determination of stability of the ML^{2+} complexes in nitrobenzene saturated with water, can be characterized by the main chemical equilibrium (3):

$$M^{2+}(aq) + SrL^{2+}(nb) \rightleftharpoons ML^{2+}(nb) + Sr^{2+}(aq) \quad (3)$$

with the general equilibrium extraction constant $K_{ex}(M^{2+}, SrL^{2+})$ given by:

$$K_{ex}(M^{2+}, SrL^{2+}) = \frac{[ML^{2+}]_{nb}[Sr^{2+}]_{aq}}{[M^{2+}]_{aq}[SrL^{2+}]_{nb}} \quad (4)$$

It is necessary to emphasize that tetra-*tert*-butyl *p*-*tert*-butylcalix[4]arene tetraacetate is a very hydrophobic ligand, practically present in the nitrobenzene phase only, where it forms very stable complexes ML^{2+} with the mentioned divalent cations. Taking into account the conditions of electroneutrality in the organic and aqueous phases of the system under study, the mass balances of the divalent cations studied at equal volumes of the nitrobenzene and aqueous phases, as well as the measured equilibrium distribution ratio of strontium, D_{Sr} = = $[SrL^{2+}]_{nb}/[Sr^{2+}]_{aq}$, combined with Eq. (4), the final expression for $K_{ex}(M^{2+}, SrL^{2+})$ is obtained in the form:

$$K_{ex}(M^{2+}, SrL^{2+}) = \frac{1}{D_{Sr}} \frac{c^{in,nb}_{Sr(DCC)_2}}{(1 + D_{Sr})c^{in,aq}_{M(NO_3)_2} - c^{in,nb}_{Sr(DCC)_2}} \quad (5)$$

where $c^{in,aq}_{M(NO_3)_2}$ is the initial concentration of $M(NO_3)_2$ (M^{2+} = Ca^{2+}, Ba^{2+}, Cu^{2+}, Zn^{2+}, Cd^{2+}, Pb^{2+}, UO_2^{2+}, Mn^{2+}, Co^{2+} or Ni^{2+}) in the aqueous phase of the system under consideration.

In this study, from the extraction experiments and γ-activity measurements by means of Eq. (5), the logarithms of the constants $K_{ex}(M^{2+}, SrL^{2+})$ were determined and are given in Table I.

Moreover, according to previous studies,[24–26] for the extraction constants $K_{ex}(M^{2+}, Sr^{2+})$ and $K_{ex}(M^{2+}, SrL^{2+})$ defined above, as well as for the stability constants of the complexes ML^{2+} and SrL^{2+} in nitrobenzene saturated with water, denoted by $\beta_{nb}(ML^{2+})$ and $\beta_{nb}(SrL^{2+})$, respectively, one obtains:

$$\log \beta_{nb}(ML^{2+}) = \log \beta_{nb}(SrL^{2+}) + \log K_{ex}(M^{2+}, SrL^{2+}) - \\ - \log K_{ex}(M^{2+}, Sr^{2+}) \quad (6)$$

Finally, using the values of $\log K_{ex}(M^{2+},Sr^{2+})$ and $\log K_{ex}(M^{2+},SrL^{2+})$ given in Table I, $\log \beta_{nb}$ (SrL^{2+}) = 7.1, determined from the distribution of strontium picrate in the water–nitrobenzene system containing the considered calix[4]arene

ligand by the method described in detail previously,[23] and applying Eq. (6), the stability constants of the ML^{2+} complexes in water-saturated nitrobenzene are obtained. These data are also summarized in Table I. Thus, the β_{nb} (ML^{2+}) values from this table indicate that the stability of the ML^{2+} cationic complex species in the mentioned medium increases in the series $Ba^{2+} < Mn^{2+} < Pb^{2+}$, $Co^{2+} <$ $< Cu^{2+}$, $Zn^{2+} < Cd^{2+}$, $Ni^{2+} < Sr^{2+} < UO_2^{2+} < Ca^{2+}$.

Acknowledgements. The presented work was supported by the Czech Ministry of Education, Youth and Sports, Projects MSM 4977751303 and MSM 6076137307.

ИЗВОД

ЕКСТРАКЦИЈА Ca^{2+}, Ba^{2+}, Cu^{2+}, Zn^{2+}, Cd^{2+}, Pb^{2+}, UO_2^{2+}, Mn^{2+}, Co^{2+} И Ni^{2+} СТРОНЦИЈУМ ДИКАРБОНИЛ КОБАЛТАТА И ТЕТРА-*tert*-БУТИЛ-*p*-*tert*-БУТИЛКАЛИКС[4]АРЕН ТЕТРААЦЕТАТА У РАСТВОР НИТРОБЕНЗЕНА

E. MAKRLÍK[1], J. BUDKA[2], P. VAŇURA[2] и P. SELUCKÝ[3]

[1]*Faculty of Applied Sciences, University of West Bohemia, Husova 11, 306 14 Pilsen,* [2]*Institute of Chemical Technology, Technická 5, 166 28 Prague и* [3]*Nuclear Research Institute, 250 68 Řež, Czech Republic*

На основу измерених коефицијената активности γ, добијених из екстракционих мерења, одређена је константа екстракционе равнотеже на основу опште једначине $M^{2+}(aq) + SrL^{2+}(nb) \rightleftharpoons ML^{2+}(nb) + Sr^{2+}(aq)$, где су: $M^{2+} = Ca^{2+}$, Ba^{2+}, Cu^{2+}, Zn^{2+}, Cd^{2+}, Pb^{2+}, UO_2^{2+}, Mn^{2+}, Co^{2+}, Ni^{2+}; L = тетра-*tert*-бутил-*p*-*tert*-бутилкаликс[4]арен тетраацетат; aq = водена фаза, nb = фаза нитробензена. Одређене константе стабилности комплекса ML^{2+} у раствору нитробензена засићеног водом расту према катјону у комплексу по следећем редоследу: $Ba^{2+} <$ $< Mn^{2+} < Pb^{2+}$, $Co^{2+} < Cu^{2+}$, $Zn^{2+} < Cd^{2+}$, $Ni^{2+} < UO_2^{2+} < Ca^{2+}$.

(Примљено 4. фебруара, ревидирано 26. маја 2008)

REFERENCES

1. E. Makrlík, P. Vaňura, *Talanta* **32** (1985) 423
2. J. D. Law, K. N. Brewer, R. S. Herbst, T. A. Todd, D. J. Wood, *Waste Management* **19** (1999) 27
3. V. N. Romanovskiy, I. V. Smirnov, V. A. Babain, T. A. Todd, R. S. Herbst, J. D. Law, K. N. Brewer, *Solvent Extr. Ion Exch.* **19** (2001) 1
4. J. D. Law, R. S. Herbst, T. A. Todd, V. N. Romanovskiy, V. A. Babain, V. M. Esimantovskiy, I. V. Smirnov, B. N. Zaitsev, *Solvent Extr. Ion Exch.* **19** (2001) 23
5. V. Böhmer, Angew. Chem., *Int. Ed. Eng.* **34** (1995) 713
6. C. D. Gutsche, *Calixarenes Revisited*, The Royal Society of Chemistry, Cambridge, 1998
7. A. Arduini, A. Pochini, S. Reverberi, R. Ungaro, *Tetrahedron* **42** (1986) 2089
8. A. Arduini, E. Ghidini, A. Pochini, R. Ungaro, G. D. Andreetti, G. Calestani, F. Ugozzoli, *J. Inclusion Phenom. Macrocyclic Chem.* **6** (1988) 119
9. F. Arnaud-Neu, E. M. Collins, M. Deasy, G. Ferguson, S. J. Harris, B. Kaitner, A. J. Lough, M. A. McKervey, E. Marques, B. L. Ruhl, M. J. Schwing-Weill, E. M. Seward, *J. Am. Chem. Soc.* **111** (1989) 8681
10. F. Arnaud-Neu, G. Barrett, S. J. Harris, M. Owens, M. A. McKervey, M. J. Schwing-Weill, P. Schwinté, *Inorg. Chem.* **32** (1993) 2644

11. K. Ohto, E. Murakami, T. Shinohara, K. Shiratsuchi, K. Inoue, M. Iwasaki, *Anal. Chim. Acta* **341** (1997) 275
12. Z. Ye, W. He, X. Shi, L. Zhu, *J. Coord. Chem.* **54** (2001) 105
13. A. F. Danil de Namor, S. Chahine, D. Kowalska, E. E. Castellano, O. E. Piro, *J. Am. Chem. Soc.* **124** (2002) 12824
14. P. M. Marcos, J. R. Ascenso, M. A. P. Segurado, J. L. C. Pereira, *J. Inclusion Phenom. Macrocyclic Chem.* **42** (2002) 281
15. P. M. Marcos, S. Félix, J. R. Ascenso, M. A. P. Segurado, J. L. C. Pereira, P. Khazaeli--Parsa, V. Hubscher-Bruder, F. Arnaud-Neu, *New J. Chem.* **28** (2004) 748
16. E. Makrlík, J. Budka, P. Vaňura, P. Selucký, *J. Radioanal. Nucl. Chem.* **277** (2008) 487
17. E. Makrlík, *Collect. Czech. Chem. Commu*n. **57** (1992) 289
18. J. Rais, *Collect. Czech. Chem. Commun*. **36** (1971) 3253
19. P. Vaňura, *Czech. J. Phys.* **49 Suppl. S1** (1999) 761
20. P. Vaňura, E. Makrlík, J. Rais, M. Kyrš, *Collect. Czech. Chem. Commun.* **47** (1982) 1444
21. I. Podzimek, M. Kyrš, J. Rais, *J. Inorg. Nucl. Chem.* **42** (1980) 1481
22. E. Makrlík, P. Vaňura, *Z. Phys. Chem.*, in press
23. E. Makrlík, P. Vaňura, *J. Radioanal. Nucl. Chem.* **267** (2006) 699
24. M. Daňková, E. Makrlík, P. Vaňura, *J. Radioanal. Nucl. Chem.* **221** (1996) 251
25. E. Makrlík, P. Vaňura, *J. Radioanal. Nucl. Chem.* **214** (1996) 339
26. E. Makrlík, P. Vaňura, *Monatsh. Chem.* **137** (2006) 157.

www.shd.org.rs

Journal of the Serbian Chemical Society

JSCS@tmf.bg.ac.yu • www.shd.org.rs/JSCS

J. Serb. Chem. Soc. *73* (12) 1187–1196 (2008)
JSCS–3798

UDC 547.672:54.02:54–74:537.872
Original scientific paper

Electronic structures and spectra of conducting anthracene derivatives

ZHONGFA WANG and SHI WU*

Department of Chemistry, Zhejiang University, Hangzhou 310027, PRC

(Received 20 June, revised 26 November 2007)

Abstract: Theoretical studies on anthracene and a series of its derivatives were performed using the AM1 method and DFT. Based on B3LYP/6-31G(d) optimized geometries, the electronic, IR and NMR spectra of anthracene oligomers were calculated using the Indo/Cis, AM1 and B3LYP/6-31G(d) methods, respectively. The energy gaps of the oligomers decreased and the main absorptions in the electronic spectra of the oligomers were red-shifted, whereas the IR frequencies for some of the C=C and C–H bonds were blue-shifted with increasing chain length and in the presence of substituents. The ^{13}C-NMR chemical shifts of the bridged carbon atoms were upfield shifted in the presence of an electron-donating group, while the chemical shifts of the carbon atoms on the two side rings of the anthracene moiety shifted downfield in the presence of an electron-withdrawing group.

Keywords: anthracene; conducting polymer; energy gap; chemical shift; B3LYP/6-31G(d).

INTRODUCTION

Many polymers possess conductive properties, which has stimulated intensive interest of scientists. These conducting polymers are often classified into polythiophene,[1–3] polypyrrole,[4] polyheterocycles,[5,6] polyaniline[7] and polyaryl rings.[8–12] Henze *et al*. reported that the stabilities of polythiophene assemblies are enhanced with increasing chain length.[1] Methoxyl substitution in conducting polymers containing conjugated bithiazole moieties led to an improvement of the solubility.[5] For conducting copolymers of pyridine with thiophene, *n*-doped states are more stable than *p*-doped states.[6] Conducting and insulating phases are possibly located in the same polymer.[7] Polymers containing dimethyldihydropyene can be designed for optoelectronic redox switching by the introduction of a photochromic unit.[8] New phenanthroline dicarboxamide-based helical foldamers can promote the polymerization of aromatics and oligoamides for potential applica-

* Corresponding author. E-mail: wushi@zju.edu.cn
doi: 10.2298/JSC0812187W

tions in biology and material science.[11] Weibin *et al*. achieved the synthesis and characterization of soluble oligo(9,10-bisalkynylanthrylene)s.[12]

There are some reports on important properties of anthracene polymers, which are of interest for possible applications. Many anthracene moieties are photoluminescent, and polymers containing such units as a part of the extended π-electron system are also likely to be electroluminescent. A film of poly(anthracene--2,6-diyl) was found to be electroconducting after being doped with potassium naphthalenide polymers and ferric chloride, with conductivities of 4.0×10^{-2} and 0.12 S cm^{-1}, respectively. These film showed yellow-green luminescence.[13] Polyanthracene is partly soluble in organic solvents and its soluble part is a strong blue light emitter.[14] On the other hand, poly(9,10-anthracene diylidene) exhibits thermochromism and high thermal stability.[15–17]

However, there are only a few theoretical reports on the electronic structure and spectroscopy of anthracene derivatives. Herein, a series of such oligomers were designed to explore the effects of chain length and substituents on the energy gaps and spectra. These properties are useful to explain the conductivities and stabilities of conducting polymers.

METHODOLOGY

A linear polymer can be considered as a one-dimensional box. Electrons are delocalized and move over the whole system. Then, a minimum on the potential curve can be found. Based on the monomer anthrylene (compound **1**), compounds **2**–**4** and **5**–**11** were designed by increasing the chain length and changing the substituents, respectively (Fig. 1). The chain was elongated *via* 2,6-linkage and the substituents were inserted at the 9,10-positions on the anthrylene unit.

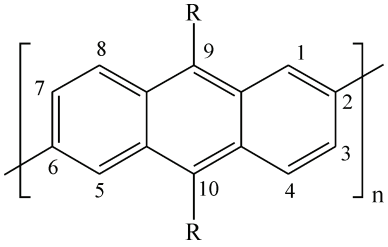

Fig. 1. The structures of compounds **1**–**11**. Compound **1**: n = 1, R = H; Compound **2**: n = 2, R = H; Compound **3**: n = 3, R = H; Compound **4**: n = 4, R = H; Compound **5**: n = 1, R = NH_2; Compound **6**: n = 1, R = NO_2; Compound **7**: n = 2, R = NH_2; Compound **8**: n = 2, R = NO_2; Compound **9**: n = 3, R = NH_2; Compound **10**: n = 3, R = NO_2; Compound **11**: n = 4, R = NH_2.

Full geometry optimization of these compounds without any symmetry restriction was performed step by step using the AM1 method and DFT at the B3LYP/STO-3G, B3LYP/3--21G and B3LYP/6-31G(d) levels (the optimized geometry of compound **11** at B3LYP/6--31G(d) level is shown in Fig. S1 in the Supplement, available only in electronic form at http://www.shd.org.rs/jscs).

The AM1 method and DFT in the Gaussian 03 program[18] were successfully employed to study the electronic structures and spectroscopic characteristics of supramolecular complexes,[19–22] intramolecular hydrogen bonding species,[23] conducting polymers[24,25] and carbon clusters.[26–29] Based on the B3LYP/6-31G(d) optimized geometries of the compounds, the configuration interaction was investigated using the Indo/Cis method.[30] By exciting electrons from the 14 highest occupied molecular orbits into the 14 lowest unoccupied orbits, this led to

the generation of 196 configurations. Subsequently, the IR frequencies were computed using the AM1 method. Finally, ^{13}C-NMR chemical shifts were calculated using the Giao method at the B3LYP/6-31G(d) level.

RESULTS AND DISCUSSION

LUMO–HOMO energy gaps

The LUMO–HOMO energy gaps of the unsubstituted compounds **1**–**4** gradually decreased with increasing value of n (Table I); those of compounds **5**, **7**, **9** and **11** with R = NH_2 and of compounds **6**, **8** and **10** with R = NO_2 showed the same regularity. With decreasing energy gap, electrons can be easily excited from the ground state and, hence, the conductivities of the oligomers increased over those of the monomers. It was experimentally shown that the energy gap of oligo(9,10--bialkynylanthrylene)s decreased from 2.60 (n = 1) to 2.31 eV (n = 5),[12] supporting the above calculation results. The energy gaps of polyanthrylene, and its derivatives substituted by amino and nitrate groups were predicted *via* the extrapolation method to be 2.95, 2.38 and 2.73 eV.[25] On the other hand, the energy gaps of compounds **5** and **6** are less than that of compound **1**, owing to the presence of the substituents. The electron-donating group affects the energy gap more than the electron-withdrawing group. Comparing the energy gaps of compounds **7**–**10** with that of compound **1**, the same conclusion as above can be drawn. The HOMO energy of the oligomer increased, and the energy gap decreased in the presence of the electron-donating group,[31] which supports the present calculations. Therefore, the presence of substituents decreases the energy gaps, improves the conductivities and also enhances the solubilities of the oligomers.

TABLE I. Several variables of compounds **1**–**11** optimized at the B3LYP/6-31G(d) level

Variable	Compounds										
	1	**2**	**3**	**4**	**5**	**6**	**7**	**8**	**9**	**10**	**11**
Energy gap / eV	3.599	3.230	3.045	2.995	2.902	3.182	2.615	2.913	2.463	2.760	2.393
η / eV	1.800	1.615	1.523	1.478	1.451	1.591	1.308	1.457	1.232	1.380	1.197
χ / eV	3.429	3.480	3.506	3.520	2.803	4.652	2.871	4.780	2.910	4.849	2.926
IP / eV	5.228	5.095	5.028	4.997	4.254	6.243	4.178	6.236	4.141	6.229	4.122
EA / eV	1.629	1.865	1.983	2.042	1.352	3.061	1.563	3.323	1.678	3.469	1.729

In addition to C2–C6 coupling of the anthracene units in Fig. 1, coupling at the 9,10-positions was also considered. The energy gaps of the analogous oligomers (n = 1, 2, 3) formed *via* 9,10-linkages were calculated to be 3.599, 2.144 and 1.158 eV at the B3LYP/6-31G(d) level, respectively. The energy gaps decreased with increasing chain length. Compared with those obtained for 2,6-linkages in Table 1, the energy gaps of the oligomers with 9,10-linkage become small. Since C9 and C10 are located at the middle positions of the anthracene unit, the 9,10-lingkage is favorable for the overlapping of the electron cloud be-

tween neighboring anthracene units. Hence, polyanthracenes formed *via* 9,10-linkages will exhibit better conductivities than those formed *via* 2,6-lingkages.

Some important variables

Conducting polymers generally display poor thermodynamic stabilities due to their expanded conjugated structures. The improvement of their stability is a main problem. The influence of substituents on stability was investigated in this study. The ionization potential (*IP*), electron affinity (*EA*), absolute hardness (η) and absolute electron negativity (χ) (Table I) changed linearly as the chain length increased. The *IP* and η values of compounds **1**–**4** decreased with increasing *n*. Thus, polyanthrylene easily looses electrons and its thermal stability becomes worse. Simultaneously the *EA* and χ of compounds **1**–**4** grew more, leading to the easy reduction of polyanthrylene. Then the polymer is reactive. The experimental *IP* values of the substituted anthrylene decreased from 5.45 (n = 1) to 5.29 eV (n = 5), whereas the *EA* values increased from 2.85 (n = 1) to 2.98 eV (n = 5),[12] supporting the above calculation results. Observing the values of the four variables of compounds **5**, **7**, **9** and **11** and **6**, **8** and **10**, it can be concluded that the polyanthrylenes substituted by electron-withdrawing and donating groups also possess sensitive redox characteristics.

The *IP* and *EA* values of compound **5** are lower than those of compound **1**, thus it is easy inject holes into compound **5**. The *IP* and *EA* values of compound **6** are higher than those of compound **1**, thus compound **6** easily catch electrons. Hence, the presence of the electron-donating group leads to easy oxidation, whereas the electron-withdrawing group stimulates reduction of the substituted polyanthrylenes. The η values of compounds **5** and **6** are lower than that of compound **1**, thus the presence of the substituents does not improve the thermal stability of the polymer.

Intrinsic conducting materials with large *EA* and χ values, such as compounds **6**, **8** and **10**, are likely to undergo *n*-doping. Compounds **5**, **7**, **9** and **11** of lower *IP* have a low oxidation potential, resulting in a low resistance and good conductivity. For example, the anthrylene pentamer with the electron-donating group displays a large charge carrier mobility of 2.95×10^{-3} $cm^2\ V^{-1}\cdot s^{-1}$.[12]

Electronic absorption spectra

The main absorption peaks in the electronic spectrum of compound **1** were calculated to be at 215.8, 230.6, 276.6 and 317.4 nm. The first absorption at 317.4 nm was scaled by the multiplier 1.18, although its oscillator strength, 0.0109, was small compared with the experimental result 375 nm.[14] There was a large red-shift in the absorptions at 228.1, 267.4, 296.1, 354.4 and 364.6 nm of compound **2** compared with those of compound **1** (Fig. 2; the electronic spectra of other compounds are given in Fig. S2 of the Supplement). Simultaneously, the bands of compound **2** are split and broadened due to its low symmetry because

the two anthrylene planes are not coplanar in the presence of the large steric effect. The absorptions at 235.2 and 362.4 nm of compound **3** were red-shifted relative to 228.1 and 354.4 nm of compound **2**. Those at 306.5 and 366.0 nm of compound **4** were also red-shifted in comparison with 304.3 and 362.4 nm of compound **3**. Thus, the main absorption bands were red-shifted as the chain length increased, which is in agreement with the experimental conclusion that the first UV absorptions of substituted anthrylene are red-shifted as *n* increases from 1 to 5.[12]

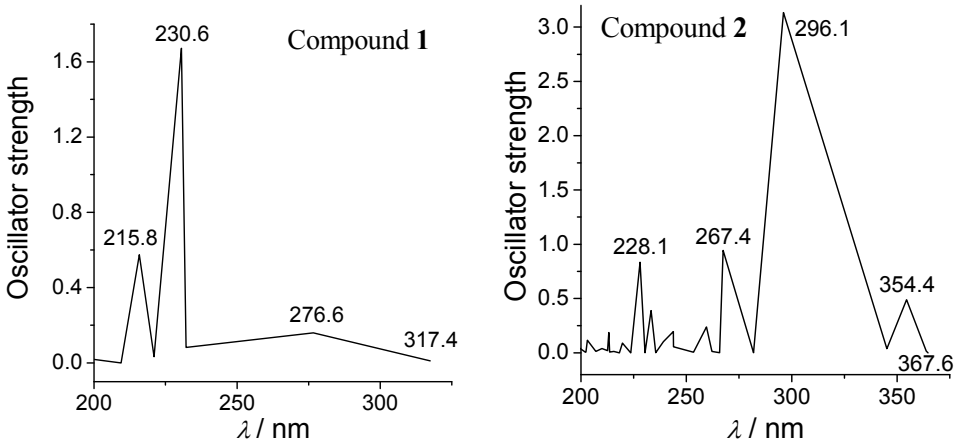

Fig. 2. The electronic spectra of compounds **1** and **2** calculated by the Indo/Cis method.

The first peak of compound **5** appeared at 395.2 nm, arising from the π-π* transition of the HOMO (39) to the LUMO (40), in view of the valence electrons of the Indo method. This absorption was red-shifted compared with that of compound **1**, which was caused by substitution with NH_2 groups. The contribution coefficients of the P_z atomic orbitals of the two nitrogen atoms to the HOMO (39) are 0.2256 and –0.2256, and those to the LUMO (40) are both –0.1104. Obviously, the atomic orbitals of the nitrogen atoms participate in the formation of the molecular orbitals and play an important role in the frontier orbitals. This effect results in a decrease of the energy gap and red-shifts of the main electronic transitions. Similarly, the main peaks of compounds **5**, **7**, and **9** are sequentially red-shifted.

The main peaks of compound **6**, appearing at 257.0 and 296.4 nm, were red--shifted compared with 230.6 and 276.6 nm of compound **1**. This is caused by the substitution of the NO_2 group. These two absorptions of compound **6** are blue--shifted in contrast to 262.5 and 395.2 nm of compound **5**. The presence of the electron-donating group in compound **5** leads to a smaller energy gap. The strongest peaks at 257.0, 287.2 and 292.0 nm of compounds **6**, **8** and **10** were gradually red-shifted, which is ascribed to the lower energy gap and decrease in symmetry with elongation of the chain length.

IR spectra

The stabilities of polymers are related to the delocalization of electrons and strength of the main chain bonds, which can be reflected in the IR spectra. The main absorption peaks in the IR spectrum of compound **1** were calculated to be at 723.4, 880.7 and 3289.0 cm^{-1}. The first two bands are assigned to the C–H out-of-plane deformation vibrations, which are consistent with the experimental results of 725 and 883 cm^{-1}.[14] The last one is attributed to the C–H stretching vibration. There were large blue-shifts in the absorptions at 736.0, 903.2 and 3289.9 cm^{-1} of compound **2** relative to those of compound **1** (Fig. 3; the IR spectra of the other compounds are given in Fig. S3 of the Supplement). Simultaneously, the number of the absorptions increased with increasing chain length. These absorptions of compound **2** were further blue-shifted to 737.5, 908.0 and 3290.0 cm^{-1} in compound **3**. This indicates that the C–H bonds were strengthened with enlargement of the conjugation system and delocalization of the electrons.

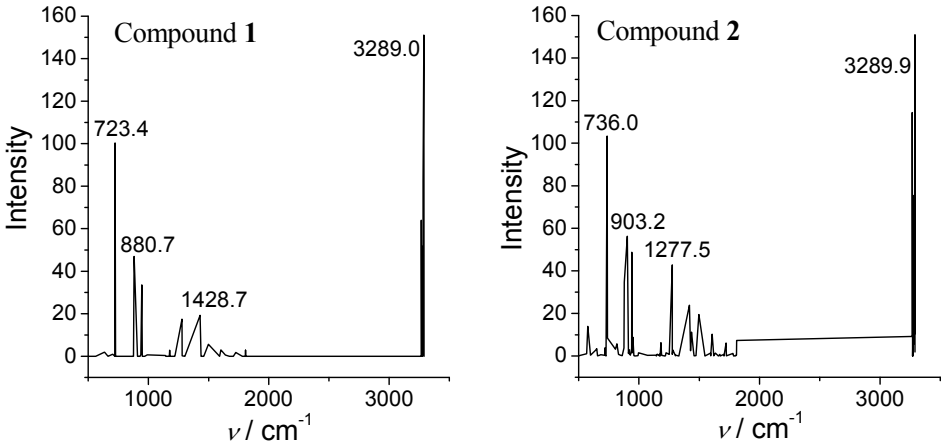

Fig. 3. The IR spectra of compounds **1** and **2** calculated by the AM1 method.

The main IR absorptions of compound **5** were at 846.4, 1660.8 and 3292.7 cm^{-1}, *i.e.*, blue-shifted relative to the corresponding bands of compound **1** at 880.7, 1428.7 and 3289.0 cm^{-1}. The absorption at 1660.8 cm^{-1} of compound **5** is generated by the stretching vibration of the C=C bonds, which is basically consistent with the experimental frequency at 1597 cm^{-1} of the C=C bonds in polynaphthylene.[10] The IR band at 1660.8 cm^{-1} of compound **5** could be due to deformation vibration of the N–H bond of the primary aromatic amine. The presence of the electron-donating groups in compound **5** elevates the electron density on the anthrylene ring and strengthens the C=C and C–H bonds. The main absorptions at 850.0, 3292.9 and 3363.8 cm^{-1} arising from the C–H and N–H bonds in compound **7** were blue-shifted compared with those of compound **5**. The N–H stretching vibration at 3363.8 cm^{-1} in compound **7** is less strong than

the O–H stretching vibration at 3383 cm^{-1} in polynaphthylene.[10] The absorption at 1658.8 cm^{-1} resulting from the C=C bonds in compound **7** was red-shifted relative to that of compound **5**. The main absorptions at 853.4, 3293.3 and 3364.7 cm^{-1} in compound **9** were blue-shifted, whereas the absorption at 1658.1 cm^{-1} was red-shifted in comparison with the corresponding bands in compound **7**. The electron density on the anthrylene ring decreased as the chain length increased, leading to a weakening of the C=C bonds and a strengthening of the C–H and N–H bonds.

The main IR absorptions caused by the C–H bonds of compounds **6**, **8** and **10** compared with those of compounds **5**, **7** and **9** were blue-shifted, whereas those arising from the C=C bonds were red-shifted. The absorptions near 1867 cm^{-1} of compounds **6**, **8** and **10** resulted from N=O bonds, which were stronger than the C=O bonds with an experimental stretching frequency at 1743 cm^{-1}.[32] The π-electron density on the anthrylene ring was delocalized in the presence of the $–NO_2$, which reduced the strength of the C=C bonds.

NMR spectra

The change in electron density of the carbon atoms and symmetry of the oligomers can be observed in the NMR spectra, which are helpful in understanding the stabilities of polymers. The chemical shifts δ of the hydrogen atoms in the ^{1}H-NMR spectra of compounds **1**–**3** were calculated to be in the ranges 5.4–9.2, 5.3–11.9 and 5.3–12.1 ppm, respectively. Thus, the range of the δ values of the hydrogen atoms was enlarged and the δ data were shifted downfield with increasing *n*. The electrons on the hydrogen atoms were delocalized and the shielding effect was reduced with the increasing chain length. The δ data of the hydrogen atoms on the naphthylene ring were determined to be at 7.1–7.6 ppm,[10] which supports the above calculation.

The δ values of the carbon atoms in the ^{13}C-NMR spectrum of compound **1** appeared in the range 126.2–195.9 ppm. The absorption at 126.2 ppm arose from C(9) and C(10), whereas the absorption at 195.9 ppm is ascribed to C(11)–C(14). The δ data of C(2) and C(6) for the linkage of the two anthrylene rings in compound **2** were shifted downfield to 167.1 ppm (Fig. 4; the NMR spectra of the other compounds are given in Fig. S4 of the Supplement), and the C–C bond was weakened because of the formation of the dimer. In the naphthylene oligomer, the δ values of the two linkage carbon atoms were also downfield shifted from 118.7 to 120.6 ppm.[10] The ^{13}C-NMR absorptions of compound **3** were split because of the decreased symmetry. The δ data of C(9) and C(10) in compound **5** were shifted downfield to 130.1 ppm, while those of C(11)–C(14) were shifted upfield till 170.3 ppm. The situation was similar for compound **7**. The presence of the electron-donating group decreased the electron density on the neighboring carbon atoms but increases that on the bridged carbon atoms. The δ data of C(9)

and C(10), and C(11)–C(14) in compound **6** were shifted upfield to 87.2 and 184.4 ppm, respectively, while those of C(1), C(4), C(5) and C(8), and C(2), C(3), C(6) and C(7) were shifted downfield to 159.6 and 169.2 ppm, respectively. A similar regularity was observed in the bands of compound **8**. The presence of the electron-withdrawing group reduces the electron density on the two side rings, but elevates that on the middle ring in the anthrylene unit.

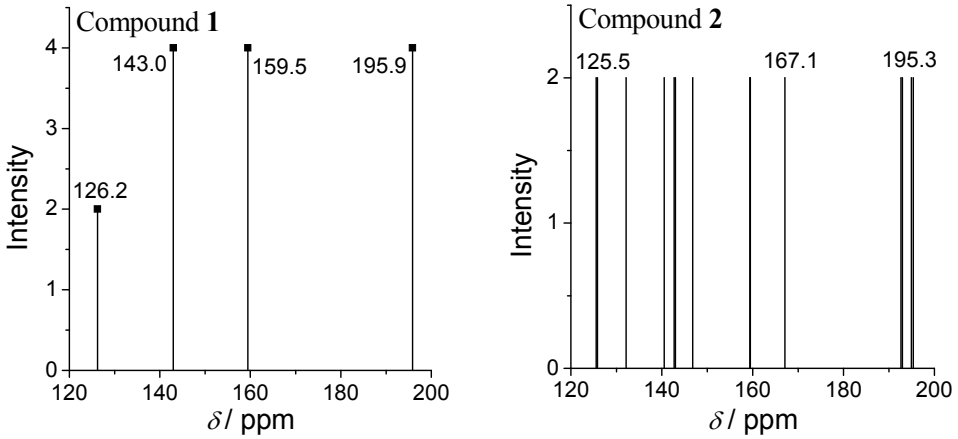

Fig. 4. ^{13}C-NMR spectra of compounds **1** and **2** calculated on the B3LYP/6-31G(d) level.

CONCLUSIONS

The electronic structures and spectroscopic characteristics of the anthrylene oligomers were affected by the chain length and substituents. The energy gaps of the oligomers decreased with increasing number of repeating units, thus polyanthrylene becomes a conducting polymer. The presence of the substituents decreases the energy gaps of the oligomers. Substitution by NO_2 or NH_2 groups and elongation of the chain length lead to red-shifts of the main absorptions in the electronic spectra of the oligomers. The electron density on the bridged carbon atoms in the anthrylene ring was elevated on substitution by amino groups; thus the C=C and C–H bonds are strengthened. The anthrylene polymer with the amino groups was predicted to be a better conducting material because of its lower oxidation potential and energy gap.

SUPPLEMENT

Available in electronic form only (http://www.shd.org.rs/JSCS/).

И З В О Д

ЕЛЕКТРОНСКА СТРУКТУРА И СПЕКТРИ ПРОВОДНИХ ДЕРИВАТА АНТРАЦЕНА

ZHONGFA WANG и SHI WU

Department of Chemistry, Zhejiang University, Hangzhou 310027, PRC

Теоријске студије антрацена и серије његових деривата изведене су помоћу AM1 методе и DFT. На основу B3LYP/6-31G(d) оптимизованих геометрија израчунати су електронски, IR и NMR спектри антраценових олигомера помоћу Indo/Cis, AM1 and B3LYP/6-31G(d) метода, респективно. Разлике у енергетским нивоима олигомера се смањују, а главни апсорпциони максимуми им се померају ка црвеном делу спектра, док су IR фреквенције неких C=C and C–H веза померене ка плавом делу спектра са повећањем дужине ланца и у присуству супституента. ^{13}C-NMR хемијска померања чворних атома угљеника померају се ка мањим δ вредностима у присуству електрон-донорских група, док се δ вредности угљеникових атома спољашњих прстенова антраценских делова молекула повећавају у присуству електрон-акцепторских група.

(Примљено 20. јуна, ревидирано 26. новембра 2007)

REFERENCES

1. O. Henze, W. J. Feast, F. Gardebien, P. Jonkheijm, R. Lazzaroni, P. Leclère, E. W. Meijer, A. P. H. J. Schenning, *J. Am. Chem. Soc.* **128** (2006) 5923
2. P. Lu, G. M. Xia, *J. Serb. Chem. Soc.* **70** (2005) 201
3. G. M. Xia, P. Lu, G. B. Xu, *J. Serb. Chem. Soc.* **69** (2004) 335
4. C. Visy, E. Pinter, T. Fülei, R. Patakfalvi, *Synth. Met.* **152** (2005) 13
5. I. H. Jenkins, P. G. Pickup, *Macromolecules* **26** (1993) 4450
6. I. H. Jenkins, U. Salzner, P. G. Pickup, *Chem. Mater.* **8** (1996) 2444
7. J. Y. Bergeron, L. H. Dao, *Macromolecules* **25** (1992) 3332
8. M. J. Marsella, Z. Q. Wang, R. H. Mitchell, *Org. Lett.* **2** (2000) 2979
9. I. Cianga, Y. Yagci, *Prog. Polymer Sci*. **29** (2004) 387
10. Y. Sasada, Y. Shibasaki, M. Suzuki, M. Ueda, *Polymer* **44** (2003) 355
11. Z. Q. Hu, H. Y. Hu, C. F. Chen, *J. Org. Chem.* **71** (2006) 1131
12. W. Cui, X. Zhang, X. Jiang, H. Tian, D. Yan, Y. Geng, X. Jing, F. Wang, *Org. Lett*. **8** (2006) 785
13. Hodge, G. A. Power, M. A. Rabjohns, *Chem. Commun*. (1997) 73
14. B. Fan, L. Qu, G. Shi, *J. Electroanal. Chem*. **575** (2005) 287
15. M. Baumgarten, U. Müller, A. Bohnen, K. Müllen, *Angew. Chem. Int. Edn. Engl*. **31** (1992) 448
16. I. Schopov, C. Jossifov, *Polymer* **19** (1978) 1449
17. M. Satoh, F. Uesugi, M. Tabata, K. Kaneto, K. Yoshino, *J. Chem. Soc. Chem. Commun.* **12** (1986) 979
18. M. J. Frisch, G. W. Trucks, H. B. Schlegel, G. E. Scuseria, M. A. Robb, J. R. Cheeseman, J. A. Montgomery Jr., T. Vreven, K. N. Kudin, J. C. Burant, J. M. Millam, S. S. Iyengar, J. Tomasi, V. Barone, B. Mennucci, M. Cossi, G. Scalmani, N. Rega, G. A. Petersson, H. Nakatsuji, M. Hada, M. Ehara, K. Toyota, R. Fukuda, J. Hasegawa, M. Ishida, T. Nakajima, Y. Honda, O. Kitao, H. Nakai, M. Klene, X. Li, J. E. Knox, H. P. Hratchian, J. B. Cross, C. Adamo, J. Jaramillo, R. Gomperts, R. E. Stratmann, O. Yazyev, A. J. Austin, R. Cammi, C. Pomelli, J. W. Ochterski, P. Y. Ayala, K. Morokuma, G. A. Voth, P.

Salvador, J. J. Dannenberg, V. G. Zakrzewski, S. Dapprich, A. D. Daniels, M. C. Strain, O. Farkas, D. K. Malick, A. D. Rabuck, K. Raghavachari, J. B. Foresman, J. V. Ortiz, Q. Cui, A. G. Baboul, S. Clifford, J. Cioslowski, B. B. Stefanov, G. Liu, A. Liashenko, P. Piskorz, I. Komaromi, R. L. Martin, D. J. Fox, T. Keith, M. A. Al-Laham, C. Y. Peng, A. Nanayakkara, M. Challacombe, P. M. W. Gill, B. Johnson, W. Chen, M. W. Wong, C. Gonzalez, J. A. Pople, *Gaussian 03, Revision B. 01*, Gaussian Inc., Pittsburgh, PA 2003
19. S. Wu, Q. Teng, X. Chen, R. Zhou, *Chem. J. Chin. Univ.* **24** (2003) 1271
20. L. Zhu, Q. Teng, S. Wu, *J. Serb. Chem. Soc.* **72** (2007) 375
21. L. Qi, Q. Teng, S. Wu, Z. Liu, *Chem. J. Chin. Univ.* **26** (2005) 1909
22. Z. Wang, S. Wu, *Chem. Pap.* **61** (2007) 313
23. A. N. Pankratov, A. V. Shalabay, *J. Serb. Chem. Soc.* **72** (2007) 151
24. L. Ding, Y. Ding, Q. Teng, K. Wang, *J. Chin. Chem. Soc.* **54** (2007) 853
25. L. Yang, A. M. Ren, J. K. Feng, J. F. Wang, *J. Org. Chem.* **70** (2005) 3009
26. S. Wu, Q. Teng, *Int. J. Quantum Chem.* **106** (2006) 526
27. Q. Teng, S. Wu, *J. Mol. Struct.* (*TheoChem*) **756** (2005) 103
28. Q. Teng, S. Wu, *J. Mol. Struct.* (*Theochem*) **719** (2005) 47
29. Q. Teng, S. Wu, *Int. J. Quantum Chem.* **104** (2005) 279
30. M. A. Thompson, M. C. Zerner, *J. Am. Chem. Soc.* **113** (1991) 8210
31. M. A. Hsu, T. J. Chou, *J. Chin. Chem. Soc.* **52** (2005) 811
32. Z. Kačarević-Popović, D. Kostoski, L. Novaković, N. Miljević, B. Šećerov, *J. Serb. Chem. Soc.* **69** (2004) 1029.

www.shd.org.rs

Journal of the Serbian Chemical Society

JSCS@tmf.bg.ac.yu • www.shd.org.rs/JSCS

J. Serb. Chem. Soc. *73* (12) 1197–1209 (2008)
JSCS–3799

UDC 546.78–261+546.92:544.6.004.2
Original scientific paper

Electrochemical properties of mixed WC and Pt-black powders

MAJA D. OBRADOVIĆ[1*#], BILJANA M. BABIĆ[2], ANDRZEJ KOWAL[3], VLADIMIR V. PANIĆ[1#] and SNEŽANA LJ. GOJKOVIĆ[4#]

[1]*Institute of Chemistry, Technology and Metallurgy, University of Belgrade, Njegoševa 12, 11001 Belgrade, Serbia,* [2]*Vinča Institute of Nuclear Sciences, P. O. Box 522, 11001 Belgrade, Serbia,* [3]*Institute of Catalysis and Surface Chemistry, Polish Academy of Sciences, Niezapominajek 8, 30-239 Krakow, Poland and* [4]*Faculty of Technology and Metallurgy, University of Belgrade, Karnegijeva 4, 11120 Belgrade, Serbia*

(Received 7 July, revised 28 August 2008)

Abstract: The electrochemical characteristics of a mixture of Pt-black and WC powders and its catalytic activity for methanol and formic acid oxidation were investigated in acid solution. XRD and AFM measurements revealed that the WC powder employed for the investigation was a single-phase material consisting of crystallites/spherical particles of average size of about 50 nm, which were agglomerated into much larger particles. Cyclic voltammetry showed that the WC underwent electrochemical oxidation, producing tungstate species. In the case of the mixed Pt + WC powders, the tungstate species were deposited on the Pt as a thin film of hydrous tungsten oxide. Enhanced hydrogen intercalation in the hydrous tungsten oxide was observed and it was proposed to be promoted in mixed powders by the presence of hydrogen adatoms on bare Pt sites. The determination of Pt surface area in the Pt + WC layer by stripping of underpotentially deposited Cu revealed that the entire Pt surface was accessible for underpotential deposition of Cu. Investigation of the electrochemical oxidation of methanol and formic acid on Pt + WC and pure Pt layers did not indicate electrocatalytic promotion due to the presence of WC.

Keywords: tungsten carbide; platinum; hydrogen intercalation; methanol oxidation; formic acid oxidation.

INTRODUCTION

It is expected that fuel cell research and development will provide an environmental friendly power source for vehicles and portable electronic devices. Proton exchange membrane fuel cells (PEMFC) are advantageous since they operate at low temperatures and hence do not require expensive or large containment structures. Oxygen reduction is the cathodic reaction in PEMFCs, while the oxi-

* Corresponding author. E-mail: obradovic@ihtm.bg.ac.rs
# Serbian Chemical Society member.
doi: 10.2298/JSC0812197O

dation of hydrogen or some small organic molecule occurs on the anode. Methanol distinguishes itself from other fuels because it is an inexpensive liquid and easy for handling, storage and transport.[1] Formic acid is another example since its oxidation commences at a less positive potential than methanol oxidation, while the crossover of formic acid through the polymer membrane is lower than that of methanol.[2]

Platinum is the most active single metal catalyst for the methanol oxidation reaction (MOR), although the onset potential is rather far from the thermodynamic value. Modification of Pt by various metals has been widely investigated, but there is general agreement that only Pt–Ru surfaces are much more active than single Pt. Recently, several researchers reported the use of tungsten carbide as a support for Pt particles[3,4] because of the influence of tungsten species on the activity of Pt for the MOR. Some earlier investigations of the MOR showed enhancement of the reaction rate on rare earth tungsten bronze doped with Pt,[5] platinum–tungsten oxide,[6,7] carbon-supported platinum modified with WO_y[8] and high surface area tungsten oxide containing Pt centers.[9] However, it was also reported that the presence of polyoxotungstates on Pt can suppress the interfacial formation of PtOH/PtO,[10] which participates in the oxidation process of organic molecules. On the other hand, Pt/WC exhibited a lower onset potential for CO oxidation than Pt nanoparticles supported on high surface area carbons, but the activities of Pt/WC and Pt/C for the MOR were similar.[4]

The results of an investigation of the electrochemical properties of a mixture of Pt-black and WC powders are reported in this work. The aim of the investigation was to give basic insight into the activity of the mixture in the oxidation of small organic molecules with respect to Pt alone. This study should supply additional information whether the synthesis of Pt nanoparticles supported on tungsten-based materials would be beneficial.

EXPERIMENTAL

Platinum black powder (Alfa Aesar, BET specific surface area: 24–29 $m^2 g^{-1}$) and tungsten carbide powder, provided by Woksal, Užice, Serbia, were used as the electrocatalysts. The powders were applied onto a glassy carbon substrate (Tacussel rotating disk electrode, 5 mm in diameter) from the ink to form a thin layer.[11] The Pt black powder was suspended in high purity water, while WC and the mixture of WC and Pt black were suspended in 2-propanol (Merck). In all cases, 50 μl of a Nafion® solution (5 wt. %, 1100 E.W., Aldrich) was added per 1.0 cm^3 of the suspension, in order to insure adhesion of the layer. The concentrations of Pt and WC in the suspensions were 10 and 40 mg cm^{-3}, respectively. After 1 h agitation in an ultrasonic bath (70 kHz), 5.0 μl of the suspension was placed onto a glassy carbon electrode by micro-pipette and left to dry overnight.

It should be noted that in preliminary experiments, WC and WC + Pt suspensions were prepared in water, but a certain change of the suspension and data non-reproducibility were observed. The voltammetric responses of thin layers made day by day from the same water suspension differed, indicating a decrease in the Pt surface area.

A three-compartment electrochemical glass cell with a large surface area Pt wire (99.998 % purity, Aesar) as the counter electrode and a saturated calomel electrode (SCE) as the reference electrode was used. All the potentials reported in this paper are expressed on the scale of the reversible hydrogen electrode (RHE). The supporting electrolyte of 0.10 M H_2SO_4 (Merck) was prepared with high purity water (Millipore, 18 MΩ cm resistivity). The electrolyte was deaerated by bubbling with N_2 previously purified by flowing through an ammonium metavanadate solution. Electrochemical oxidation of methanol and formic acid were investigated in deaerated supporting electrolyte which contained 0.10 M CH_3OH or 0.10 M HCOOH (Merck). The experiments were conducted at 298±0.5 K. A Pine RDE4 potentiostat and Philips PM 8143 *X–Y* recorder were employed.

WC powder was characterized by X-ray diffraction (XRD) analysis using a Siemens D500 diffractometer with CuKα radiation over the 2θ range from 10 to 90° at a scan rate of 0.04° s^{-1}. To determine the WC surface area, adsorption/desorption isotherms of N_2 were registered at –196 °C by the gravimetric McBain method. The appearance of WC powder was examined by atomic force microscopy (AFM) using a NanoScope 3D (Veeco, USA). A drop of WC suspension in 2-propanol was placed on a mica surface and left to dry. Then the imaging was performed in the contact mode using NanoProbes silicon nitride cantilevers with a force constant of 0.060 N m^{-1}.

RESULTS AND DISCUSSION

Characterization of the WC

The XRD pattern of the WC powder (Fig. 1) indicates pure single-phase WC of hcp symmetry with the lattice parameters $a_0 = b_0 = 0.29053$ nm and $c_0 = = 0.28385$ nm. The crystallite size, calculated from the width of the (101) peak using the Scherrer equation, was found to be about 40 nm. The BET real surface area of the WC was calculated to be 0.7 m^2 g^{-1}. Assuming spherical powder particles and taking 15.6 g cm^{-3} for the density of WC, a particle diameter corresponding to the BET surface area of 0.5 μm was calculated. Comparison of the XRD and BET results indicates that the particles of WC powder are compact agglomerates of smaller crystallites. This was proved by the AFM technique. The typical appearance of a WC agglomerate consisting of densely-packed, nearly spherical particles of 50 to 150 nm in size is presented in Fig. 2.

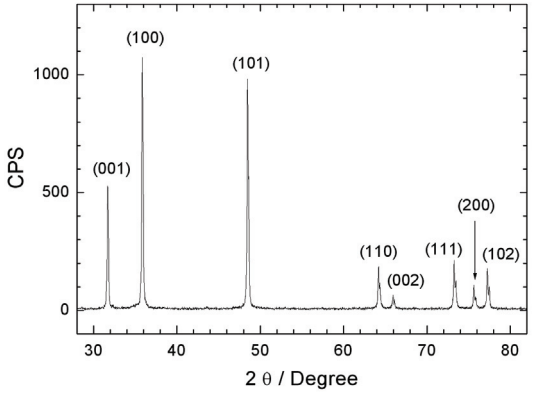

Fig. 1. XRD Pattern of the WC powder sample.

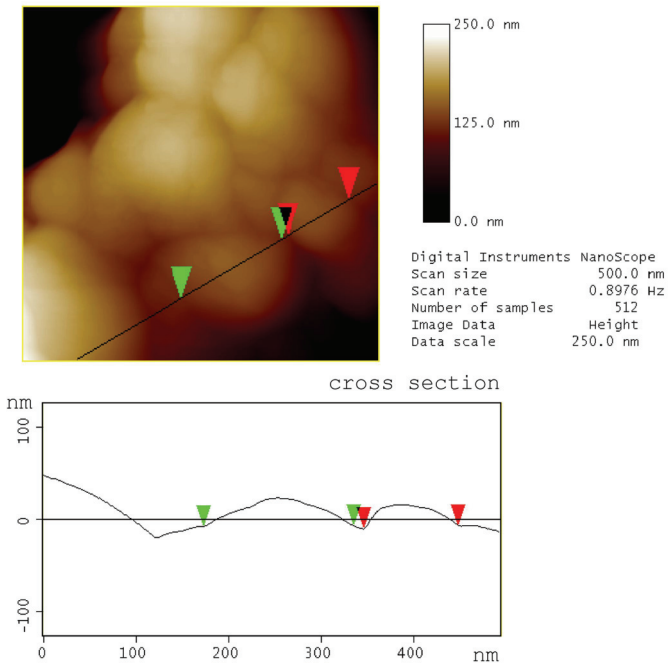

Fig. 2. The results of AFM analysis of WC powder: height image and cross section analysis.

Cyclic voltammograms of WC powder registered in 0.10 M H_2SO_4 are given in Fig. 3. When the potential was cycled between 0.050 and 0.75 V, the voltammogram was stable over time, featuring a broad anodic peak and an increase in the cathodic current at $E < 0.40$ V. In the first cycle toward more positive potentials (up to 1.25 V), an anodic peak at ≈ 1.06 V, followed by a subsequent increase in the anodic current was observed. In the second cycle, the peak and subsequent current decreased and finally reached steady-state values after the 20th cycle, as shown by the steady-state curve in Fig. 3. Upon resetting the positive potential limit back to 0.75 V, a voltammetric response like the very first one was regained.

In the presence of water and/or oxygen, WC oxidizes to surface oxide and/or soluble W(VI) species:[12,13]

$$WC + 5H_2O \rightarrow WO_3 + CO_2 + 10H^+ + 10e^- \quad (1)$$

$$WC + 6H_2O \rightarrow WO_4^{2-} + CO_2 + 12H^+ + 10e^- \quad (2)$$

The cyclic voltammogram of WC recorded in the narrow potential range (Fig. 3, 1st curve) resembles the voltammetric behavior of WO_3,[14] which indicates that the WC surface was in the oxidized state. The WO_3 layer formed spontaneously on the WC surface was partially reduced in the cathodic scan by the intercalated hydrogen:[15]

$$WO_3 + xH^+ + xe^- \rightarrow H_xWO_3 \qquad 0.1 < x < 0.5 \qquad (3)$$

The H_xWO_3 species are known as hydrogen–tungsten bronzes. The cathodic current at $E < 0.40$ V should correspond to the hydrogen intercalation process, while the broad anodic peak is very likely due to deintercalation. The anodic peak at ~1.06 V can be assigned to further oxidation of WC.[16] The products of this reaction are probably insoluble and their deposition on the electrode surface causes a decrease in the anodic current, as shown in Fig. 3.

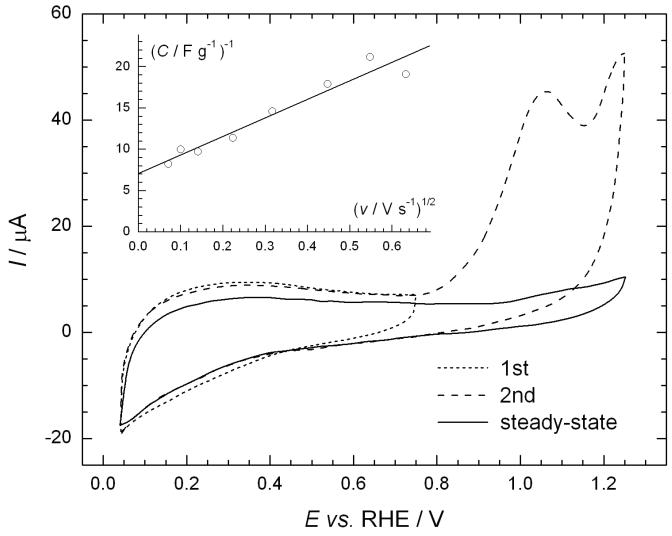

Fig. 3. The first, second and steady state cyclic voltammograms of the WC thin layer (1.27 mg WC cm^{-2}) recorded in deaerated 0.10 M H_2SO_4 at 50 mV s^{-1}. Inset: reciprocal of specific capacitance of the WC thin layer, calculated between 0.56 and 0.75 V from the steady-state voltammograms, as a function of the square root of sweep rate.

Assuming that the intercalation/deintercalation processes are accomplished at potentials above 0.55 V, the double layer capacitance of the passive film on WC was estimated from the voltammetric charge between 0.56 and 0.75 V from the steady-state voltammograms. As the inset in Fig. 3 shows, the capacitance was slightly dependent on the sweep rate, due to the porous structure. Extrapolation of the reciprocal capacitance to zero sweep rate[17] gives a total double layer capacitance of the film, C_{tot}, of 0.14 F g^{-1}. Assuming the most typical value for double layer capacitance of 20 μF cm^{-2}, a specific surface area of 0.70 m^2 g^{-1} is calculated, which coincides with the obtained BET surface area. This result indicates that native WC spherical particles within micro-sized agglomerates, as seen by AFM (Fig. 2) and calculated from XRD, are not accessible to the electrolyte, but only the surface defined by the agglomerates through the micro-pores of the layer.

Voltammetry of the Pt + WC mixture

The voltammetric behavior of mixed WC and Pt black powders is illustrated in Fig. 4. The first cycle with a positive potential limit of 0.75 V resembles the hydrogen adsorption/desorption features of Pt sites. After extension of the positive potential limit to 1.25 V, the cyclic voltammogram features the formation of Pt oxide and its reduction, as well as the development of a pair of peaks at 0.14 and 0.30 V, due to an intensive oxidation of WC. On cycling of the potential, the height of the peaks increased, while the anodic current due to the oxidation of WC decreased and eventually disappeared, similar to the behavior of pure WC powder (Fig. 3).

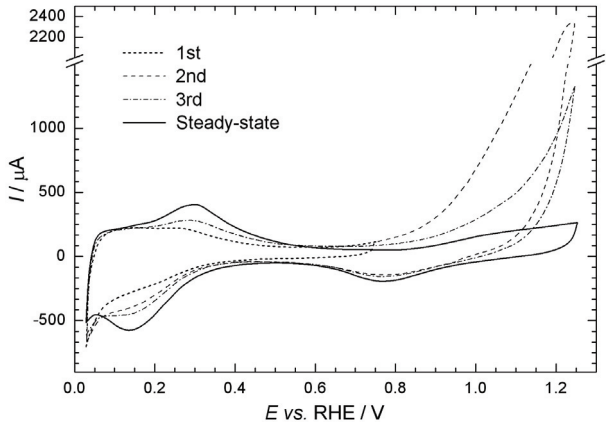

Fig. 4. Successive and steady state cyclic voltammograms of the WC + Pt thin layer (1.02 mg WC cm^{-2} + 0.25 mg Pt cm^{-2}) recorded in de-aerated 0.10 M H_2SO_4 at 50 mV s^{-1}.

The steady-state cyclic voltammograms of the single Pt black and WC powders and the mixture of Pt and WC are presented in Fig. 5. Bearing in mind that in the mixed layer and in the single layers, the amounts of Pt are identical and the amounts of WC are similar, the voltammetric charges can be directly analyzed. It is obvious from Fig. 5 that the voltammetric features of the mixture are not the simple superposition of the voltammograms of its components. The charge under the peaks at 0.14/0.30 V is significantly higher than the charge for the monolayer adsorption/desorption of hydrogen on Pt particles present in the mixture and considerably higher in comparison to the hydrogen intercalation/deintercalation charge on WC. In addition, the formation of Pt-oxide is hindered in the presence of WC. Jeon *et al.*[4] recently proposed that spillover of hydrogen from Pt to WC supplies a fresh Pt surface, resulting in the increased charge of H adsorption/desorption on the Pt sites. However, the peaks related to H adsorption/desorption on the Pt sites on the voltammogram of the Pt + WC mixture are displaced with respect to those of pure Pt or highly overlapped with the peaks at 0.14/0.30 V, related to the catalyzed oxidation of WC (Fig. 4). This observation leads to the assumption that soluble tungstate species, produced during the oxidation of WC, can be deposited onto Pt sites. The deposited layer is subjected to intercalation/deintercalation of

hydrogen, which results in the appearance of pronounced peaks at 0.14/0.30 V. When WC alone was attached to the electrode surface, anodic oxidation of WC did not produce any additional voltammetric features (Fig. 3) related to the enhanced intercalation/deintercalation process. This indicates that the deposition of intercalation-active tungstates occurs preferentially on Pt.

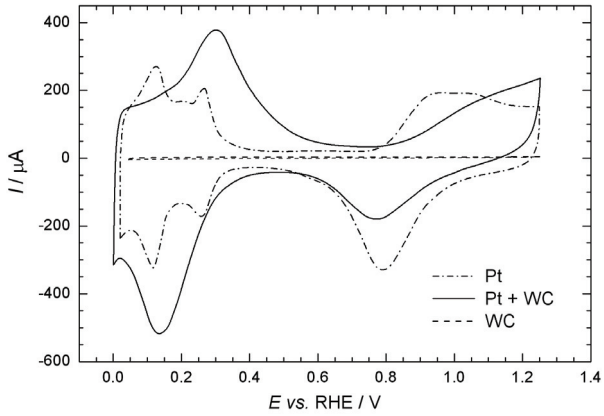

Fig. 5. Steady-state cyclic voltammograms of thin layers of WC (1.27 mg WC cm^{-2}), Pt (0.25 mg cm^{-2}) and Pt + WC (0.25 mg Pt cm^{-2} + 1.02 mg WC cm^{-2}) recorded in deaerated 0.10 M H_2SO_4 at 20 mV s^{-1}.

To calculate the pseudocapacitance of the hydrogen intercalation in the WC and WC + Pt layers, the anodic parts of the voltammograms recorded at sweep rates from 5 to 400 mV s^{-1} were integrated in the potential range from 0.050 to 0.56 V. A dependence of the pseudocapacitance on the sweep rate was registered for both the WC and WC + Pt layers. Such a behavior is due to diffusion-limited pseudocapacitive process within the porous layer of hydrous tungsten oxide formed atop the WC and Pt sites. According to the model proposed by Ardizzone *et al.*,[18] the mobility of the protons involved in Reaction (3) is hindered by the porous structure of the layer, resulting in the following pseudocapacitance *vs*. sweep rate relationships:

$$\frac{1}{C} = \frac{1}{C_{\text{tot}}} + k\sqrt{v} \tag{4}$$

$$C = C_{\text{out}} + \frac{k'}{\sqrt{v}} \tag{5}$$

where C_{tot} is the total capacitance of the porous structure, C_{out} is the capacitance of the outer layer surface (facing the bulk of the electrolyte), while the capacitance of the inner surface relates to the loose grain boundaries, C_{in}, can be calculated as $C_{\text{in}} = C_{\text{tot}} - C_{\text{out}}$.[19]

The C *vs*. $v^{-1/2}$ and C^{-1} *vs*. $v^{1/2}$ plots for WC and the mixture WC + Pt are presented in Fig. 6. Reasonably straight lines were obtained and the total pseudocapacitances were calculated. From the C *vs*. $v^{-1/2}$ plots (Fig. 6a), the pseudocapacitances related to the outer layer of hydrous tungsten oxide in both the WC

and WC + Pt layer were determined. Since the pseudocapacitances calculated in this way include the double layer capacitance, its value of 0.14 F g^{-1} (inset in Fig. 3) was subtracted. In the case of the WC + Pt mixture, the pseudocapacitance of hydrogen adsorption/desorption on Pt sites (which was found to be independent of the sweep rate) was also subtracted from the total pseudocapacitance charge. This was done assuming that hydrogen adsorption is undisturbed by the presence of WC and the products of its oxidation. The corrected pseudocapacitances of hydrogen intercalation expressed per mass of WC are given in Table I, from which it can be observed that the total pseudocapacitance is more than doubled in the presence of Pt and that the structure of the hydrous oxide layer is significantly changed. The C_{out}/C_{tot} ratio shows that for the hydrous oxide formed on WC with no Pt in the film, only about 8 % of the electroactive sites were on the surface, indicating a highly porous structure. However, when Pt was present in the film, about 80 % of the electroactive sites were easily accessible surface sites. This can be rationalized if the Pt was partially covered by thin hydrous tungsten oxide layer with the majority of its active sites being surface sites facing the electrolyte. Such a film can exhibit a higher pseudocapacitance than that on WC without Pt in the layer only if the hydrogen atoms adsorbed on Pt sites spillover to the hydrous tungsten oxide and intercalate in it.[15,20]

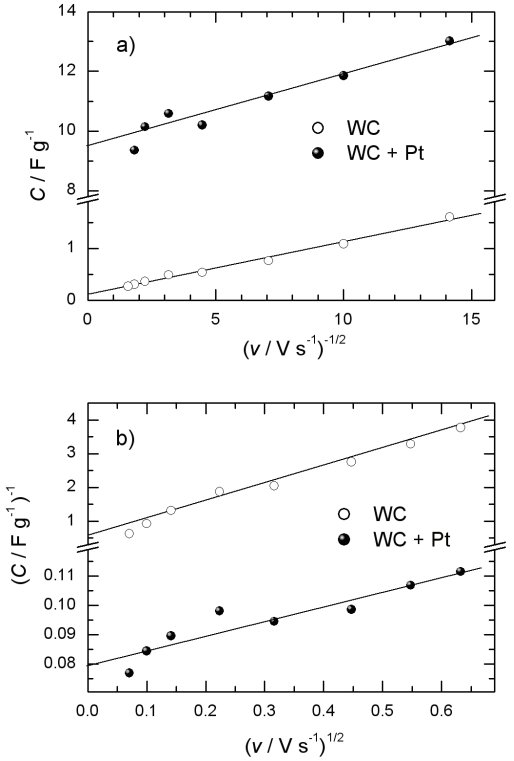

Fig. 6. a) C *vs.* $v^{-1/2}$ and b) C^{-1} *vs.* $v^{1/2}$ plots for WC and WC + Pt layer.

TABLE I. Corrected values of the pseudocapacitance for hydrogen intercalation into hydrous tungsten oxide for WC and WC + Pt thin layers, calculated per mass of WC

Electrode	C_{tot} / F g^{-1}	C_{out} / F g^{-1}	C_{out}/C_{tot}
WC	2.17	0.165	0.076
Pt + WC	4.90	3.79	0.77

Determination of the Pt surface area in the WC + Pt electrode layer

The determination of the real surface area of a catalyst is a crucial point in the assessment of its activity. The surface area of Pt can be determined from the charge of hydrogen adsorption/desorption. In the calculation, it is assumed that a complete monolayer is formed, which requires 210 μC cm^{-2}. However, the hydrogen adsorption/desorption features of Pt in the cyclic voltammogram of the WC + Pt mixture (Fig. 4) are partly discernible only when the anodic limit is set to before the onset of the oxidation of WC. After a substantial amount of WC had been oxidized, large peaks of hydrogen intercalation/deintercalation mask the Pt peaks. Therefore, some alternative method should be applied to determine Pt surface area. Recently, Green and Kucernak[21] reported that the surface area of Pt alloyed with Ru can be successfully determined from the stripping of underpotentially deposited (UPD) copper. This method is also applicable to the WC + Pt system since the anodic peak of Cu stripping is more positive than the peak for hydrogen deintercalation from the hydrous tungsten oxide. In addition, WC alone was found to be inactive for UPD Cu.

Copper was underpotentially deposited from a solution of 0.10 M H_2SO_4 and 2.0×10^{-3} M $CuSO_4$ at a potential of 0.330 V *vs*. RHE, which is about 15 mV more positive than the equilibrium potential of Cu electrodeposition in the applied electrolyte. After 2 min of deposition, which is sufficient for a complete monolayer to be formed,[21] the electrode potential was swept anodically and the stripping voltammogram was recorded. The result obtained for a polycrystalline Pt electrode and for a layer of Pt-black powder are shown in Fig. 7a and 7b, respectively. For sake of comparison, the cyclic voltammograms in the supporting electrolyte are also given. The Cu stripping curves reveal at least three different energetic states of Cu, which are similar for polycrystalline Pt and Pt-black powder. The stripping curves, corrected for the background current of Pt, were integrated and the charges were compared to the hydrogen desorption charge. The Cu(UPD)/H(UPD) ratio was calculated to be 1.8 for polycrystalline Pt and 2.3 for Pt-black, which is close to the theoretical value of 2. These results confirm that the Pt surface area can be estimated using the procedure of Cu UPD and stripping as described above. The experiment with the Pt + WC mixture show that the Cu stripping peak is shifted anodically but the charge beneath the peak corresponds to the surface area of Pt in the layer.

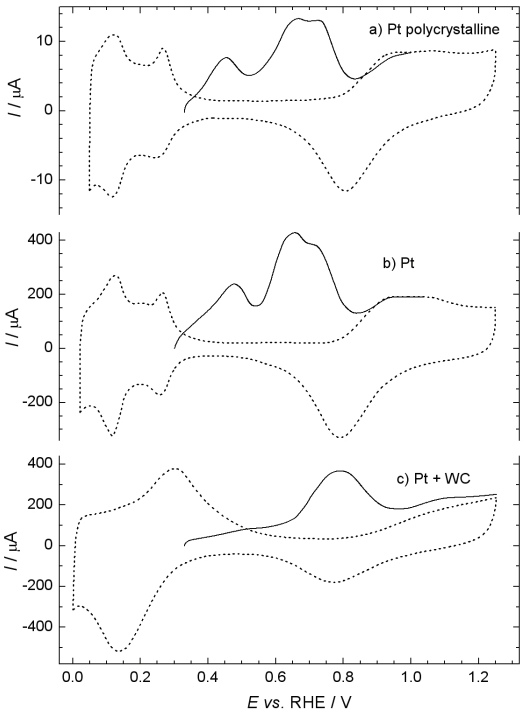

Fig. 7. Cyclic voltammograms of: a) Pt polycrystalline electrode, b) thin layer of Pt (0.25 mg cm^{-2}) and c) thin layer of Pt + WC (0.25 mg Pt cm^{-2} + 1.02 mg WC cm^{-2}) recorded in 0.10 M H_2SO_4 (dashed lines) and Cu stripping voltammograms recorded in the presence of 2.0×10^{-3} M $CuSO_4$ (solid lines) at 20 mV s^{-1}.

Voltammetric experiments for the Pt + WC mixture revealed that a thin layer of hydrous tungsten oxide was deposited on Pt (Figs. 4 and 5, Table I). However, Cu stripping showed that the entire surface area of Pt in the film was accessible to Cu UPD. It should also be noted that formation of Pt-oxide was hindered by the presence of WC (Fig. 4) and that the Cu stripping peak was shifted anodically with respect to the peak on pure Pt (Fig. 7). Thus, it can be anticipated that small organic molecules, such as CH_3OH and HCOOH, would be able to approach the Pt surface through the tungsten oxide film, but the electrocatalytic properties of the Pt might be changed due to the presence of the film, as indicated in the literature.[5–9]

Oxidation of methanol and formic acid

The oxidation of methanol and formic acid were investigated on a layer of the WC + Pt mixture after the steady-state voltammogram (Fig. 5) had been established. Methanol or formic acid was added into the cell while holding the potential at 0.10 V. After 2 min, a potential sweep was applied at a rate of 1.0 mV s^{-1} and the polarization curve was recorded. Concerning the results of Cu stripping on the WC + Pt mixture, the current densities were calculated with respect to the entire surface area of Pt in the catalyst layer, assuming that the Pt sites were equally available for UPD of Cu and the oxidation of the organics. The same

experiments were performed on pure Pt-black layers and the results were compared. The diagrams in Fig. 8 show overlapping of the results for pure Pt and the WC + Pt mixture, meaning that hydrous tungsten oxide formed by the oxidation of WC does not influence the activity of Pt for the oxidation of methanol and formic acid.

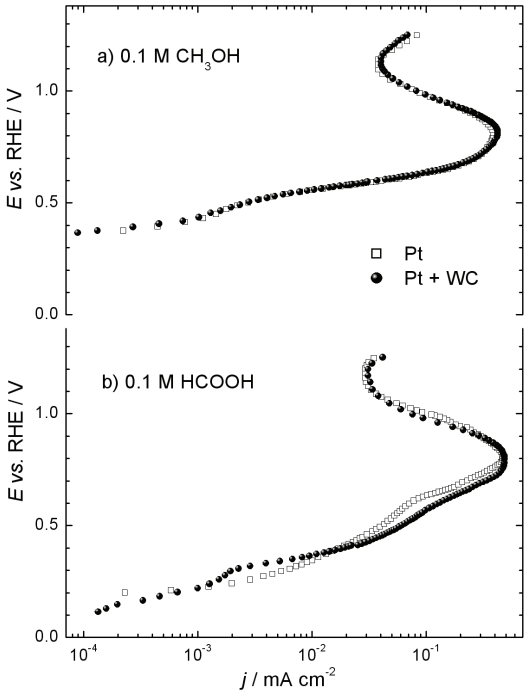

Fig. 8. Tafel plots for the oxidation of a) 0.10 M CH_3OH and b) 0.10 M HCOOH on the thin layers of Pt and WC + Pt in deaerated 0.10 M H_2SO_4. Sweep rate: 1.0 mV s^{-1}.

CONCLUSIONS

Cyclic voltammetry revealed that WC undergoes electrochemical oxidation, which produces tungstate species. In the case of the mixed WC + Pt powders, these species appeared to be deposited onto Pt in a form of a hydrous tungsten oxide. Enhanced hydrogen intercalation in the hydrous tungsten oxide was observed and it is proposed that this process was promoted by the spillover of the hydrogen adatoms on the bare Pt sites. The presence of WC in the Pt catalyst layer had no effect on the kinetics of methanol and formic acid oxidation, assuming that the part of Pt surface covered by hydrous tungsten oxide did not hinder the approach of the organics to the Pt beneath.

Acknowledgements. This work was financially supported by the Ministry of Science of the Republic of Serbia, contract Nos. 142048 and 142056.

ИЗВОД

ЕЛЕКТРОХЕМИЈСКА СВОЈСТВА СМЕШЕ ПРАХОВА WC И Pt

МАЈА Д. ОБРАДОВИЋ[1], БИЉАНА М. БАБИЋ[2], ANDRZEJ KOWAL[3], ВЛАДИМИР В. ПАНИЋ[1] и СНЕЖАНА Љ. ГОЈКОВИЋ[4]

[1]Институт за хемију, технологију и металургију, Универзитет у Београду, Његошева 12, 11001 Београд, [2]Институт за нуклеарне науке "Винча", п. пр. 522, 11001 Београд, [3]Institute of Catalysis and Surface Chemistry, Polish Academy of Sciences, Niezapominajek 8, 30-239 Krakow, Poland и [4]Технолошко–металуршки факултет, Универзитет у Београду, Карнегијева 4, 11120 Београд

У раду су испитиване електрохемијске карактеристике смеше прахова Pt и WC и њена каталитичка активност за реакције оксидације метанола и мрављe киселине у киселом раствору. Анализа резултата дифракције X-зрака (XRD) и микроскопије атомских сила (AFM) показују да је прах WC једнофазни материјал са просечном величином кристалита од око 50 nm, који су агломерисани у много веће честице. Циклична волтаметрија указује на то да WC подлеже оксидацији којом настају волфраматне врсте. У случају смеше прахова Pt и WC, волфраматне врсте највероватније се таложе на Pt у облику танког слоја хидратисаних оксида волфрама. Примећено је повећање интеркалације водоника у слоју хидратисаних волфрамата и претпоставља се да присуство адатома водоника на површини Pt потпомаже процес водоничне интеркалације. Одређивање површине Pt у слоју Pt + WC десорпцијом монослоја Cu таложеног на потпотенцијалима указује да је читава површина Pt доступна за таложење атома Cu. Испитивање електрохемијских реакција оксидације метанола и мрављe киселине на слоју смеше Pt + WC и слоју чисте Pt указује да присуство праха WC не утиче на електрокаталитичка својства Pt.

(Примљено 7. јула, ревидирано 28. августа 2008)

REFERENCES

1. S. Wasmus, A. Küver, *J. Electroanal. Chem*. **461** (1999) 14
2. X. Yu, P. Pickup, *J. Power Sources* **182** (2008) 24
3. R. Ganesan, J. S. Lee, *Angew. Chem. Int. Ed*. **44** (2005) 6557
4. M. K. Jeon, H. Daimon, K. R. Lee, A. Nakahara, S. I. Woo, *Electrochem. Commun*. **9** (2007) 2692
5. K. Machida, M. Enyo, G. Adachi, J. Shiokawa, *J. Electrochem. Soc*. **135** (1988) 1955
6. M. B. Oliveira, L. P. R. Profeti, P. Olivi, *Electrochem. Commun*. **7** (2005) 703
7. P. K. Shen, A. C. C. Tseung, *J. Electrochem. Soc*. **141** (1994) 3082
8. A. K. Shukla, M. K. Ravikumar, A. S. Aricò, G. Candiano, V. Antonucci, N. Giordano, A. Hamnett, *J. Appl. Electrochem*. **25** (1995) 528
9. C. Bock, B. MacDougall, *Electrochim. Acta* **47** (2002) 3361
10. M. Chojak, A. Kolary-Zurowska, R. Wlodarczyk, K. Miecznikowski, K. Karnicka, B. Palys, R. Marassi, P. Kulesza, *Electrochim. Acta* **52** (2007) 5574
11. S. Lj. Gojković, A. V. Tripković, R. M. Stevanović, *J. Serb. Chem. Soc*. **72** (2007) 1419
12. J. D. Voorhies, *J. Electrochem. Soc*. **119** (1972) 219
13. M. H. Ghandehari, *J. Electrochem. Soc*. **127** (1980) 2144
14. E. J. McLeod, V. I. Birss, *Electrochim. Acta* **51** (2005) 684
15. P. J. Kulesza, L. R. Faulkner, *J. Electrochem. Soc*. **136** (1989) 707
16. H. Chhina, S. Campbell, O. Kesler, *J. Power Sources* **164** (2007) 431

17. R. De Levie, in *Advances in electrochemistry and electrochemical engineering*, Vol. 6, P. Delahay Ed., Interscience, New York, 1967, p. 329
18. S. Ardizzone, G. Fregonara, S. Trasatti, *Electrochim. Acta* **35** (1990) 263
19. V. Panić, A. Dekanski, S. Milonjić, V. B. Mišković-Stanković, B. Nikolić, *J. Serb. Chem. Soc.* **71** (2006) 1173
20. J. Shim, C.-R. Lee, H.-K. Lee, J.-S. Lee, E. J. Cairns, *J. Power Sources* **102** (2001) 172
21. C. L. Green, A. Kucernak, *J. Phys. Chem. B* **106** (2002) 1036.

www.shd.org.rs

Journal of the Serbian Chemical Society

JSCS@tmf.bg.ac.yu • www.shd.org.rs/JSCS

J. Serb. Chem. Soc. *73* (12) 1211–1221 (2008)
JSCS–3800

UDC 546.82–31:544.773.42:544.5/.6.004.2
Original scientific paper

Photoelectrochemical properties of sol–gel obtained titanium oxide

VLADIMIR V. PANIĆ[1]*#, SANJA I. STEVANOVIĆ[1#], VESNA B. MIŠKOVIĆ-STANKOVIĆ[2#], BRATISLAV Ž. JOVANOVIĆ[2#] and BRANISLAV Ž. NIKOLIĆ[2#]

[1]*Institute of Chemistry, Technology and Metallurgy, University of Belgrade, Njegoševa 12, 11001 Belgrade and* [2]*Faculty of Technology and Metallurgy, University of Belgrade, Karnegijeva 4, 11120 Belgrade, Serbia*

(Received 2 July, revised 12 October 2008)

Abstract: The photoelectrochemical properties of a sol–gel prepared titanium oxide coating applied onto a Ti substrate were investigated. The oxide coating was formed from an inorganic sol thermally treated in air at 350 °C. The coating consisted of agglomerates of narrow size distribution around 100 nm. The photoelectrochemical characteristics were evaluated by investigating the changes in the open circuit potential, current transients and impedance characteristics of a Ti/TiO_2 electrode upon illumination by UV light in H_2SO_4 solution and in the oxidation of benzyl alcohol. The electrode was found to be active for photoelectrochemical reactions in the investigated solutions.

Keywords: photoelectrochemical activity; titanium oxide; oxide sol; sol–gel procedure; electrochemical impedance spectroscopy.

INTRODUCTION

Owing to its good chemical stability, physico–chemical characteristics, electrical and optical properties, titanium oxide is a widespread material investigated in many fields of fundamental and applied science. The anatase crystalline form is known for its photocatalytic properties upon UV illumination, while the rutile form is most famous as a white pigment in dye technology.[1] In organic reactions, TiO_2 is widely used as a photocatalyst in an aqueous (waste water treatment)[2] as well as in a non-aqueous environment (organic synthesis).[3–5] Additionally, it can be used as a carrier for highly dispersed heteropolyacids,[6] electrochemical composite catalysts[7] and as a stabilizing component of electrochemically active oxide coatings on titanium.[8–10] The application of titanium oxide thus envelopes different branches, from the white pigment industry, through sunscreen lotions, so-

* Corresponding author. E-mail: panic@ihtm.bg.ac.rs
# Serbian Chemical Society member.
doi: 10.2298/JSC0812211P

lar cells and toothpastes, to electrochemistry, random access memory, outdoor air purification and waste water treatments.[11]

The photoreactivity of titanium oxide for oxidation reactions is usually explained by the excitation of valence band (vb) electrons.[1] When TiO_2 is illuminated by light of energy greater than that required by the band gap, electrons are transferred to the conduction band (cb), and positive holes (h^+) remain in the vb. The charge carriers very quickly migrate to surface traps lying within the forbidden gap. From there, the holes are populated by electrons from, *e.g.*, organics (R) adsorbed at the surface of the illuminated TiO_2:[12,13]

$$TiO_2 + h\nu \rightleftharpoons TiO_2|e^-_{cb} + TiO_2|h^+_{vb} \quad (1)$$

$$TiO_2|h^+_{vb} + R \rightarrow TiO_2 + R^\bullet \quad (2)$$

In aqueous solutions, the generated holes can also react with adsorbed water molecules or OH^- to produce $^\bullet OH$ radicals, which are able to react with the organics in parallel to reaction (2).[12]

Reversibility by the electron–hole recombination step (Eq. (1)) decreases the reactivity of illuminated TiO_2. This disadvantage can be suppressed if some sink of excited electrons would be available in the system. For example, in oxygen-containing solutions, the excited electrons can reduce O_2 and generate an avalanche of free radicals:[13]

$$e^-_{cb} + O_2 \rightarrow O^-_2 \quad (3)$$

$$O_2 + 2e^-_{cb} + 2H^+ \rightarrow H_2O_2 \quad (4)$$

$$O^-_2 + H_2O_2 \rightarrow HO^- + {}^\bullet OH + O_2 \quad (5)$$

$$O^-_2 + 2H^+ \rightarrow 2{}^\bullet OH \quad (6)$$

$$H_2O_2 + e^-_{cb} \rightarrow {}^\bullet OH + OH^- \quad (7)$$

$$H_2O_2 + h\nu \rightarrow 2{}^\bullet OH \quad (8)$$

However, if titanium oxide would be assembled to conducting materials within a closed electrical circuit, the reactivity can be improved by a bias potential, which will drive away exited electrons to the external circuit of the photoelectrochemical (PEC) cell.[14–16]

The PEC activity of TiO_2 towards numerous organics, from methanol[17] to herbicides,[18] has been investigated intensively.[1,13,16,19,20] It was found that PEC reactivity depends strongly on the conditions of formation of TiO_2, such as preparation procedure,[21,22] precursor type,[18] annealing temperature,[19,23] but also on the possible implantation of electrochemically active metals, such as Pt.[24] Titanium oxides prepared by different procedures can show different PEC activity, although their crystalline structures are quite similar.[22] Generally, a mixture of

anatase and rutile crystalline forms is more active than these forms alone,[19,22] although in the case of commercial Degussa P25 TiO_2, increasing the rutile content (higher annealing temperature) can lead to a considerable decrease in, *e.g.*, the total organic carbon removal efficiency in phenol oxidation.[19]

The aim of this work was to investigate the PEC activity of TiO_2 prepared *via* the sol–gel route employing forced hydrolysis of titanium chloride.[25] Titanium oxide prepared by this procedure already showed some advantages for chlorine and oxygen evolution and phenol oxidation[26] on activated titanium anodes.[10,27] The PEC activity was investigated in H_2SO_4 solution and for the oxidation of benzyl alcohol, which is known for its simple oxidation kinetics.

EXPERIMENTAL

The synthesis of the oxide sol

Titanium oxide sol was prepared by the forced hydrolysis of titanium chloride (15 % $TiCl_3$ in 10 % HCl, Merck) in acid solution.[25] An appropriate amount of titanium chloride was slowly added into boiling 5.0 mol dm^{-3} HCl and aged for 24 h under reflux in an experimental setup equipped with a magnetic stirrer. Vigorous agitation at the boiling temperature results in slow hydrolysis, which results in a solid oxide phase of narrow particle size distribution.[27,28] The size of oxide particles increases with ageing time, while the TiO_2 sols aged more than 20 h were found to be beneficial for good electrochemical properties of binary RuO_2–TiO_2 coatings of activated titanium anodes.[10,27]

The concentration of the solid phase in the prepared oxide colloidal monodispersion, evaluated by evaporation to dryness at 120 °C for 24 h, was 17 mg cm^{-3}.

Preparation of the photoelectrode

The photoelectrochemical properties of the prepared titanium oxide were examined using an electrode assembly consisting of a titanium substrate coated with the prepared oxide sol. A Ti plate, 1 cm×1 cm×0.7 cm in size, etched in 1:1 v/v hot 35 % HCl:H_2O mixture, was used as the substrate. The coating was prepared by painting the oxide sol over the substrate, which was followed by slow evaporation at 70–90 °C. The painting and evaporation steps were repeated until a coating mass of 3 mg per cm^2 of the geometric surface area was attained. The electrode was then subjected to the thermal treatment at 350 °C for 2 h.

The coating was characterized by atomic force microscopy (AFM) technique in air at room temperature. The structural characterization was performed with a NanoScope 3D (Veeco, USA) microscope. The AFM observations were performed in tapping mode using etched silicon probes with a spring constant 20–80 N m^{-1}.

Photoelectrochemical (PEC) characterization

The PEC properties of the prepared Ti/TiO_2 electrode and its photovoltaic activity in the oxidation of benzyl alcohol (BA), 0.010 mol dm^{-3}, were investigated in 1.0 mol dm^{-3} H_2SO_4. Chronopotentiometric, chronoamperometric and electrochemical impedance spectroscopy (EIS) measurements were performed in a standard electrochemical cell equipped with a Pt wire as the counter electrode and a saturated calomel electrode (SCE) as the reference electrode. All experiments were performed at room temperature.

The photoelectrode working area of 0.79 cm^2 faced the electrolyte/air interface at a distance of 5 mm and was illuminated directly in the PEC experiments from above using a UV lamp (λ = 356 nm, 2×8 W, DESAGA UVIS, Germany) placed about 5 cm away from the electrode surface.

RESULTS AND DISCUSSION

The typical appearance of the TiO_2 coating surface is illustrated in Fig. 1 by AFM images taken at two different magnifications. The spherical grains of a uniform size of around 100 nm are continuously distributed all over the coating surface. Earlier X-ray diffraction investigations of the solid phase of prepared sol[25] indicated the oxide amorphous structure, while anatase crystalline structure was formed by thermal treatments up to 450 °C, with only a negligible presence of the rutile phase at higher temperatures. The crystallite size, according to the Scherrer Equation, was about 8 nm. The examination by transmission electron

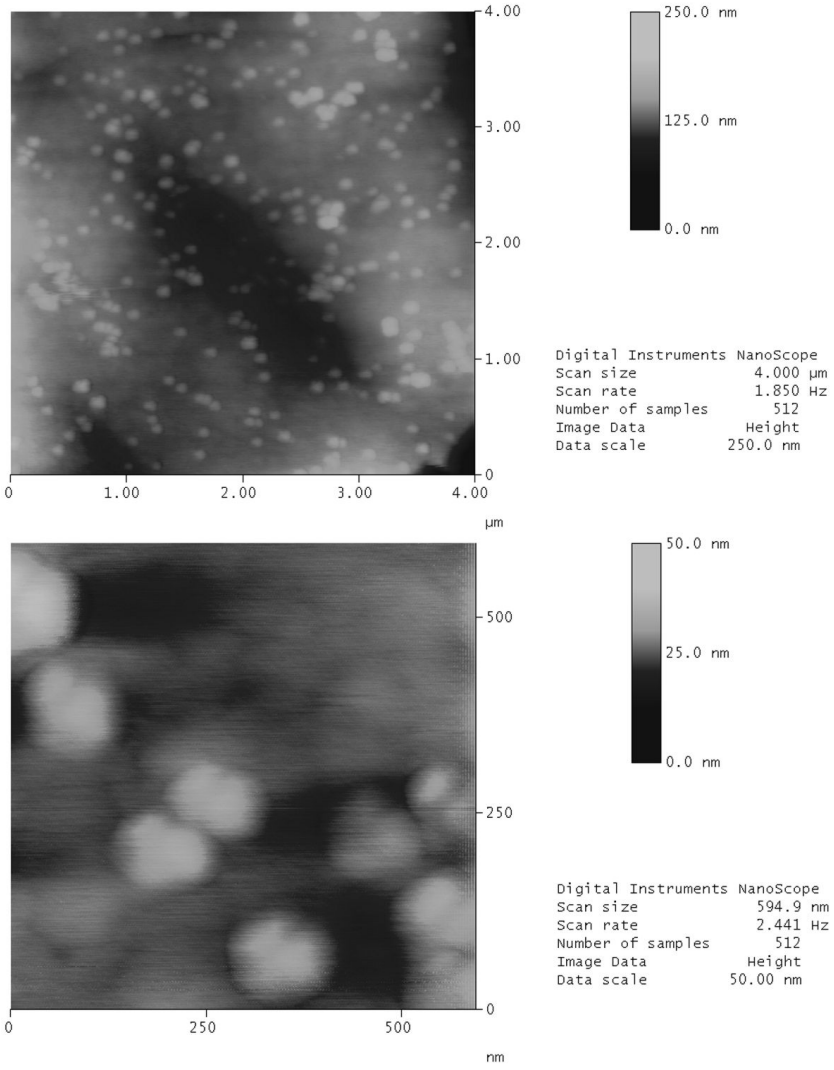

Fig. 1. Typical AFM images of the Ti/TiO_2 electrode surface.

microscopy showed the presence of the 5–25 nm particles, depending on the ageing time.[27] According to these earlier results, it can be emphasized that the grains seen by AFM (Fig. 1) must be agglomerates of small crystallites. The structural AFM investigations indicate that the ageing of the oxide sol under the applied conditions of sol synthesis rather results in the sticking of the formed nanoparticles into large agglomerates than in their primary growth, as is to be expected in the forced hydrolysis process.[27,28]

Photoelectrochemical properties

The influence of UV light on the value of the open circuit potential (OCP) of Ti/TiO_2 electrode in H_2SO_4 solution is illustrated in Fig. 2. Illumination with UV light caused the OCP to take the negative values with respect to those registered under "UV off" condition. The OCP always shifted cathodically since the number of electrons occupying the conduction band was increased by those excited by photons. The photon–electron interaction process appears to be not completely reversible since the preceding "UV off" OCP value can be hardly recovered after illumination. This also holds for the "UV on" OCP value, which shifts anodically with every subsequent UV on/off period. Consequently, the difference between the "UV off" and "UV on" OCP value decreases with the number of UV on/off periods, which indicates a decreasing ability of the photons to excite the electrons.

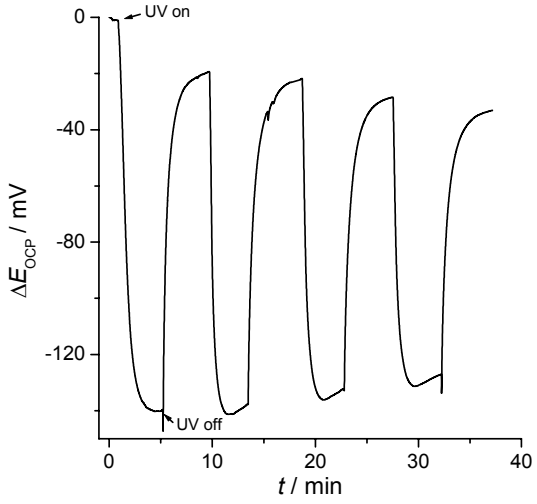

Fig. 2. The time dependence of the open circuit potential of Ti/TiO_2 electrode in presence and the absence of UV light. Electrolyte: 1.0 mol dm^{-3} H_2SO_4.

The Nyquist and Bode plots of EIS data registered at the "UV off" and "UV on" OCP of the Ti/TiO_2 electrode in H_2SO_4 solution are shown in Fig. 3. In the absence and the presence of UV light, loops ascribable to capacitor and resistor in parallel were registered (Fig. 3a). However, the impedance under UV illumination was considerably lower, as the consequence of increased conductivity due to the presence of photon-exited electrons in the conduction band.

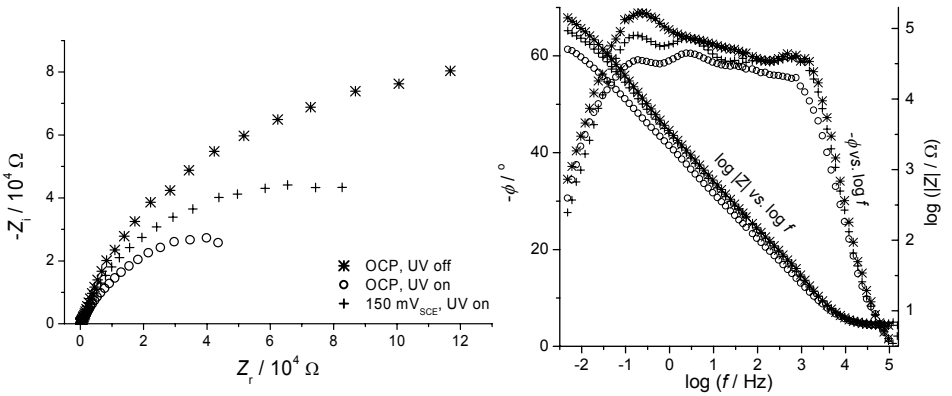

(a) (b)

Fig. 3. Nyquist (a) and Bode plots (b) of EIS data of Ti/TiO_2 electrode registered at the "UV off" and "UV on" OCP and at 150 mV_{SCE} (UV on) in 1.0 mol dm^{-3} H_2SO_4.

Although the impedance data generally form a loop in the complex plane plot (Fig. 3a), its fine structure, which depends on whether the UV light was on or off, is clearly resolved in the Bode phase angle plot (Fig. 3b). In the absence of UV light, two well-resolved phase angle maxima are registered at 1 kHz and 200 mHz, both related to the equivalence of a capacitor and resistor in parallel, which indicates that the loop in Fig. 3a is actually comprised of overlapping loops. On the other hand, in the presence of UV light, these maxima were suppressed, while a new, more intense, maximum appeared at around 3 Hz.

In order to resolve which part of the registered impedance characteristics are intrinsic to the presence of UV light, EIS data were registered at a potential of 150 mV_{SCE}, which is close to "UV off" OCP value, but in the presence of the UV light. These data are also shown in Fig. 3. As can be seen in Fig. 3b, the EIS characteristics at 150 mV_{SCE} are insensitive to UV down to a frequency of 100 Hz. A new maximum is seen at 3 Hz as in the case of the EIS data at the "UV on" OCP value, while the phase angle peak at 200 mHz is less suppressed. This comparison indicates that the phase angle peak at 3 Hz was completely UV light-induced. On the other hand, the peaks at 1 kHz and 200 mHz, being dependent on electrode potential, are electrochemical in nature.

The photovoltaic contribution to the current transients of the Ti/TiO_2 electrode in H_2SO_4 solution can be seen in Fig. 4. The photoelectrochemical activity was controlled at potentials close to the "UV on" (55 mV_{SCE}) and "UV off" OCP (150mV_{SCE}). The illumination by UV light caused an increase in the currents due to a positive photocurrent contribution. The photocurrent was stable during several UV on/off periods and depended neither on the bias potential nor on the sign of the UV light-absent current. Since oxidation of water is the only possible anodic process in the given electrolyte, the relatively small photocurrents visible

in Fig. 4 can be ascribed to photocatalytic oxygen evolution. The absolute photovoltaic effect is rather small, which can be the consequence of the stringent kinetic demands for the oxygen evolution reaction.

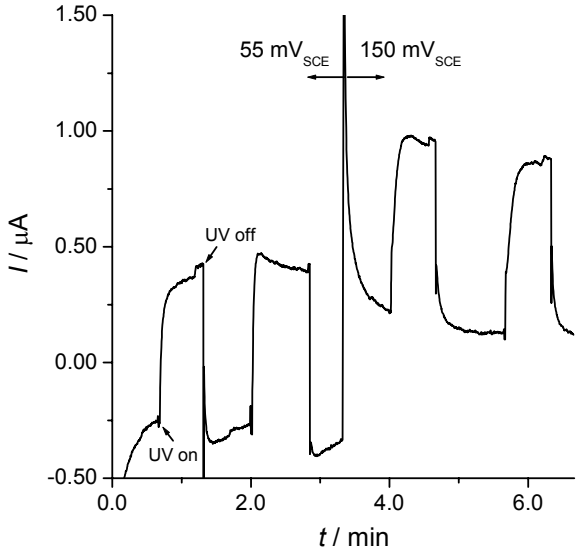

Fig. 4. The current transients of the Ti/TiO_2 electrode at the potentials of 55 and 150 mV_{SCE} in the presence and the absence of UV light. Electrolyte: 1.0 mol dm^{-3} H_2SO_4.

Photoelectrochemical activity for benzyl alcohol oxidation

The change of the OCP of the Ti/TiO_2 electrode, induced by UV light in the presence of BA in the electrolyte, is shown in Fig. 5. The OCP values shifted cathodically, as in the case of the BA-free electrolyte (Fig. 2), but in the presence of BA the shift was considerably more pronounced. The OCP can become even

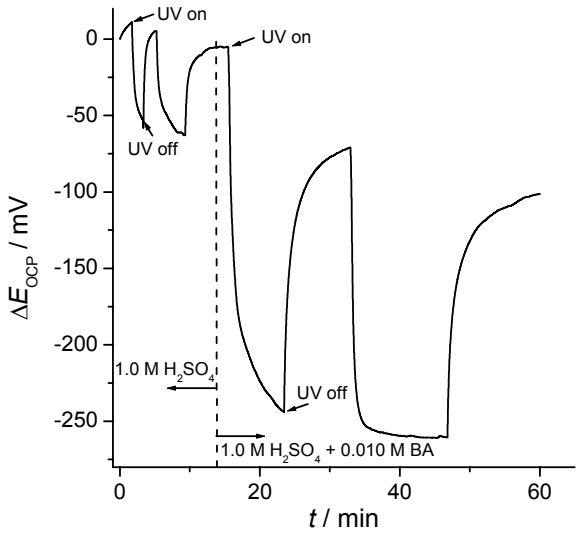

Fig. 5. The time dependence of the open circuit potential of the Ti/TiO_2 electrode in presence and the absence of UV light. Electrolyte: 1.0 mol dm^{-3} H_2SO_4 + 0.010 mol dm^{-3} BA.

250 mV more negative with respect to the "UV off" value. It should be stressed that the "UV off" OCP value did not change upon addition of BA.

Although the "UV off" OCP value can be hardly recovered after the very first UV light switch, as in the case of the BA-free electrolyte, the "UV on" value in the BA-containing electrolyte appeared to be stable and independent of the number of UV on/off periods.

The photoelectrochemical activity of the Ti/TiO_2 electrode considerably increased in the presence of BA; the photocurrent was double that of the BA-free electrolyte, as is shown in Fig. 6 by current transient at a potential close to the "UV off" OCP value.

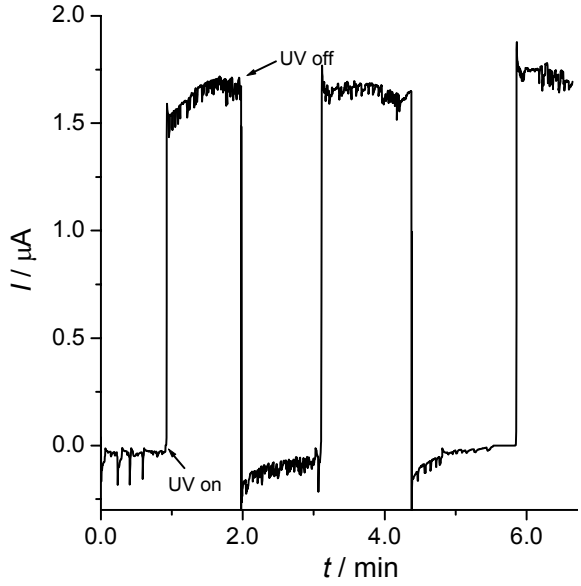

Fig. 6. Current transients of the Ti/TiO_2 electrode in the presence and the absence of UV light. Electrolyte: 1.0 mol dm^{-3} H_2SO_4 + + 0.010 mol dm^{-3} BA.

The considerably larger cathodic shift of the OCP (Fig. 5) and the increased photocurrent (Fig. 6) in the presence of BA indicate that BA is more easily oxidized at TiO_2 than water molecules (BA-free electrolyte) because the holes in the TiO_2 generated by the excitation of electrons are easily populated by electrons from the BA molecules. BA oxidation to benzenecarbaldehyde proceeds through the benzyl radical as an intermediate and a tentative mechanism of PEC oxidation could be as follows:

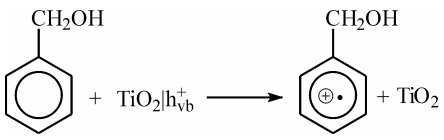

(9)

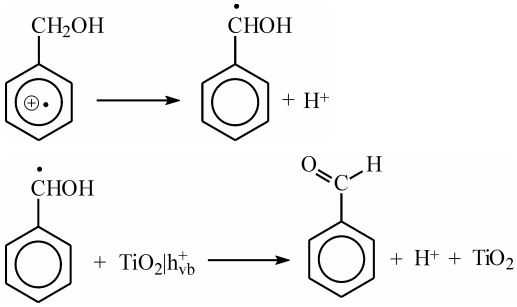

(10)

(11)

The protons released from the benzyl radical-cation (Eqs. (10) and (11)) are easily adopted by O_2^- (Eq. (6)) generated in the reaction between the exited electrons and oxygen (Eq. (3)).

The Nyquist and Bode plots for the Ti/TiO_2 electrode registered at the OCP in the BA-containing electrolyte, in the presence and the absence of UV light, are shown in Fig. 7.

As in the BA-free electrolyte (Fig. 3a), loops were registered in the presence and the absence of UV light, although the impedance is considerably lower than in the BA-free electrolyte (Fig. 7a). The influence of UV light is not so pronounced; only a decrease in the imaginary value can be seen in the low-frequency domain. Two phase angle maxima are registered (Fig. 7b) with no appearance of a UV light-induced third one, as was registered in the BA-free electrolyte (Fig. 3b). However, the low-frequency phase angle peak is considerably more pronounced in the presence of BA.

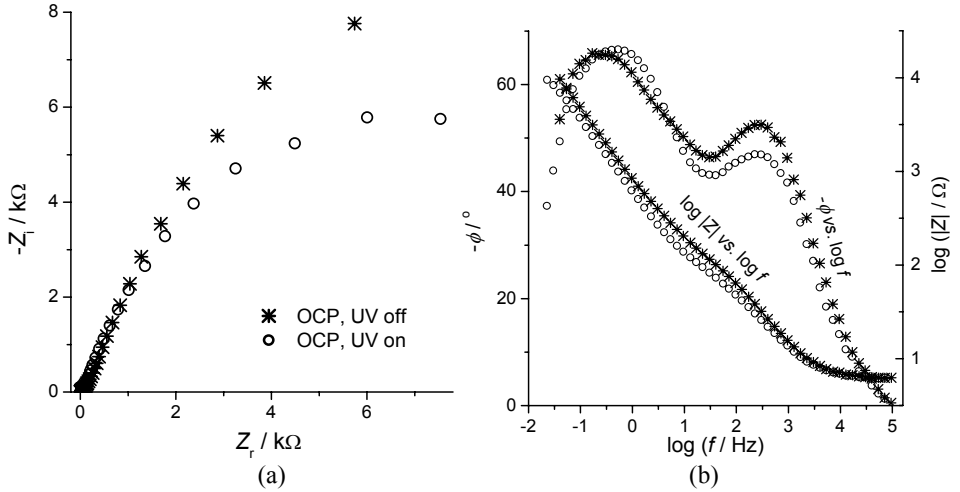

(a) (b)

Fig. 7. Nyquist (a) and Bode plots (b) of the EIS data for the Ti/TiO_2 electrode registered at the "UV off" and "UV on" OCP in 1.0 mol dm^{-3} H_2SO_4 + 0.010 mol dm^{-3} BA.

CONCLUSIONS

A titanium oxide coating on a titanium substrate, prepared by the inorganic sol–gel procedure, showed photoelectrochemical activity in H_2SO_4 solution and for the oxidation of benzyl alcohol.

Microscopic investigations of the coating showed the presence of agglomerates of narrow size distribution, around 100 nm. The agglomerates are consisted of 8 nm-sized crystallites.

Illumination with UV light influenced the open circuit potential, current transient and impedance characteristics of the prepared Ti/TiO_2 photoelectrode, in a H_2SO_4 solution and in a H_2SO_4 + benzyl alcohol solution. The cathodic shift of the open circuit potential was more pronounced in the presence of benzyl alcohol than in its absence, while the photocurrent was doubled due to the oxidation of benzyl alcohol. Due to UV illumination, a new phase angle peak appeared in the Bode plot of the EIS data of the photoelectrode in H_2SO_4 solution. However, this peak was not registered in the H_2SO_4 + benzyl alcohol solution.

Acknowledgements. This work was financially supported by the Ministry of Science and Technological Development of the Republic of Serbia, contract No. 142061. Useful discussion with Dr Lynne Katsikas of the Faculty of Technology and Metallurgy, Belgrade, is also acknowledged.

И З В О Д

ФОТОЕЛЕКТРОХЕМИЈСКА СВОЈСТВА ТИТАН-ОКСИДА ДОБИЈЕНОГ СОЛ–ГЕЛ ПОСТУПКОМ

ВЛАДИМИР В. ПАНИЋ[1], САЊА М. СТЕВАНОВИЋ[1], ВЕСНА Б. МИШКОВИЋ-СТАНКОВИЋ[2], БРАТИСЛАВ Ж. ЈОВАНОВИЋ[2] и БРАНИСЛАВ Ж. НИКОЛИЋ[2]

[1]*Институт за хемију, технологију и металургију, Универзитет у Београду, Његошева 12, 11001 Београд и* [2]*Технолошко–металуршки факултет, Универзитет у Београду, Карнегијева 4, 11120 Београд*

Фотоелектрохемијска својства титан-оксида добијеног сол–гел портупком испитивана су на оксидној превлаци нанетој на титанску подлогу. Превлака је термички третирана у ваздуху на температури од 350 °C. Превлака се састоји од зрна уједначене расподеле по величини од око 100 nm. Фотоелектрохемијске карактеристике установљене су испитивањем промена потенцијала отвореног кола, временске зависности струје и импедансних карактеристика Ti/TiO_2 електроде при осветљености UV светлошћу у раствору H_2SO_4 и при оксидацији бензил-алкохола. Установљена је фотоактивност електроде у испитиваним системима.

(Примљено 2. јула, ревидирано 12. октобра 2008)

REFERENCES

1. G. Li Puma, A. Bono, D. Krishnaiah, J. G. Collin, *J. Hazardous Mater*. **157** (2008) 209
2. B. F. Abramović, V. B. Anderluh, D. V. Sojić, F. F. Gaál, *J. Serb. Chem. Soc.* **72** (2007) 1477
3. C. E. Taylor, *Catal. Today* **84** (2003) 9
4. K. I. Shimizu, H. Akahane, T. Kodama, Y. Kitayama, *Appl. Catal.* **A269** (2004) 75
5. D. Ž. Mijin, D. Z. Zlatić, G. S. Ušćumlić, P. M. Jovančić, *Hem. Ind.* **62** (2008) 275 (in Serbian)

6. A. Popa, V. Sasca, M. Stefanescu, E. E. Kiš, R. Marinković-Neducin, *J. Serb. Chem. Soc.* **71** (2006) 235
7. S. V. Mentus, I. Bošković, J. M. Pješčić, V. Grudić, Z. Bogdanov, *J. Serb. Chem. Soc*. **72** (2007) 1403
8. S. Trasatti, *Electrochim. Acta* **36** (1991) 225
9. V. V. Panić, B. Ž. Nikolić, *J. Serb. Chem. Soc.* **72** (2007) 1393
10. V. Panić, A. Dekanski, S. Milonjić, R. Atanasoski, B. Nikolić, *Electrochim. Acta* **46** (2000) 415
11. D. Ollis, E. Pellizzetti, N. Serpone, *Environ. Sci. Technol.* **25** (1991) 1522
12. W. H. Wang, Z. Zhang, J. Q. Zhang, C. N. Cao, *J. Phys. Chem. B* **109** (2005) 15008
13. H. Selcuk, J. J. Sene, M. A. Anderson, *J. Chem. Technol. Biotechnol.* **78** (2003) 979
14. H. Hidaka, Y. Asai, J. Zhao, K. Nohara, E. Pelizzetti, N. Serpone, *J. Phys. Chem*. **99** (1995) 8244
15. M. E. Calvo, R. J. Candal, S. A. Bilmes, *Environ. Sci. Technol*. **35** (2001) 4132
16. W. H. Leng, Z. Zhang, J. Q. Zhang, *J. Mol. Catal. A* **206** (2003) 239
17. M. C. Li, J. N. Shen, *J. Solid State Electrochem*. **10** (2006) 980
18. T. Docters, J. M. Chovelon, J. M. Herrmann, J. P. Deloume, *Appl. Catal. B*. **50** (2004) 219
19. J. F. Porter, Y.-G. Li, C. K. Chan, *J. Mater. Sci*. **34** (1999) 1523
20. W. H. Leng, Z. Zhang, S. A. Cheng, J. Q. Zhang, C. N. Cao, *Chin. Chem. Lett.* **12** (2001) 1019
21. J. Marsh, D. Gorse, *Electrochim. Acta* **43** (1998) 659
22. G. Li, L. Chen, M. E. Graham, K. A. Gray, *J. Mol. Catal. A* **275** (2007) 30
23. M. Rashidzadeh, *Int. J. Photoenergy*, 2008, Article ID 245981
24. C. He, Y. Xiong, D. Shu, X. Zhu, X. Li, *Thin Solid Films* **503** (2006) 1
25. V. Panić, A. Dekanski, S. Milonjić, R. Atanasoski, B. Nikolić, *Colloids Surfaces: A* **157** (1999) 269V. V. Panić, A. B. Dekanski, T. R. Vidaković, V. B. Mišković-Stanković, B. Jovanović, B. Ž. Nikolić, *J. Solid State Electrochem.* **9** (2005) 43
27. V. Panić, A. Dekanski, G. Wang, M. Fedoroff, S. Milonjić, B. Nikolić, *J. Colloid Interface Sci*. **263** (2003) 68
28. E. Matijević, M. Budnik, L. Meites, *J. Colloid Interface Sci.* **61** (1977) 302.

www.shd.org.rs

Journal of the Serbian Chemical Society

JSCS@tmf.bg.ac.yu • www.shd.org.rs/JSCS

J. Serb. Chem. Soc. 73 (12) 1223–1233 (2008)
JSCS–3801

UDC 547.675+546.11.027:543.544.3:
:543.51:612.461
Original scientific paper

Determination of dimethoxyphenethylamine derivatives in urine by deuterium labeled internal standards

YA-ZHU XU[1], HUEI-RU LIN[2], AHAI-CHANG LUA[2,3] and CHINPIAO CHEN[1]*

[1]*Department of Chemistry, National Dong Hwa University, Hualien 974,* [2]*Institute of Medical Sciences, Tzu Chi University, Hualien 970 and* [3]*Department of Laboratory Medicine and Biotechnology, Tzu Chi University, Hualien 970, Taiwan, R. O. C.*

(Received 4 February, revised 21 June 2008)

Abstract: The use of gas chromatography–mass spectrometry (GC–MS) in forensic analysis is increasing. To exploit fully the capabilities of MS, labeled standards, that can be used to improve the performance of the quantitative analysis, and to increase accuracy and precision, are required. A series of deuterated internal standards, corresponding to the 2C-series of phenethylamine derivatives, including 4-bromo-2,5-dimethoxyphenethylamine-d_6 (2C-B), 4-chloro-2,5-dimethoxyphenethylamine-d_6 (2C-C), 4-iodo-2,5-dimethoxy-phenethylamine-d_6 (2C-I), 4-ethylthio-2,5-dimethoxy-phenethylamine-d_6 (2C-T-2) and 2,5-dimethoxy-4-*n*-propylthiophenethylamine-d_6 (2C-T-7), were synthesized. These deuterated compounds were used to analyze for the corresponding unlabeled compounds in urine. The analysis was performed using GC–MS, with the selected ion monitoring (SIM) technique, whereby good results were achieved.

Keywords: phenethylamine; designer drugs; 2C-C; 2C-B; 2C-I; 2C-T-2; 2C-T-7.

INTRODUCTION

The increased availability of the 2C-series of phenethylamine derivatives on the illicit market has become a serious social problem.[1] Shulgin *et al.,* in their publication, *Phenethylamines I have Known and Loved* (PiHKAL), documented 179 phenethylamine derivatives, including 3,4-methylenedioxymethamphetamine (MDMA), mescaline, 2C-B, 2C-C, 2C-I, 2C-T-2 and 2C-T-7. They also described relevant synthetic procedures.[2] Phenethylamine derivatives are increasingly abused psychoactive drugs, the abuse of which is well documented.[3–8] The series of homologous designer drugs continues to be explored and their widespread consumption has led to increasing number of reports of abuse and intoxication. The abuse of psychoactive drugs from the phenylethylamine and phenylisopropylamine groups has become a very serious social problem in Taiwan over the last decade.[9–22]

* Corresponding author. E-mail: chinpiao@mail.ndhu.edu.tw
doi: 10.2298/JSC0812223X

Unknown drugs are typically detected and identified by gas chromatography–mass spectrometry (GC–MS) because this approach is highly sensitive and can separate organic compounds in complex mixtures.[23–26] The compounds are often derivatized on the amine to yield more specific fragmentation information. This process seriously influences the ability to detect novel amphetamine controlled substance analogs.[27,28] Many studies have addressed the preparation of deuterium-labeled control drugs as internal standards for GC–MS analysis.[29–39] The synthetic routes to 2C-C-d_6, 2C-B-d_6, 2C-I-d_6, 2C-T-2-d_6 and 2C-T-7-d_6 have been described elsewhere.[31] The present investigation explores the applications of 2C-C-d_6, 2C-B-d_6, 2C-I-d_6, 2C-T-2-d_6 and 2C-T-7-d_6 as internal standards.

EXPERIMENTAL

Reagents

Methanol and ethyl acetate (EA) were purchased from Mallinckrodt (Paris, KY, USA). Trifluoroacetic anhydride was purchased from Fluka (Buchs, Switzerland). Stock solutions of the analytes (100 μg mL^{-1}) were prepared in methanol. Subsequent working solutions of calibration samples were prepared by diluting the stock solutions with blank urine. An internal standard (IS) solution of 2C-C-d_6, 2C-B-d_6, 2C-I-d_6, 2C-T-2-d_6 and 2C-T-7-d_6, each at 20 μg mL^{-1}, was prepared in methanol. The preparation of 2C-B-d_6, 2C-C-d_6, 2C-I-d_6, 2C-T-2-d_6 and 2C--T-7-d_6 has been described elsewhere.[31] The structures of 2C-B-d_6, 2C-C-d_6, 2C-I-d_6, 2C-T--2-d_6 and 2C-T-7-d_6.are presented in Fig. 1.

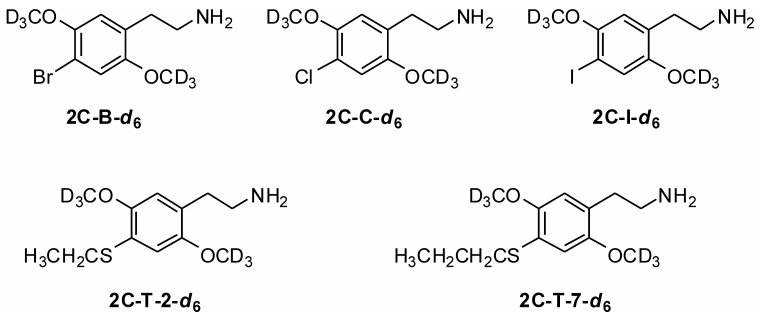

Fig. 1. The structures of 2C-B-d_6, 2C-C-d_6, 2C-I-d_6, 2C-T-2-d_6 and 2C-T-7-d_6.

Procedure

Blank urine samples, which had been collected from volunteer laboratory personnel, were used for the development of the method. Blank urine samples were spiked with appropriate amounts of analytes at concentrations of 0, 50, 100, 500, 1000 and 2000 ng mL^{-1} to prepare calibration curves. Samples were maintained in the refrigerator at 4 °C until analysis.

Instrumentation

A Hewlett Packard 6890 gas chromatograph was coupled to a Hewlett Packard 5973 quadrupole mass spectrometer under EI conditions. Injection was performed in the splitless mode. The flow rate of the carrier gas (He) was 0.60 mL min^{-1}. An HP-5MS column (12.5 m×0.20 mm ID, 0.33 μm film thickness; Agilent Technologies, Palo Alto, CA, USA) was used. The injection port temperature was maintained at 250 °C. The GC oven temperature program started at 70 °C, which was maintained for 0.5 min, and then increased at 30 °C min^{-1} to 255 °C,

which was maintained for 0.5 min. One μL was injected for GC–MS analysis in the full scan monitoring mode. The total analysis time was 12 min per sample with a solvent delay of 3.0 min. The transfer line temperature and MS source temperature were 280 and 230 °C, respectively. The electron energy of the MS was set to 70 eV. Full scan mass spectra of analytes and their deuterium analogs were collected in the *m*/*z* range 50–450 at a scan rate of 3.62 scan/s. The data were collected using Hewlett-Packard ChemStation software.

Sample preparation

To a clean 12–mL screw-cap glass tube was added 2.0 mL of urine sample and 50 μL of IS solution. The mixture was alkalinized with 2.0 mL of 1.0 M NaOH, and extracted with 3.0 mL of EA after vortexing and subsequent centrifugation at 3000 rpm for 5 min. The organic layer was carefully transferred to a clean tube. The mixture was evaporated to dryness under a stream of nitrogen gas at 50–60 °C. The dried extract was dissolved in 50 μL of EA and derivatized with 50 μL of trifluoroacetic anhydride for 30 min at 60 °C. The samples were then cooled to room temperature, evaporated to dryness, and reconstituted with 50 μL of EA. One μL was injected for GC–MS analysis.

RESULTS AND DISCUSSION

The total ion current chromatogram (monitored in the full scan mode) of five phenethylamine designer drugs and four structurally related sympathomimetic amines [amphetamine (A, AMP), methamphetamine (MA), 3,4-methylenedioxyamphetamine (MDA), and MDMA] are presented in Fig. 2. All compounds were chromatographically well separated. The retention times of the drugs and their deuterated analogues are given in Table I. Although the retention times according to the GCs of five sets of labeled and unlabeled compounds vary very little (0.01 min), the selected ion monitoring (SIM) technique discriminates the labeled and unlabeled compounds. Therefore, these deuterium-labeled compounds have the potential to be used as internal standards in GC–MS analysis. The $[M]^+$ of the labeled and unlabeled compounds did not overlap each other and no interference from the urine samples was observed. Accordingly, the 14 $[M]^+$ were monitored using GC–MS with a SIM. The SIM chromatogram was obtained from 2.0 mL of urine sample with 1.0 μg of A, MA, MDA, MDMA and IS. Although A, MA, MDA and MDMA were not the standard samples in this study, generally these compounds were analogous to the IS samples, and could be distinguished in the GC–MS chromatogram.

The electron impact mass spectra of 2C-B-TFA, 2C-B-d_6-TFA, 2C-C-TFA, 2C-C-d_6-TFA, 2C-I-TFA, 2C-I-d_6-TFA, 2C-T-2-TFA, 2C-T-2-d_6-TFA, 2C-T-7--TFA and 2C-T-7-d_6 are presented in Figs. 3–7. Very high $[M]^+$ peaks were observed for 2C-B-TFA, 2C-C-TFA, 2C-I-TFA, 2C-T-2-TFA and 2C-T-7-TFA at *m*/*z* 355, 311, 403, 337 and 351, respectively. For 2C-B-d_6-TFA, 2C-C-d_6-TFA, 2C-I-d_6-TFA, 2C-T-2-d_6-TFA and 2C-T-7-d_6-TFA, very strong $[M]^+$ peaks appeared at *m*/*z* 361, 317, 409, 343 and 357, respectively.

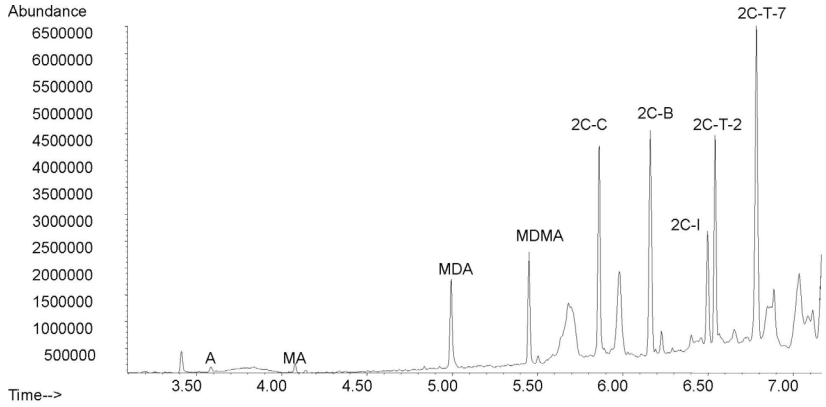

Fig. 2. Total ion chromatography (time in min). The concentrations of the analytes were 0.50 μg mL^{-1}.

TABLE I. Retention times and ions monitored for GC/MS analysis

Compound	Retention time, min	Ions monitored[a] (relative intensity, %)
2C-C-d_6	5.98	204, 191 (69.4), 317 (67.8)
2C-C	5.99	198, 185 (78.7), 311 (74.2)
2C-B-d_6	6.26	248, 361 (76.3), 235 (61.2)
2C-B	6.27	242, 355 (75.6), 229 (77.7)
2C-I-d_6	6.61	409, 296 (80.9), 283 (50.8)
2C-I	6.62	403, 290 (85.6), 277 (53.1)
2C-T-2-d_6	6.66	217, 343 (82.6), 230 (26.5)
2C-T-2	6.67	211, 337 (74.1), 224 (23.8)
2C-T-7-d_6	6.93	231, 357 (78.1), 244 (23.5)
2C-T-7	6.94	225, 351 (89.6), 238 (23.9)
AMP	3.64	140, 118 (91.9), 91 (40.6)
MA	4.14	154, 118 (29.9), 110 (22.7)
MDA	5.05	162, 275 (49.0), 135 (234.4)
MDMA	5.51	154, 162 (78.4), 135 (56.1)

[a]Quantification ions underlined

The EI mass spectrum of 2C-B-d_6-TFA (Fig. 3) has a base peak ion at *m*/*z* 248. This odd electron ion was formed by a McLafferty rearrangement to eliminate trifluoroacetamide (Scheme 1). The ion *m*/*z* 235 was also generated by eliminating an *N*-ethylidene-2,2,2-trifluoroacetamide from the molecular ion *m*/*z* 361. The ion *m*/*z* 203 was formed from the ion *m*/*z* 235 by the well-known specific six-center H-rearrangement of a *γ*-D-atom of the methoxy-d_3 (OCD_3) side chain to the benzylic part, eliminating neutral formaldehyde-d_2 (CD_2O). This rearrangement was proven by comparing the mass spectrum of 2C-B-TFA and 2C-B-d_6--TFA (Fig. 3), *i.e.*, the ion *m*/*z* 199 corresponds to ion *m*/*z* 203 in 2C-B-d_6-TFA and the ion *m*/*z* 203 has four deuterium atoms. 2C-B-d_6-TFA contains a bromine and thus the ions *m*/*z* 361, 248, 235 and 203 always have corresponding isotopic ions *m*/*z* 363, 251, 237 and 205. The ion *m*/*z* 151 was generated by eliminating a

bromomethane ($BrCD_3$) from the molecular ion *m*/*z* 248. Compounds 2C-B, 2C-C, 2C-I, 2C-C-d_6 and 2C-I-d_6 have the same fragmentation pathway, and their corresponding mass spectra are shown in Fig. 3–5.

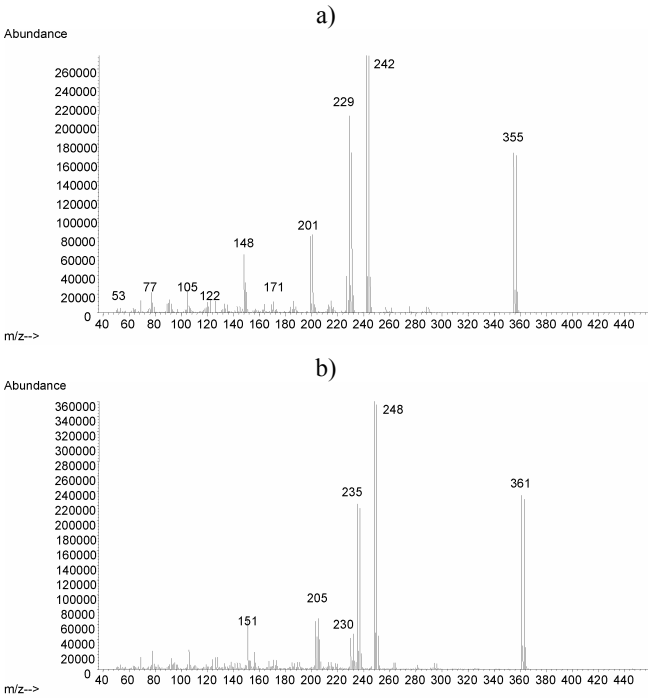

Fig. 3. The mass spectra of TFA derivatives of 2C-B (a) and 2C-B-d_6 (b).

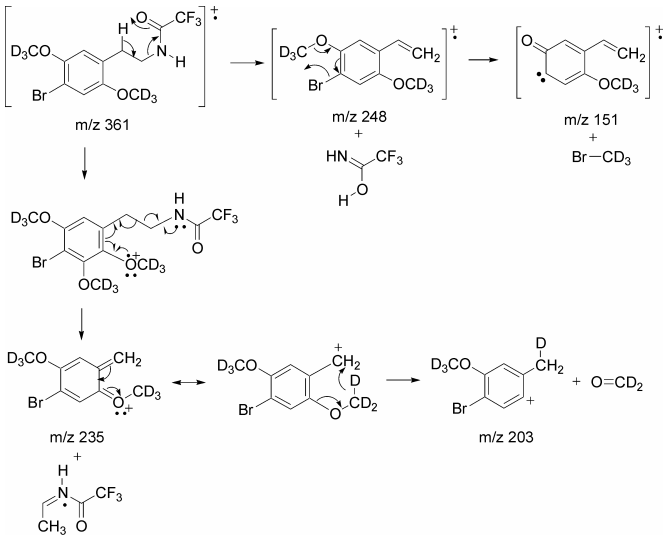

Scheme 1. Spectral interpretation of *N*-[2-(4-bromo-2,5-dimethoxyphenyl)ethyl]--2,2,2-trifluoroacetamide-d_6 (2C-B-d_6-TFA).

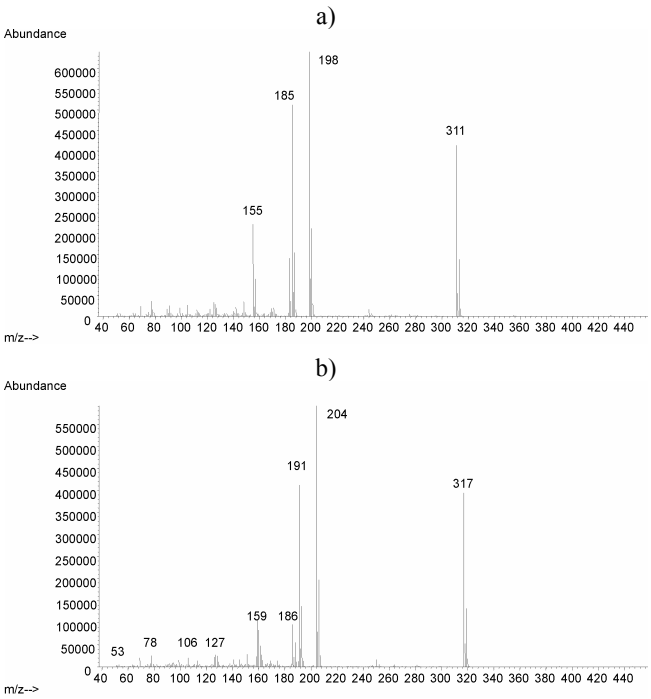

Fig. 4. The mass spectra of TFA derivatives of 2C-C (a) and 2C-C-d_6 (b).

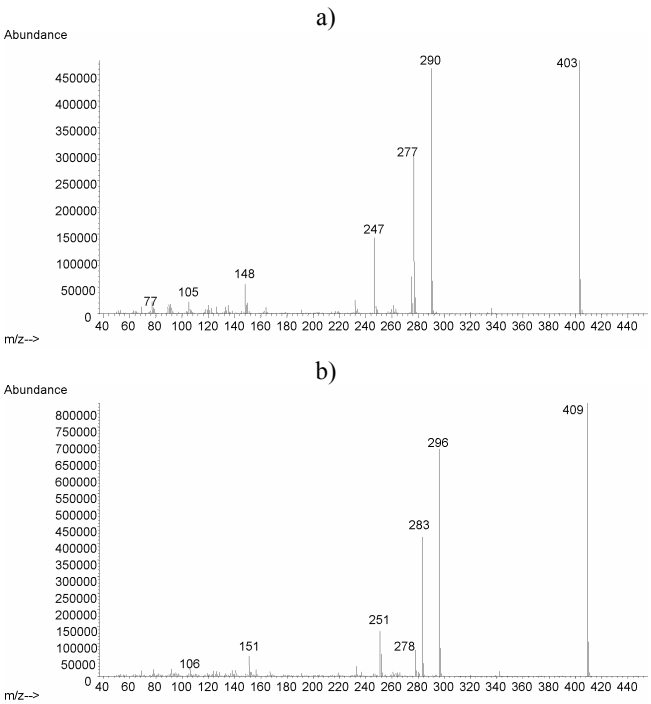

Fig. 5. The mass spectra of TFA derivatives of 2C-I (a) and 2C-I-d_6 (b).

The EI mass spectrum of 2C-T-2-d_6-TFA (Fig. 6) has a base peak ion at *m*/*z* 217. The ion *m*/*z* 217 was generated by eliminating *N*-ethylidene-2,2,2-trifluoroacetamide from the molecular ion *m*/*z* 343. This odd electron ion *m*/*z* 230 was formed by a McLafferty rearrangement to eliminate a trifluoroacetamide (Scheme 2). The ion *m*/*z* 185 was formed from the ion *m*/*z* 217 by the well-known specific six-center H-rearrangement of a γ-D-atom of the methoxy-d_3 (OCD_3) side chain to the benzylic part, eliminating neutral formaldehyde-d_2 (CD_2O). This rearrangement was proven by comparing the mass spectrum of 2C-T-2-TFA and 2C-T--2-d_6-TFA (Fig. 6), *i.e.*, the ion *m*/*z* 181 corresponds to ion *m*/*z* 185 in 2C-T-2-d_6--TFA, and ion *m*/*z* 185 has four deuterium atoms. The ion *m*/*z* 157 was generated by eliminating an ethylene (CH_2=CH_2) from the molecular ion *m*/*z* 185. Compounds 2C-T-2, 2C-T-7 and 2C-T-7-d_6 have the same fragmentation pathway and their corresponding mass spectra are shown in Figs. 6 and 7.

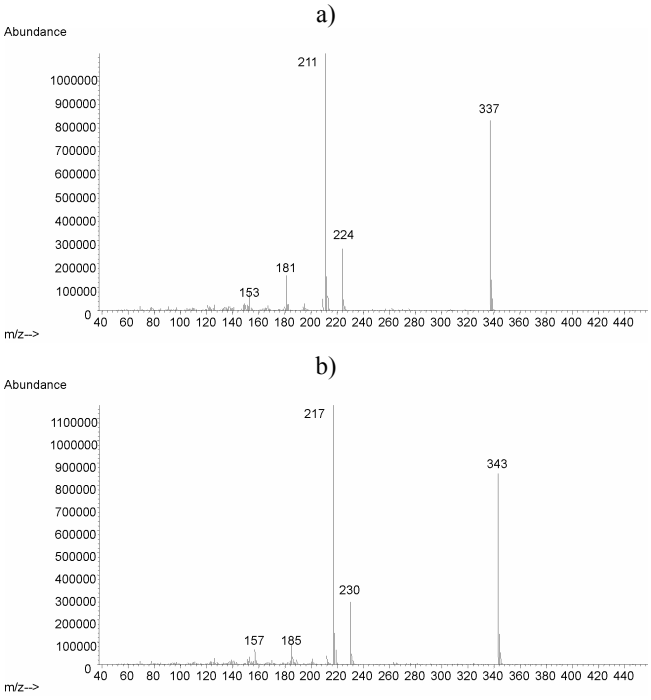

Fig. 6. The mass spectra of TFA derivatives of 2C-T-2 (a) and 2C-T-2-d_6 (b).

The extraction and derivatization were performed using ethyl acetate as solvent. Due to the need to heat for derivatization, a solvent with boiling point above 60 °C was selected. The boiling point of ethyl acetate is 77 °C. The derivatization time (30 min) and temperature (60 °C) were selected, because these derivatization conditions are well established.[16]

The linearity of the quantification method was determined using calibration standards at 0, 50, 100, 500, 1000, 2000 ng of analyte. The selected ion monitoring (SIM) mode was employed throughout the study. Linear regression of the

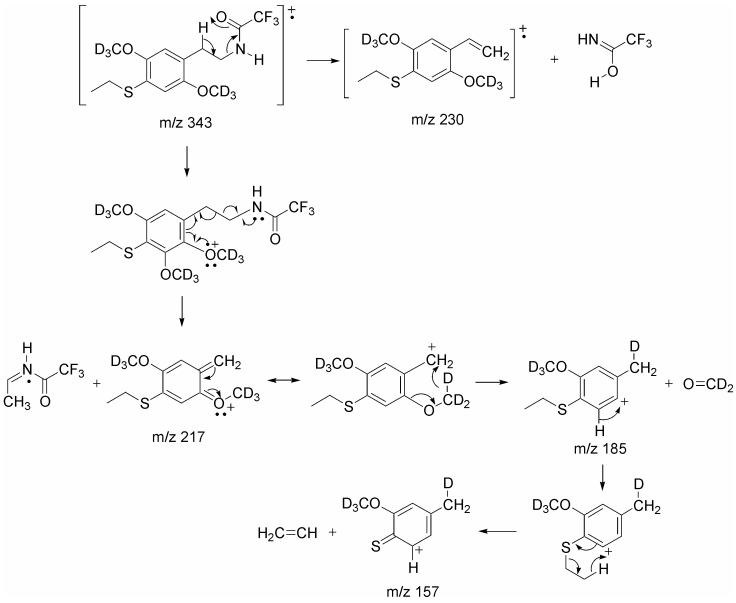

Scheme 2. Spectral interprettation of *N*-[2-(4-ethylsulfanyl-2,5-dimethoxyphenyl) ethyl]-2,2,2-trifluoroacetamide-d_6 (2C-2-T-*d*6-TFA).

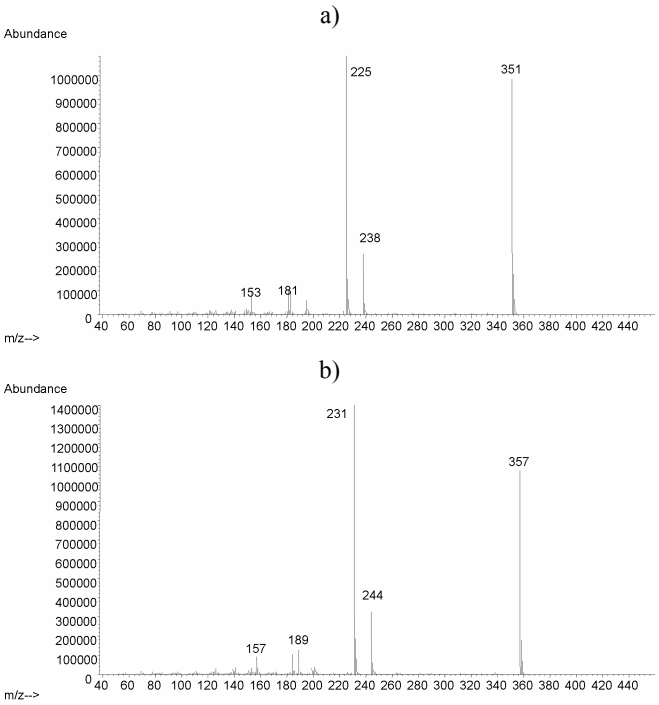

Fig. 7. The mass spectra of TFA derivatives of 2C-T-7 (a) and 2C-T-7-d_6 (b).

calibration curves gave r^2 values between 0.9946 and 0.9999, with most values > 0.9990. The limit of detection (*LOD*) was defined as the signal noise ratio, equal to 3. The *LOD* values of the target compounds are given in Table II, from which it can be seen that the calibration curves for the studied compounds gave excellent straight lines over the range of 0–2000 ng mL^{-1}. Thus, excellent accuracy and precision could be obtained by this method.

Table II. Linear regression of the calibration curves

Compound	Coefficient of correlation (r^2)	Regression line	*LOD* (*S*/*N* = 3) ng mL^{-1}
2C-C	0.9998	$y = 0.0026x - 0.0084$	5.1
2C-B	0.9946	$y = 0.0023x + 0.0259$	8.0
2C-I	0.9999	$y = 0.0015x - 0.0061$	6.7
2C-T-2	0.9991	$y = 0.0018x - 0.0128$	1.6
2C-T-7	0.9999	$y = 0.0015x - 0.0061$	2.9

CONCLUSIONS

This study demonstrates the applications of 2C-B-d_6, 2C-C-d_6, 2C-I-d_6, 2C-T-2-d_6 and 2C-T-7-d_6 as internal standards in GC–MS. Although the GC retention times of the five sets of labeled and unlabeled compounds vary very little (0.01 min), quantification by MS with the selected ion monitoring (SIM) technique enhances the performance of the quantitative analysis. Therefore, five deuterium-labeled compounds possess the potential to be used as the internal standard for GC–MS analysis.

Acknowledgment. The authors thank Ms. Hsu, L. M., at the Instruments Center, National Chung Hsing University and Ms. Lin, S. C., at the Instrument Center, National Tsing Hwa University for their help in obtaining the HRMS spectra, and the National Bureau of Controlled Drugs, Department of Health, Taiwan, Republic of China, for financially supporting this research under contract DOH94-NNB-1007.

ИЗВОД

ОДРЕЂИВАЊЕ ДЕРИВАТА ДИМЕТОКСИФЕНЕТИЛАМИНА У УРИНУ ПРИМЕНОМ ДЕУТЕРИСАНИХ ИНТЕРНИХ СТАНДАРДА

YA-ZHU XU[1], HUEI-RU LIN[2], AHAI-CHANG LUA[2,3] и CHINPIAO CHEN[1]

[1]Department of Chemistry, National Dong Hwa University, Hualien 974, [2]Institute of Medical Sciences, Tzu Chi University, Hualien 970 и [3]Department of Laboratory Medicine and Biotechnology, Tzu Chi University, Hualien 970, Taiwan, R. O. C.

У форензичкој анализи примена гасне хроматографије са масеном спектрометријом (GC–MS) је све већа. Употреба обележених стандарда може побољшати перформансе квантитативне хемијске анализе, повећањем тачности и прецизности одређивања методом GC–MS. Синтетисана је серија деутерисаних интерних стандарда, која одговара 2C серији деривата фенетиламина, укључујући 4-бром-2,5-диметоксифенетиламин-d_6 (2C-B), 4-хлор-2,5-диметоксифенетиламин-d_6 (2C-C), 4-јод-2,5-диметокси-фенетиламин-d_6 (2C-I), 4-етилтио-2,5-диметокси-фенетиламин-d_6 (2C-T-2) и 2,5-диметокси-4-*n*-пропилтиофенетиламин-d_6 (2C-T-7). Деутерисана једињења су коришћена у анализи одговарајућих необележених једињења у узор-

цима урина. Анализа је изведена применом GC–MS у SIM (техника мониторинга одабраних јона) моду, при чему су добијани аналитички поуздани резултати.

(Примљено 4. фебруара, ревидирано 21. јуна 2008)

REFERENCES

1. D. de Boer, I. Bosman, *Pharm. World Sci.* **26** (2004) 110
2. *Erowid*, http://www.erowid.org/library/books_online/pihkal/pihkal.shtml#index (November, 2008)
3. C. Giroud, M. Augsburger, L. Rivier, P. Mangin, F. Sadeghipour, E. Varesio, J. L. Veuthey, P. Kamalaprija, *J. Anal. Toxicol.* **22** (1998) 345
4. C. Furnari, V. Ottaviano, F. Rosati, *Ann. Ist. Super. Sanita* **37** (2001) 297
5. C. Lora-Tamayo, T. Tena, A. Rodriguez, D. Moreno, J. R. Sancho, P. Ensenat, F. Muela, *Forensic Sci. Int*. **140** (2004) 195
6. F. Schifano, A. Oyefeso, J. Corkery, K. Cobain, R. Jambert-Gray, G. Martinotti, A. H. Ghodse, *Hum. Psychopharmacol*. **18** (2003) 519
7. D. G. Caldicott, N. A. Edwards, A. Kruys, K. P. Kirkbride, D. N. Sims, R. W. Byard, M. Prior, *J. Toxicol. Clin. Toxicol.* **41** (2003) 143
8. K. W. Simonsen, E. Kaa, E. Nielsen, D. Rollmann, *Forensic Sci. Int.* **131** (2003) 162
9. J. S. Chen, K. J. Chang, R. C. Charng, S. J. Lai, S. R. Binder, H. Essien, *J. Toxicol. Clin. Toxicol.* **33** (1995) 581
10. C. C. Yang, J. F. Wu, H. C. Ong, S. C. Hung, Y. P. Kuo, C. H. Sa, S. S. Chen, J. F. Deng, *J. Toxicol. Clin. Toxicol.* **34** (1996) 651
11. K. P. Shaw, *J. Forensic Sci.* **44** (1999) 27
12. P. Chou, M. Y. Liou, M. Y. Lai, M. L. Hsiao, H. J. Chang, *Formos Med. Assoc.* **98** (1999) 827
13. C. C. Yang, J. F. Wu, H. C. Ong, Y. P. Kuo, J. F. Deng, J. Ger, *Indian J. Pediatr*. **64** (1997) 469
14. C. F. Yen, M. Y. Chong, Y. H. Liu, *Subst. Use Misuse* **38** (2003) 141
15. S. K. Lin, C. H. Lee, C. H. Pan, W. H. Hu, *Psychiatry Clin. Neurosci.* **57** (2003) 425
16. A. C. Lua, H. R. Lin, Y. T. Tseng, A. R. Hu, P. C. Yeh, *Forensic Sci. Int.* **136** (2003) 47
17. C. K. Chen, S. K. Lin, P. C. Sham, D. Ball, E. W. Loh, C. C. Hsiao, Y. L. Chiang, S. C. Ree, C. H. Lee, R. M. Murray, *Psychol. Med.* **33** (2003) 1407
18. S. K. Lin, D. Ball, C. C. Hsiao, Y. L. Chiang, S. C. Ree, C. K. Chen, *Psychiatry Clin. Neurosci.* **58** (2004) 206
19. H. C. Liu, S. K. Lin, S. K. Liu, S. L. Chen, C. J. Hu, J. G. Chang, S. J. Leu, *Psychiatr. Genet.* **14** (2004) 33
20. C. F. Yen, C. H. Ko, J. Y. Yen, S. J. Liu, *Public Health* **119** (2005) 50
21. C. F. Yen, Y. P. Chang, *Psychiatry Clin. Neurosci.* **59** (2005) 77
22. C. F. Yen, B. L. Shieh, *J. Nerv. Ment. Dis.* **193** (2005) 444
23. C. R. Clark, J. DeRuiter, A. Valaer, F. T. Noggle, *J. Chromatogr. Sci.* **33** (1995) 328
24. F. T. Noggle, C. R. Clark, K. H. Bondir, J. DeRuiter, *J. Chromatogr. Sci.* **29** (1991) 103
25. T. A. Dal Cason, *Forensic Sci. Int.* **35** (1990) 675
26. W. H. Soine, R. E. Shark, D. T. Agee, *J. Forensic Sci.* **28** (1983) 386
27. P. Roesner, T. Junge, *Microgram* **27** (1994) 411
28. S. Borth, W. Haensel, P. Roesner, T. Junge, *Forensic Sci. Int.* **114** (2000) 139
29. Y. Z. Xu, C. Chen, *J. Chin. Chem. Soc.* **54** (2007) 493
30. Y. Z. Xu, C. Chen, *J. Labelled Comp. Radiopharm.* **49** (2006) 897
31. Y. Z. Xu, C. Chen, *J. Labelled Comp. Radiopharm.* **49** (2006) 1187

32. A. C. Shaikh, Y. Y. Wang, C. Chen, *J. Labelled Comp. Radiopharm.* **50** (2007) 660
33. F. Balssa, Y. Bonnaire, *J. Labelled Comp. Radiopharm.* **50** (2007) 207
34. J. Y. Sancéau, D. Larouche, B. Caron, P. Bélanger, A. Coquet, A. Bélanger, F. Labrie, S. Gauthier, *J. Labelled Comp. Radiopharm.* **50** (2007) 197
35. J. Hooper, P. Watts, *J. Labelled Comp. Radiopharm.* **50** (2007) 189
36. J. B. Springer, O. M. Colvin, S. M. Ludeman, *J. Labelled Comp. Radiopharm.* **50** (2007) 115
37. M. A. Ismail, W. David, D. W. Boyki, *J. Labelled Comp. Radiopharm.* **49** (2006) 985
38. M. Pająk, M. Kańska, *J. Labelled Comp. Radiopharm*. **49** (2006) 1061
39. A. A. B. Robertson, N. P. Botting, *J. Labelled Comp. Radiopharm.* **49** (2006) 1201.

www.shd.org.rs

Journal of the Serbian Chemical Society

JSCS@tmf.bg.ac.yu • www.shd.org.rs/JSCS

J. Serb. Chem. Soc. *73* (12) 1235–1246 (2008)
JSCS–3802

UDC 547.581.2+547.831–32:532.13:541.25
Original scientific paper

Study of solute–solvent interactions of nicotinic acid and benzoic acid in methanol and its binary solvent systems

MAHENDRA NATH ROY*, LOVELY SARKAR and BIPUL KUMAR SARKAR

Department of Chemistry, University of North Bengal, Darjeeling-734013, India

(Received 22 November 2007, revised 23 April 2008)

Abstract: The apparent molar volumes, ϕ_V, and viscosity B-coefficients, B, for nicotinic acid (NA) and benzoic acid (BA) in mixed solvents containing 10, 20, 30 mass % of *n*-amyl alcohol (*n*-AmOH) or isoamyl alcohol (i-AmOH) in methanol and in pure methanol (MeOH) were determined from the solution density and viscosity measurements at 298.15 K as function of concentrations of NA and BA. These results were, in conjunction with the results obtained in pure methanol, used to deduce the partial molar volumes of transfer, $\Delta\phi_V^0$, and viscosity B-coefficients of transfer, ΔB, for NA and BA from methanol to different mixed methanol solvents, in order to rationalize various interactions in the ternary solutions. An increase in the transfer properties of NA and BA with increasing mass % of *n*-AmOH and i-AmOH in methanol was observed and explained by the effect of structural changes and preferential solvation. Also, the free energies of viscous flow, $\Delta\mu_1^{0\neq}$ and $\Delta\mu_2^{0\neq}$, per mole of solvent and solute, respectively, were calculated and analyzed on the basis of the transition state theory of relative viscosity.

Keywords: apparent molar volumes; viscosity B-coefficients; nicotinic acid; benzoic acid; solute–solvent interactions.

INTRODUCTION

Many enzymes require a non-protein co-factor for their catalytic activities. Vitamins are essential precursors for various co-enzymes. These co-enzymes are therefore required in almost all metabolic pathways.[1] Nicotinic acid (pyridine-3--carboxylic acid) is an essential micro-nutrient, a reactive moiety of the co-enzyme nicotinamide adenine dinucleotide (NAD) and nicotinamide adenine dinucleotide phosphate (NADP).[2] NAD is involved in the catabolism of carbohydrates, fats, and proteins with simultaneous energy production. The NADP functions consist especially of anabolic processes of fatty acids and cholesterol synthesis.[3–5] Sometimes nicotinic acid is referred to as nothing more than vitamin PP (Pellagra Preventive),[2,6,7] since its deficiency in human diet causes pellagra.

* Corresponding author. E-mail: mahendraroy2002@yahoo.co.in
doi: 10.2298/JSC0812235R

Benzoic acid is a good adsorbing reagent for insulin[8,9] and is used in medicine as a urinary antiseptic and in the vapor form for disinfecting bronchial tubes.[10] This acid also finds many important applications in the manufacture of alkyl resins, plasticizers and pharmaceuticals.[11]

Volumetric properties of the binary or ternary mixtures have recently been studied extensively. In particular, much effort has gone into the determination of partial molar volumes at infinite dilution, as they are the key to solvation phenomena. Although there are studies on various properties of nicotinic acid (NA) [7,12–17,20] and benzoic acid (BA) [9,18–22] in the literature, studies on partial molar volumes and viscosities of these compounds in mixed solvent systems are still scarce. Hence in this study an attempt was made to study these properties for NA and BA in binary mixtures of methanol with *n*-amyl (*n*-AmOH) and isoamyl alcohol (i-AmOH) at 298.15 K to unravel the various interactions prevailing in the ternary systems under investigation.

EXPERIMENTAL

Nicotinic acid and benzoic acid were purchased from the Sigma Chemical Company, USA and used as received. Their purity as supplied by the vendor was 99 %. A. R. Grade methanol, *n*-amyl alcohol and isoamyl alcohol were purchased from Merck, India. The purity of the alcohols as given by the vendor was also 99 %. The purification of methanol was cited in an earlier paper.[23] Both *n*-AmOH and i-AmOH were dried with anhydrous K_2CO_3 and fractionally distilled. The middle fraction was collected and kept free from humidity with 3 Å molecular sieves.[24] The physical properties of the different pure liquids and mixed methanol solvents are listed in Table I.

TABLE I. Physical properties of different pure and mixed methanol solvents at 298.15 K

Solvent	ρ / g cm^{-3}		η / mPa s	
	Experimental	Literature	Experimental	Literature
Methanol	0.7869	0.7869[26]	0.547	0.547[26]
n-Amyl alcohol	0.8115	0.8110[24]	3.350	3.350[24]
Isoamyl alcohol	0.8071	0.8071[24]	3.475	3.480[24]
10 mass % of *n*-amyl alcohol	0.7883	–	0.569	–
20 mass % of *n*-amyl alcohol	0.7898	–	0.645	–
30 mass % of *n*-amyl alcohol	0.7923	–	0.732	–
10 mass % of isoamyl alcohol	0.7882	–	0.574	–
20 mass % of isoamyl alcohol	0.7900	–	0.648	–
30 mass % of isoamyl alcohol	0.7911	–	0.720	–

Stock solutions of NA and BA in different mixed methanol solvents and in pure methanol were prepared by mass and the working solutions were prepared by mass dilution. The conversion of molality into molarity was accomplished using the experimental density values. Great care was taken in minimizing evaporation losses and preventing moisture pick-up. The uncertainty in the molarity of the nicotinamide solutions was evaluated to ±0.0001 mol dm^{-3}.

The densities were measured with an Ostwald–Sprengel type pycnometer having a bulb volume of 25 cm^3 and an internal diameter of the capillary of about 0.1 cm. The pycnometer was calibrated at 298.15 K with doubly distilled water and purified benzene. The pycnometer

with the test solution was equilibrated in a water bath maintained at ±0.01 K of the desired temperature. The pycnometer was then removed from the thermostatic bath, properly dried, and weighed. The mass measurements accurate to ±0.01 mg were made on a digital electronic analytical balance (Mettler Toledo, AG 285, Switzerland). The total uncertainty in density was estimated to be ±0.0001 g cm^{-3} and that of the temperature ±0.01 K.

The viscosity was measured by means of a suspended Ubbelohde type viscometer, which had been thoroughly cleaned, dried and calibrated at 298.15 K with triply distilled water and purified methanol. It was filled with experimental liquid and placed vertically in a glass sided thermostat bath maintained constant to ±0.01 K. The efflux times of flow of the liquids were recorded with a stopwatch correct to ±0.1 s. The viscosity of a solution, η, is given by the following equation:

$$\eta = (kt - \frac{L}{t})\rho \quad (1)$$

where k and L are viscometer constants and t and ρ are the efflux time of flow and the density of the experimental liquid, respectively. The uncertainty in the viscosity measurements was within ±0.003 mPa s. Details of the methods and techniques of density and viscosity measurements were described elsewhere.[25,26] The experimental values of concentrations c, densities viscosities, and derived parameters of the studied ternary solutions at 298.15 K are reported in Table II.

TABLE II. Concetration, density, viscosity, apparent molar volume, ϕ_V, and $(\eta_r - 1)/\sqrt{c}$ for nicotinic acid and benzoic acid in methanol and mixed methanol solvents at 298.15 K

c / mol dm^{-3}	ρ / g cm^{-3}	η / mPa s	ϕ_V / cm^3 mol^{-1}	$(\eta_r - 1)/\sqrt{c}$
Nicotinic acid				
In methanol				
0.0197	0.7880	0.551	88.32	0.0521
0.0320	0.7886	0.553	87.09	0.0613
0.0517	0.7898	0.559	85.57	0.0965
0.0690	0.7908	0.563	84.28	0.1113
0.0779	0.7913	0.565	83.91	0.1179
0.0821	0.7916	0.566	83.70	0.1212
In 10 mass % of *n*-AmOH + MeOH				
0.0200	0.7893	0.575	93.55	0.0746
0.0325	0.7900	0.579	92.20	0.0975
0.0524	0.7910	0.584	90.45	0.1152
0.0699	0.7920	0.590	89.08	0.1396
0.0874	0.7930	0.596	87.95	0.1605
0.0901	0.7932	0.597	87.80	0.1639
In 20 mass % of *n*-AmOH + MeOH				
0.0200	0.7908	0.647	92.90	0.0219
0.0325	0.7915	0.651	90.04	0.0516
0.0524	0.7927	0.656	86.29	0.0745
0.0699	0.7938	0.662	83.76	0.0996
0.0874	0.7949	0.668	81.67	0.1206
0.0900	0.7951	0.669	81.31	0.1240

TABLE II. Continued

c / mol dm^{-3}	ρ / g cm^{-3}	η / mPa s	ϕ_V / cm^3 mol^{-1}	$(\eta_r - 1)/\sqrt{c}$
Nicotinic acid				
In 30 mass % of *n*-AmOH + MeOH				
0.0199	0.7931	0.737	104.64	0.0484
0.0325	0.7937	0.742	101.01	0.0758
0.0524	0.7948	0.752	95.17	0.1194
0.0698	0.7957	0.760	93.90	0.1448
0.0812	0.7964	0.765	91.65	0.1582
0.0815	0.7964	0.765	91.89	0.1579
In 10 mass % of i-AmOH + MeOH				
0.0198	0.7893	0.579	83.32	0.0619
0.0321	0.7900	0.582	83.12	0.0778
0.0519	0.7912	0.589	82.85	0.1147
0.0692	0.7922	0.595	82.68	0.1391
0.0865	0.7932	0.601	82.50	0.1599
0.0878	0.7933	0.601	82.49	0.1587
In 20 mass % of i-AmOH + MeOH				
0.0197	0.7909	0.651	98.01	0.0330
0.0321	0.7916	0.655	92.74	0.0603
0.0518	0.7927	0.662	89.86	0.0949
0.0690	0.7938	0.668	86.12	0.1175
0.0780	0.7943	0.671	86.05	0.1271
0.0822	0.7946	0.673	85.00	0.1346
In 30 mass % of i-AmOH + MeOH				
0.0197	0.7920	0.729	97.87	0.0891
0.0321	0.7927	0.738	92.61	0.1395
0.0518	0.7941	0.754	82.41	0.2075
0.0691	0.7954	0.765	76.96	0.2378
0.0839	0.7967	0.777	72.00	0.2733
0.0849	0.7967	0.778	71.70	0.2765
Benzoic acid				
In methanol				
0.0200	0.7885	0.553	88.60	0.0776
0.0320	0.7890	0.556	88.45	0.0920
0.0519	0.7898	0.560	88.25	0.1043
0.0719	0.7907	0.564	88.11	0.1159
0.0878	0.7915	0.567	88.01	0.1234
0.0999	0.7919	0.569	87.96	0.1272
In 10 mass % of *n*-AmOH + MeOH				
0.0204	0.7894	0.573	86.51	0.0492
0.0325	0.7901	0.576	84.66	0.0682
0.0528	0.7913	0.580	82.84	0.0841
0.0732	0.7926	0.585	80.40	0.1039
0.0894	0.7936	0.588	79.71	0.1117
0.0996	0.7943	0.591	78.50	0.1225

TABLE II. Continued

c / mol dm^{-3}	ρ / g cm^{-3}	η / mPa s	ϕ_V / cm^3 mol^{-1}	$(\eta_r - 1)/\sqrt{c}$
Benzoic acid				
In 20 mass % of *n*-AmOH + MeOH				
0.0200	0.7906	0.648	101.50	0.0329
0.0320	0.7912	0.650	99.46	0.0433
0.0521	0.7922	0.656	97.10	0.0747
0.0722	0.7932	0.661	95.06	0.0923
0.0883	0.7941	0.665	93.60	0.1043
0.0983	0.7946	0.668	92.79	0.1137
In 30 mass % of *n*-AmOH + MeOH				
0.0200	0.7931	0.734	103.65	0.0193
0.0320	0.7938	0.738	100.59	0.0458
0.0520	0.7947	0.743	97.13	0.0659
0.0719	0.7957	0.749	94.19	0.0866
0.0879	0.7968	0.755	91.73	0.1060
0.0999	0.7971	0.759	90.57	0.1167
In 10 mass % of i-AmOH + MeOH				
0.0199	0.7891	0.577	95.84	0.0370
0.0318	0.7897	0.579	94.86	0.0488
0.0518	0.7907	0.583	93.57	0.0689
0.0716	0.7917	0.587	92.55	0.0846
0.0876	0.7926	0.590	91.67	0.0942
0.0995	0.7932	0.593	91.14	0.1049
In 20 mass % of i-AmOH + MeOH				
0.0199	0.7910	0.650	104.64	0.0219
0.0318	0.7914	0.652	102.54	0.0346
0.0516	0.7924	0.657	99.67	0.0611
0.0716	0.7933	0.662	97.32	0.0807
0.0874	0.7941	0.666	95.69	0.0940
0.0994	0.7945	0.670	94.75	0.1077
In 30 mass % of i-AmOH + MeOH				
0.0199	0.7918	0.725	109.90	0.0492
0.0319	0.7923	0.729	106.82	0.0700
0.0517	0.7932	0.736	103.02	0.0977
0.0716	0.7944	0.743	96.11	0.1194
0.0875	0.7950	0.749	98.03	0.1362
0.0994	0.7956	0.755	97.14	0.1542

RESULT AND DISCUSSION

For the analysis of the solvation state of NA and BA in mixed methanol solvents and the interactions existing between different components in the studied solutions, the apparent molar volumes (ϕ_V) were determined from the solution densities using the following equation:[25,27]

$$\phi_V = \frac{M}{\rho_0} - \frac{1000(\rho - \rho_0)}{\rho_0 c} \quad (2)$$

where M is the molar mass of the solute, c is the concetration of the solution and ρ_0 and ρ are the densities of the solvent and solution, respectively. The experimental ϕ_V values were fitted to Masson Equation:[28]

$$\phi_V = \phi_V^0 + S_V^* \sqrt{c} \quad (3)$$

where ϕ_V^0 is the partial molar volume at infinite dilution and S_V^* is the experimental slope. The ϕ_V^0 values were determined by fitting the dilute data ($c < 0.1$) to Eq. (3) using the least-square fit. The values of ϕ_V^0 and S_V^* at the experimental temperature are reported in Table III. The estimated uncertainties in ϕ_V^0 are equal to standard deviation, σ, the root mean square of the deviations between the experimental and calculated ϕ_V for each data point. Table III shows that the ϕ_V^0 values are generally positive and increase with increasing amount of *n*-AMOH/i-AmOH in the ternary solutions. This indicates the presence of strong solute–solvent interactions which are further strengthened at higher amounts of *n*-AMOH/i-AmOH in the ternary solutions. Also, the ϕ_V^0 values are comparatively more positive for the solutions containing BA than for those containing NA. This is a clear manifestation that solute–solvent interactions are more prominent in BA solutions. The negative S_V^* values indicated that the investigated solutions are characterized by weak solute–solute interactions.

TABLE III. Limiting partial molar volume (ϕ_V^0) and experimental slope (S_V^*) for nicotinic acid and benzoic acid in methanol and different mixed methanol solvents with standard deviations (σ) at 298.15 K

Solute	Solvent	ϕ_V^0 / cm^3 mol^{-1}	S_V^* / cm^2 dm$^{1/2}$ mol$^{-3/2}$	σ
NA	MeOH	92.81	–31.99	0.01
	10 mass % of *n*-AmOH+MeOH	98.74	–36.46	0.01
	20 mass % of *n*-AmOH+MeOH	103.17	–73.07	0.01
	30 mass % of *n*-AmOH+MeOH	116.75	–88.25	0.22
	10 mass % of i-AmOH+MeOH	84.07	–5.35	0.02
	20 mass % of i-AmOH+MeOH	108.99	–84.42	1.74
	30 mass % of i-AmOH+MeOH	123.23	–175.74	0.45
BA	MeOH	89.11	–3.70	0.01
	10 mass % of *n*-AmOH+MeOH	92.97	–45.35	1.21
	20 mass % of *n*-AmOH+MeOH	108.55	–50.28	0.02
	30 mass % of *n*-AmOH+MeOH	114.16	–74.96	0.02
	10 mass % of i-AmOH+MeOH	99.66	–26.87	0.01
	20 mass % of i-AmOH+MeOH	112.73	–57.38	0.01
	30 mass % of i-AmOH+MeOH	120.69	–79.33	0.02

Partial molar volumes of transfer from methanol to different mixed methanol solvents, $\Delta\phi_V^0$, were determined using the relation:[29,30]

$$\Delta\phi_V^0 = \phi_V^0 \text{ (mixed methanol solvent)} - \phi_V^0 \text{ (methanol)} \quad (4)$$

The $\Delta\phi_V^0$ value is, by definition, free from solute–solute interactions and therefore provides information regarding solute–co-solute interactions.[29] Alcohols are characterized by the presence of extensive intermolecular hydrogen bonding in the pure state,[31] as well as in their mixtures. However, the strength of hydrogen bonding depends on the position of the –OH group and molecular shape. Due to the branched structure of i-AmOH, intermolecular hydrogen bonding is less[32,33] in i-AmOH + MeOH mixtures than in the *n*-AmOH + MeOH system. This fact may also be due to the order of the +I-effect: MeOH < *n*-AmOH < < i-AmOH and thereby decreasing the polarity of the alcoholic O–H bonds. This decreased polarity of the alcoholic O–H bonds decreases the degree of intermolecular hydrogen bonding in the mixtures but increases the solvation of the studied solutes, predominantly by hydrophobic–hydrophobic group interactions.[34] As can be seen from Table IV, the value of $\Delta\phi_V^0$ is positive and increases monotonically with the amount of *n*-AmOH/i-AmOH in the ternary mixtures, indicating increased solute–solvents interactions in the mixed methanol solvents. Also, it is evident that this increasing trend is, on average, greater for the i-AmOH + methanol system than for the *n*-AmOH + methanol system. This suggests that NA and BA are preferentially more solvated by *n*-AmOH/i-AmOH than by methanol and the branched structure of i-AmOH renders it a more efficient solvent for the studied solutes. Also, the $\Delta\phi_V^0$ values are generally more positive for mixtures containing BA, *i.e.*, the solute–solvent interactions are comparatively more prominent for the BA mixtures than for the NA mixtures. This may be attributed to their structural difference and, inasmuch as the local structure in solutions depends on the forces between molecules and on the form and volume of the molecules, it will change with the composition. The $\Delta\phi_V^0$ values are depicted graphically in Figs. 1 and 2 as a function of mass % of *n*-AmOH/i-AmOH in the solutions for the studied solutes at 298.15 K.

A perusal of Table V shows that the values of the *A* coefficient are generally negative for all the investigated solutions at the experimental temperature. These results indicate the presence of weak solute–solute interactions and that these interactions further decrease with increasing mass % of *n*-AmOH/i-AmOH in the solutions. The viscosity B-coefficient[36] reflects the effects of solute–solvent interactions on the solution viscosity. Table V illustrates that the values of the viscosity B-coefficient for selected solutes in the studied solvent systems are positive, thereby suggesting the presence of strong solute–solvent interactions and these interactions are further strengthened with increasing mass % of *n*-AmOH/i--AmOH in the ternary solutions.

The viscosity B-coefficients of transfer (ΔB) from methanol to different mixed methanol solvents were determined using the relation:[29,30]

$$\Delta B = B(\text{mixed methanol solvent}) - B(\text{methanol}) \quad (6)$$

The ΔB values, shown in Table IV, and depicted graphically in Figs. 1 and 2 as a function of mass % of *n*-AmOH/i-AmOH in solutions at 298.15 K, support the results obtained from the $\Delta\phi_V^0$ values discussed above.

TABLE IV. Values of $\Delta\phi_V^0$ and ΔB of transfer from methanol to different mixed methanol solvents for NA and BA at 298.15 K. The viscosity data of the studied non-aqueous solutions of NA and BA were analyzed using the Jones–Dole Equation:[35]

$$(\frac{\eta}{\eta_0} - 1)c^{-1/2} = (\eta_r - 1)c^{-1/2} = A + Bc^{1/2} \quad (5)$$

where $\eta_r = \eta/\eta_0$; η_0 and η are the viscosities of the solvent and solution, respectively. A and B are constants estimated by the least-squares method and reported in Table V

Solute	Solvent	$\Delta\phi_V^0$ / cm^3 mol^{-1}	ΔB / cm^3 mol^{-1}
NA	10 mass % of *n*-AmOH	5.93	0.052
	20 mass % of *n*-AmOH	10.36	0.127
	30 mass % of *n*-AmOH	23.94	0.270
	10 mass % of i-AmOH	–8.74	0.152
	20 mass % of i-AmOH	16.18	0.183
	30 mass % of i-AmOH	30.42	0.721
BA	10 mass % of *n*-AmOH	3.86	0.127
	20 mass % of *n*-AmOH	19.44	0.202
	30 mass % of *n*-AmOH	25.05	0.259
	10 mass % of i-AmOH	10.55	0.106
	20 mass % of i-AmOH	23.62	0.213
	30 mass % of i-AmOH	31.58	0.304

TABLE V. Values of viscosity A and B coefficients with standard errors in parenthesis for NA and BA in methanol and different mixed methanol solvents at 298.15 K

Solute	Solvent	A / cm$^{3/2}$ mol$^{-1/2}$	B / cm^3 mol^{-1}
NA	MeOH	–0.022 (±0.007)	0.502 (±0.031)
	10 mass % of *n*-AmOH	–0.005 (±0.011)	0.554 (±0.030)
	20 mass % of *n*-AmOH	–0.066 (±0.006)	0.629 (±0.022)
	30 mass % of *n*-AmOH	–0.061 (±0.002)	0.772 (±0.007)
	10 mass % of i-AmOH	–0.034 (±0.006)	0.654 (±0.010)
	20 mass % of i-AmOH	–0.063 (±0.004)	0.685 (±0.015)
	30 mass % of i-AmOH	–0.080 (±0.007)	1.223 (±0.018)
BA	MeOH	0.040(±0.000)	0.281 (±0.001)
	10 mass % of *n*-AmOH	–0.008(±0.007)	0.408 (±0.015)
	20 mass % of *n*-AmOH	–0.038(±0.001)	0.483 (±0.013)
	30 mass % of *n*-AmOH	–0.055(±0.002)	0.540 (±0.007)
	10 mass % of i-AmOH	–0.019(±0.001)	0.387 (±0.002)
	20 mass % of i-AmOH	–0.051(±0.006)	0.494 (±0.017)
	30 mass % of i-AmOH	–0.035(±0.012)	0.585 (±0.040)

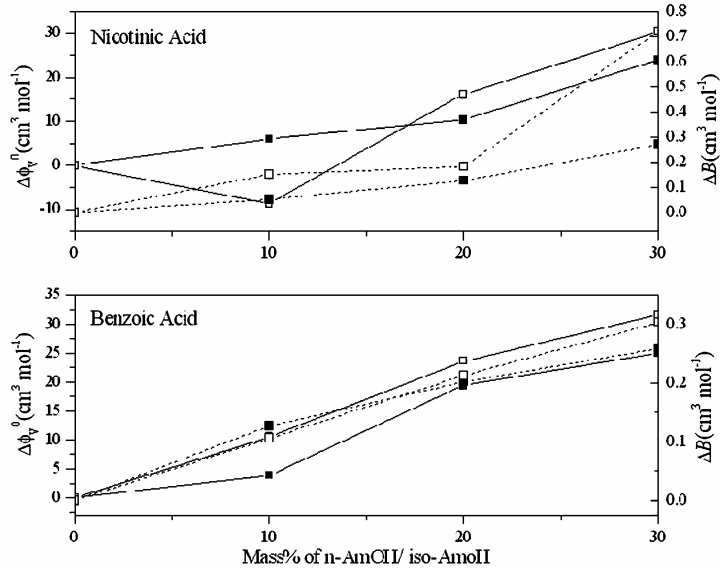

Fig. 1. Plots of partial molar volume of transfer, $\Delta\phi_V^0$, and viscosity B-coefficient of transfer, ΔB, from methanol to methanol + *n*-AmOH (■)/i-AmOH (□) solvents for nicotinic acid and benzoic acid at 298.15 K; Solid and dotted lines are for $\Delta\phi_V^0$ and ΔB, respectively.

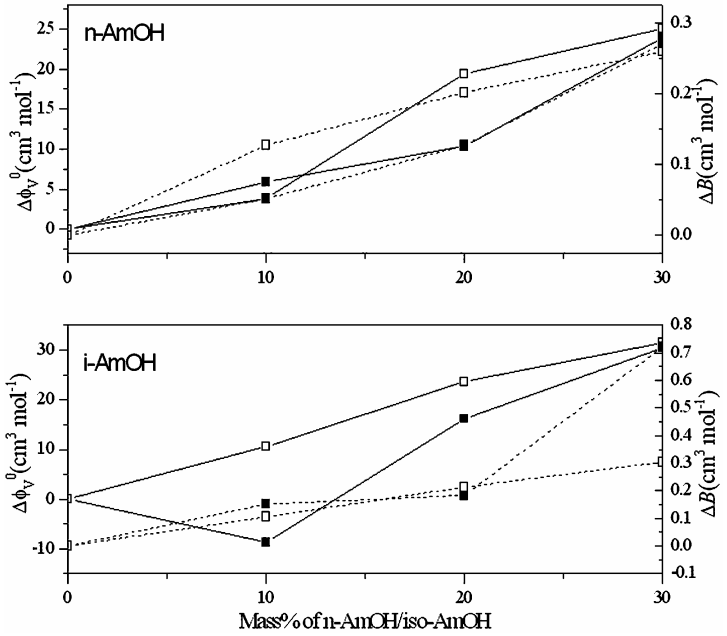

Fig. 2. Plots of partial molar volume of transfer, $\Delta\phi_V^0$, and viscosity *B*-coefficient of transfer, ΔB, from methanol to different mixed methanol solvents for nicotinic acid (■) and benzoic acid (□) at 298.15 K; Solid and dotted lines are for $\Delta\phi_V^0$ for ΔB, respectively.

The viscosity data were also analyzed on the basis of the transition state theory of relative viscosity as suggested by Feakings *et al.*[37] using the following equation:

$$\Delta\mu_2^{0\neq} = \Delta\mu_2^{0\neq} + \frac{RT(1000B + \overline{V}_2^0 - \overline{V}_1^0)}{\overline{V}_1^0} \quad (7)$$

where $\Delta\mu_2^{0\neq}$ is the contribution per mole of the solute to the free energy of activation of viscous flow of the solutions. $\overline{V}_1^0$ and $\overline{V}_2^0$ are the partial molar volumes of the solvent and solute, respectively. $\Delta\mu_2^{0\neq}$ of the solutions was determined from the above relation. The free energy of activation of viscous flow for the pure solvent/solvent mixture, $\Delta\mu_1^{0\neq}$, is given by the relation:[37,38]

$$\Delta\mu_1^{0\neq} = \Delta G_1^{0\neq} = RT \ln\left(\frac{\eta_0 \overline{V}_1^0}{hN_A}\right) \quad (8)$$

where N_A is the Avogadro constant, h the Planck constant, η_0 the viscosity of the solvent, R the gas constant and T the absolute temperature. The values of the parameters $\Delta\mu_1^{0\neq}$ and $\Delta\mu_2^{0\neq}$ are given in Table VI. They show that $\Delta\mu_1^{0\neq}$ is almost constant at all the solvent compositions, implying that $\Delta\mu_2^{0\neq}$ is dependent mainly on the viscosity B-coefficients and the $\overline{V}_2^0 - \overline{V}_1^0$ terms. However, the $\Delta\mu_2^{0\neq}$ values were found to be positive at the experimental temperature and this suggests that the process of viscous flow becomes more difficult as the amount of *n*-AmOH/i-AmOH increases in the ternary solutions. Thus, the viscous behavior of the studied solutes reinforces the earlier contention that strong solute–solvent interaction exists in the present systems. According to Feakings *et al.*,[37] $\Delta\mu_2^{0\neq}$ >

TABLE VI. Values of $\overline{V}_2^{\upsilon} - \overline{V}_1^{\upsilon}$, $\Delta\mu_1^{0\neq}$ and $\Delta\mu_2^{0\neq}$ for NA and BA in methanol and different mixed methanol solvents at 298.15 K

Solute	Solvent	$(\overline{V}_2^0 - \overline{V}_1^0)\times10^6$ / m^3 mol^{-1}	$\Delta\mu_1^{0\neq}$ / kJ mol^{-1}	$\Delta\mu_2^{0\neq}$ / kJ mol^{-1}
NA	MeOH	52.09	9.97	43.72
	10 mass % of *n*-AmOH	55.33	10.23	45.02
	20 mass % of *n*-AmOH	56.69	10.71	47.27
	30 mass % of *n*-AmOH	66.77	11.20	52.80
	10 mass % of i-AmOH	40.65	10.25	49.91
	20 mass % of i-AmOH	62.52	10.72	50.59
	30 mass % of i-AmOH	73.17	11.16	75.35
BA	MeOH	48.39	9.97	30.02
	10 mass % of *n*-AmOH	49.56	10.23	36.35
	20 mass % of *n*-AmOH	62.07	10.71	39.77
	30 mass % of *n*-AmOH	64.18	11.20	41.16
	10 mass % of i-AmOH	56.24	10.25	35.55
	20 mass % of i-AmOH	66.26	10.72	40.60
	30 mass % of i-AmOH	70.63	11.16	43.58

$> \Delta\mu_1^{0\neq}$ for solutes with positive viscosity B-coefficients indicates stronger solute–solvent interactions, thereby suggesting that the formation of the transition state is accompanied by the rupture and distortion of the intermolecular forces in the solvent structure.[37] In the present study, the found relation $\Delta\mu_2^{0\neq} > \Delta\mu_1^{0\neq}$ suggests an increase in the bulk structure of methanol in the presence of NA and BA due to the preferential solvation of the said solutes by *n*-AmOH/i-AmOH, releasing some methanol molecules to the bulk structure. In fact, Feakings *et al*[37] showed $\Delta\mu_2^{0\neq} > \Delta\mu_1^{0\neq}$ for solutes that are structure promoters.

CONCLUSION

In summary, the $\Delta\phi_V^0$ and viscosity B-coefficient values for nicotinic acid and benzoic acid indicate the presence of strong solute–solvent interactions and these interactions are further strengthened at higher amount of *n*-AmOH/i-AmOH in the ternary solutions. Also, they were found to act as methanol-structure promoters and their solvation behavior towards the mixed alcoholic solvents were more or less similar to in nature.

Acknowledgements. The authors are grateful to the Departmental Special Assistance Scheme under the University Grants Commission, New Delhi (No. 540/6/DRS/2002, SAP-1) for financial support.

И З В О Д

ИЗУЧАВАЊЕ ИНТЕРАКЦИЈА РАСТВОРЕНА СУСПСТАНЦА–РАСТВАРАЧ У РАСТВОРИМА НИКОТИНСКЕ И БЕНЗОЕВЕ КИСЕЛИНЕ У МЕТАНОЛУ И БИНАРНОЈ СМЕШИ РАСТВАРАЧА

MAHENDRA NATH ROY, LOVELY SARKAR и BIPUL KUMAR SARKAR

Department of Chemistry, University of North Bengal, Darjeeling-734013, India

На основу зависности густине и вискозности од концентрације никотинске (NA) и бензоеве (BA) киселине у бинарном растварачу, који садржи 10, 20 и 30 mass % *n*-амил алкохола (*n*-AmOH) или изоамил алкохола у метанолу (i-AmOH), и чистом метанолу, на температури 298,15 K, одређене су вредности привидних моларних запремина, ϕ_V, и B коефицијента вискозности. Ови резултати су искоришћени за одређивање парцијалне моларне запремине, $\Delta\phi_V^0$, и B коефицијента вискозности, ΔB, преноса за NA и BA од метанола ка различитим бинарним метанолским растварачима, да би се рационализовале различите интеракције у терцијарним растворима. Уочен је пораст величина преноса NA и BA са порастом садржаја *n*-AmOH или i-AmOH у метанолу, који је објашњен ефектима структурних промена и преференцијалне солватације. Такође, израчунате су и моларне промене хемијског потенцијала за растварач и растворену сустанцу, $\Delta\mu_1^{0\neq}$ и $\Delta\mu_2^{0\neq}$, респективно, и анализиране у складу са теоријом прелазног стања и релативном вискозношћу.

(Примљено 22. новембра 2007, ревидирано 23. априла 2008)

REFERENCES

1. F. A. Robinson, *The Vitamin B-Complexes*, Chapman & Hall, London, 1951, Ch. 4

2. A. S. Fauci, E. Braunwald, K. J. Isselbacher, J. D. Wilson, J. B. Martin, D. L. Kasper, S. L. Hauser, D. L. Long, *Harrison's Principles of Internal Medicine*, Vol. 1, 14th Ed., McGraw- Hill, New York, 1998
3. T. Brody, *Nutritional Biochemistry*, 2nd Ed., Academic Press, San Diego, CA, 1999
4. M. Shils, J. A. Olson, M. Shike, A. C. Ross, *Nutrition in Health and Diseases*, 9th Ed., Williams & Wilkins, Baltimore, MD, 1999
5. E. E. Snell, D. E. Metzler, *Annu. Rev. Biochem.* **25** (1956) 435
6. A. N. Nesmeyanov, N. A. Nesmeyanov, *Fundamentals of Organic Chemistry*, Vol. 3, Mir Publishers, Moscow, 1981, p. 393
7. D. Cacaval, A. C. Blaga, M. Camarup, A. I. Galaction, *Separation Sci. Technol*. **42** (2007) 389
8. I. L. Finar, *Organic Chemistry*, *Vol 1: The Fundamental Principles*, 6th Ed., Longman Singapore Publishers (Pte) Ltd, Singapore, 1990
9. P. J. Moloney, D. M. Findlay, *J. Biol. Chem.* **67** (1923) 359
10. B. S. Bhal, A. Bhal, *Advanced Organic Chemistry*, S. Chand and Company Ltd., New Delhi, 1981, p. 1097
11. W. A. Sharp, *Dictionary of Chemistry*, 2nd Ed., Penguin Books Ltd., London, 1990, p. 56
12. H. H. Loh, C. P. Berg, *J. Nutrition* **101** (1971) 1601
13. S. Schuette, R. C. Rose, *Am. J. Physiol. Cell. Physiol.* **250** (1986) C694
14. I. Cho, C. L. Chang, X. Quing, *J. Agri. Food. Chem.* **53** (2005) 7307
15. W. I. M. Holman, *Biochemistry* **56** (1954) 513
16. Z. Orekhova, M. Ben-Hamo, E. Manzurola, A. Apelblat, *J. Soln. Chem.* **34** (2005) 687
17. C. Yiyun, X. Tongwen, *Eur. J. Med. Chem.* **40** (2005) 1384
18. K. Sagarik, S. Chaiwongwattana, P. Sisot, *J. Chem. Phys.* **306** (2004) 1
19. P. K. Mandal, D. K. Chatterjee, B. K. Seal, A. K. Basu, *J. Soln. Chem.* **7** (1978) 1572
20. A. G. Kharitonova, O. K. Krasilnikova, R. Sh.Vastapetyan, A. V. Bulanova, *Colloid J.* **67** (2005) 375
21. J. W. Mauger, A. N. Paralta, *J. Pharm. Sci.* **63** (1974) 576
22. E. Ayranci, N. Hoda, E. Bayram, *J. Colloid Interface Sci.* **284** (2005) 83
23. M. N. Roy, B. Sinha, *J. Soln. Chem.* **34** (2005) 1311
24. R. Riggio, H. E. Martinez, H. N. Sollomo, *J. Chem. Eng. Data* **31** (1986) 235
25. M. N. Roy, B. Sinha, V. K. Dakua, *J. Chem. Eng. Data* **51** (2006) 590
26. M. N. Roy, B. Sinha, *J. Mol. Liq.* **133** (2007) 89
27. B. Sinha, V. K. Dakua, M. N. Roy, *J. Chem. Eng. Data* **52** (2007) 1768
28. A. Kundu, N. Kishore, *J. Soln. Chem.* **32** (2003) 703
29. K. Belibagli, E. Agranci, *J. Soln. Chem.* **19** (1990) 867
30. A. Ali, S. Khan, F. Nabi, *J. Serb. Chem. Soc.* **72** (2007) 495
31. Y. Marcus, *Introduction to Liquid State Chemistry*, Wiley, New York, 1977
32. V. K. Dakua, B. Sinha, M. N. Roy, *J. Indian. Chem. Soc*. **84** (2007) 37
33. A. Aucejo, M. C. Burguet, R. Munoz, M. Sanchotello, *J. Chem. Eng. Data* **41**(1996) 508
34. A. Ben-Naim, *Solvation Thermodynamics*, Plenum Press, New York, 1987
35. G. Jones, M. Dole, *J. Am. Chem. Soc.* **51** (1929) 2950
36. F. J. Millero, A. Losurdo, C. Shin, *J. Phys. Chem.* **82** (1978) 784
37. D. Feakings, D. J. Freemantle, K. G. Lawrence, *J. Chem. Soc., Faraday Trans. I* **70** (1974) 795
38. S. Glasston, K. Laidler, H. Eyring, *The Theory of Rate Processes*, McGraw-Hill, New York, 1941.

J. Serb. Chem. Soc. 73 (12) 1247 (2008)

Errata (printed version only)

Issue No. 11 (2008), Vol. **73**, page 1110:

– Line 24 from the top should read: "…Development of the Republic of Serbia under Grant No. 14061 is acknowledged. Thanks are…"

– Line 32 from the top should read: "…ДОБИЈЕНОМ НЕОРГАНСКИМ СОЛ––ГЕЛ ПОСТУПКОМ…"

www.shd.org.rs

Journal of the Serbian Chemical Society

JSCS@tmf.bg.ac.yu • www.shd.org.rs/JSCS

J. Serb. Chem. Soc. 73 (12) 1249–1257 (2008)

Contents of Volume 73

NUMBER 1

NUMBER 6

NUMBER 10

NUMBER 12

J. Serb. Chem. Soc. 73 (12) 1259–1263 (2008)

Subject index

J. Serb. Chem. Soc. 73 (12) 1265–1269 (2008)

Author index

End of Volume 73.